GLASS CULLET AS A NEW SUPPLEMENTARY CEMENTITIOUS MATERIAL (SCM)

by

MOHAMMADREZA MIRZAHOSSEINI

M.Sc., Iran University of Science and Technology, Tehran, 2009

AN ABSTRACT OF A DISSERTATION

submitted in partial fulfillment of the requirements for the degree

DOCTOR OF PHILOSOPHY

Department of Civil Engineering

College of Engineering

KANSAS STATE UNIVERSITY
Manhattan, Kansas

2014

Abstract

Finely ground glass has the potential for pozzolanic reactivity and can serve as a supplementary cementitious material (SCM). Glass reaction kinetics depends on both temperature and glass composition. Uniform composition, amorphous nature, and high silica content of glass make ground glass an ideal material for studying the effects of glass type and particle size on reactivity at different temperature. This study focuses on how three narrow size ranges of clear and green glass cullet, 63–75 µm, 25–38 µm, and smaller than 25 µm, as well as combination of glass types and particle sizes affects the microstructure and performance properties of cementitious systems containing glass cullet as a SCM. Isothermal calorimetry, chemical shrinkage, thermogravimetric analysis (TGA), quantitative analysis of X-ray diffraction (XRD), and analysis of scanning electron microscope (SEM) images in backscattered (BS) mode were used to quantify the cement reaction kinetics and microstructure. Additionally, compressive strength and water sorptivity experiments were performed on mortar samples to correlate reactivity of cementitious materials containing glass to the performance of cementitious mixtures. A recently-developed modeling platform called "µic the model" was used to simulated pozzolanic reactivity of single type and fraction size and combined types and particle sizes of finely ground glass. Results showed that ground glass exhibits pozzolanic properties, especially when particles of clear and green glass below 25 µm and their combination were used at elevated temperatures, reflecting that glass cullet is a temperature-sensitive SCM. Moreover, glass composition was seen to have a large impact on reactivity. In this study, green glass showed higher reactivity than clear glass. Results also revealed that the simultaneous effect of sizes and types of glass cullet (surface area) on the

degree of hydration of glass particles can be accounted for through a linear addition, reflecting that the surface area would significantly affect glass cullet reactivity and that the effects of SCM material interaction on reaction kinetics were minimal. However, mechanical properties of cementitious systems containing combined glass types and sizes behaved differently, as they followed the weaker portion of the two particles. This behavior was attributed to the pores sizes, distruibution, and connectiity. Simulations of combined glass types and sizes showed that more work on microstructural models is needed to properly model the reactivity of mixed glass particle systems.

GLASS CULLET AS A NEW SUPPLEMENTARY CEMENTITIOUS MATERIAL (SCM)

by

MOHAMMADREZA MIRZAHOSSEINI

M.Sc., Iran University of Science and Technology, Tehran, 2009

A DISSERTATION

submitted in partial fulfillment of the requirements for the degree

DOCTOR OF PHILOSOPHY

Department of Civil Engineering

College of Engineering

KANSAS STATE UNIVERSITY
Manhattan, Kansas

2014

Approved by:

Major Professor
Dr. Kyle A. Riding

Copyright

Abstract

Finely ground glass has the potential for pozzolanic reactivity and can serve as a supplementary cementitious material (SCM). Glass reaction kinetics depends on both temperature and glass composition. Uniform composition, amorphous nature, and high silica content of glass make ground glass an ideal material for studying the effects of glass type and particle size on reactivity at different temperature. This study focuses on how three narrow size ranges of clear and green glass cullet, 63–75 µm, 25–38 µm, and smaller than 25 µm, as well as combination of glass types and particle sizes affects the microstructure and performance properties of cementitious systems containing glass cullet as a SCM. Isothermal calorimetry, chemical shrinkage, thermogravimetric analysis (TGA), quantitative analysis of X-ray diffraction (XRD), and analysis of scanning electron microscope (SEM) images in backscattered (BS) mode were used to quantify the cement reaction kinetics and microstructure. Additionally, compressive strength and water sorptivity experiments were performed on mortar samples to correlate reactivity of cementitious materials containing glass to the performance of cementitious mixtures. A recently-developed modeling platform called "µic the model" was used to simulated pozzolanic reactivity of single type and fraction size and combined types and particle sizes of finely ground glass. Results showed that ground glass exhibits pozzolanic properties, especially when particles of clear and green glass below 25 µm and their combination were used at elevated temperatures, reflecting that glass cullet is a temperature-sensitive SCM. Moreover, glass composition was seen to have a large impact on reactivity. In this study, green glass showed higher reactivity than clear glass. Results also revealed that the simultaneous effect of sizes and types of glass cullet (surface area) on the

degree of hydration of glass particles can be accounted for through a linear addition, reflecting that the surface area would significantly affect glass cullet reactivity and that the effects of SCM material interaction on reaction kinetics were minimal. However, mechanical properties of cementitious systems containing combined glass types and sizes behaved differently, as they followed the weaker portion of the two particles. This behavior was attributed to the pores sizes, distruibution, and connectiity. Simulations of combined glass types and sizes showed that more work on microstructural models is needed to properly model the reactivity of mixed glass particle systems.

Table of Contents

List of Figures

List of Tables

Acknowledgements

Firstly I like to give my thanks to my one of a kind adviser, Dr. Kyle A. Riding, whose guidance, support, and motivation helped me perform well in research and academic activities.

I would also like to thank my committee members Dr. Esmaeily, Dr. Hossain, Dr. Singh, and Dr. Washburn for their valuable discussions and comments.

With special thanks to the National Science Foundation (CMMI-1032636) for funding this project, I would like to thank Ash Grove Cement Company for performing the chemical analysis and measuring the surface area and density of materials; Dr. Jeffrey Bullard for providing great discussions. The help of Ryan Benteman, Jan Vosahlik, and all my assistants including Durrel Harper, Abdelbaset Traplsi, Brandon Heavener, Garrette E. Sharpe, Alaa Eldin Abouelleil, Luke Spaich, Austin Conrady, and Antoine Borden are gratefully appreciated.

Dedication

I would enthusiastically like to dedicate this work to my beloved and amazing wife and friend ***Samira*** whose love and support are the major reasons for me to achieve accomplishments.

Chapter 1 - Introduction

Waste glass can be either landfilled or recycled after collection. The volume of landfilled glass all over the world is estimated as 200 million tons per year [1]. Because landfilling has some issues like limited capacity and environmental concerns [2], an increasing tendency for glass recycling has been observed within past decades. In 2007, glass recycling has increased to 3.2 million tons in the United States [3]. Even though waste glass can be theoretically recycled completely without any reduction in physical quality, unlimited recycling could be restricted due to mixed color glass [4]. Although large glass particles can be color-sorted by means of optical sensors of recycling devices, sorting small particles is not justifiable from an economic viewpoint and they are disposed in landfills. For example, 1.65 million tons of waste glasses are yearly landfilled in U.K because they are non-recyclable [5]. Considering these economic and environmental concerns, alternatives for reusing glass particles need to be considered. One possible method of reusing waste glass is in concrete, either as aggregate or supplementary cementitious material (SCM).

A past concern about the utilization of glass particles in concrete as aggregate is a durability concern caused by the reaction between alkali of pore solution and amorphous silica of the glass, i.e. alkali-silica reaction (ASR). This has resulted in limited use of glass aggregate in concrete [6]. On the other hand, since the glass contains high amorphous silica – a prerequisite for pozzolanic reaction – it can be a supplementary cementitious material, if it is ground small enough [2-3,7-11]. Hence, finely ground glass can not only increases concrete strength, but can also make it more sustainable and durable.

Objectives of the Study

This study aims to answer the following questions about cementitious mixtures containing single particle size and type of glass cullet, as well as mixed glass cullet at different curing temperatures:

- How does glass powder reactivity vary with changes in curing temperature?
- How do the reaction rate of glass powder, reaction products, and reaction product density change at different curing temperatures?
- How do glass type and particle size ranges influence their reactivity?
- How does using finely ground glass affect mechanical and water sorptivity properties of concrete?
- How do cementitious mixtures containing different blended glass types and sizes behave from the stand points of hydration rate, mechanical properties, and durability?
- Is it possible to model the microstructure of cementitious systems using individual and/or blended glass types and particles?

Thesis Organization

Chapter 1 provides an introduction about the major concept of the study. The objectives of this study and thesis organization are also outlined.

Chapter 2 provides a background on the reaction kinetics of portland cement and points out the most important factors affecting hydration rate. The philosophy of using SCMs in concrete is also discussed. Additionally, a literature review over the history and the results of

using glass cullet in concrete either as aggregate or SCM is carried out. A summary of the background of microstructural modeling of cement hydration is also provided.

Chapter 3 describes the materials used in this study, including their chemical and physical composition. It also discusses the procedure used to classify the glass particles by size.

Chapter 4 discusses the test methods in the experimental program of this study to enable us to answer the questions mentioned in Chapter 1.

In Chapter 5, the effects of curing temperature and glass type on hydration behavior and mechanical properties of cementitious mixtures containing very finely ground glass are discussed. Additionally, the temperature sensitivity and pozzolanicity of the glass powders are evaluated.

Chapter 6 discusses the effects of particle size on the hydration rate and performance properties of the cementitious systems containing different glass particle types at different curing temperature.

Chapter 7 discusses the effects of combining glass types and sizes in cementitious mixtures on reaction kinetics and performance properties. The measured results from isothermal calorimetry, scanning electron microscopy (SEM), and mortar compressive strength are compared to the calculated results obtained from the measured results of single particles and type of glass to investigate the effects of mixing glass particle type.

Chapter 8 discusses the use of microstructural modeling to understand the reactivity and performance of single and combined glass particles.

Chapter 9 summarizes the findings of the study and provides suggestions for further research.

Chapter 2 - Literature Review

Concrete is the second most commonly used industrial material in the world after water [12]. Concrete typically contains water, cement, coarse aggregates, and fine aggregates. Portland cement is the world's most commonly used cement in concrete. Global production and consumption of portland cement have been increased within past years [13]. In 2012, cement consumption throughout the world were 3736 million tons [12].

Portland cement is manufactured by heating up limestone, clay or ground silica sand, and a small amount of iron to about 1350 – 1450°C. This produces a material called clinker which is the size of marble. Clinker is interground with a small amount of gypsum to produce portland cement [14]. When portland cement is mixed with water, an adhesive mixture is formed which binds other concrete components such as sand and gravel together. This process takes place through a chemical reaction called cement hydration.

Cement Hydration

Cement hydration is the fundamental process which is responsible for heat release, strength gain, and microstructural development of concrete [15]. Clinker contains four main compounds (Table 2.1) whose proportions depend on the raw materials proportion and the temperature in the kiln.

Table 2.1 Four main compounds of portland cement

Compound	Notation[1]	Phase Name
Tricalcium Silicate	C_3S	Alite (impure version of C_3S)
Dicalcium Silicate	C_2S	Belite (impure version of C_2S)
Tricalcium Aluminate	C_3A	Aluminate
Tetracalcium Aluminoferrite	C_4AF	Ferrite

1. C: CaO, S: SiO_2, A: Al_2O_3, and F: Fe_2O_3

The principle hydration reactions of the main compounds of clinker are shown in Eq. (2.1) through Eq. (2.4).

$C_3S + 5.3H \rightarrow C\text{-}S\text{-}H + 1.3CH$ Eq. (2.1)

$C_2S + 4.3H \rightarrow C\text{-}S\text{-}H + 0.3CH$ Eq. (2.2)

$C_3A + 3C\$H_2 + 26H \rightarrow C_6A\$_3H_{32}$ Eq. (2.3)

$C_4AF + 3C\$H_2 + 21H \rightarrow C_6(A,F)\$_3H_{32} + (F,A)H_3$ Eq. (2.4)

The $ is used in cement chemist notation to denote sulfate. The hydration of C_3S and C_2S produce calcium silicate hydrate (C-S-H) and calcium hydroxide (CH).

During these reactions, each of these four phases releases some heat, making hydration an exothermal chemical reaction [16]. Monitoring and measuring the amount of heat evolved during cement hydration can provide valuable information to investigate mechanical and performance properties of concrete. Figure 2.1 shows the isothermal heat of hydration (HOH) of a portland cement. There are five distinct reaction stages shown in Figure 2.1: dissolution, induction, acceleration, deceleration, and the transition/diffusion-controlled stage [16]. Dissolution (Stage 1) happens during the first few minutes (5-7 minutes) after the initial contact of cement and water [14]. The heat of this stage, which is also known as heat of wetting [14], evolves from the quick dissolution of some alite and rapid hydration of some of the aluminate phase [17]. During this stage, the rate of reaction is a function of particle size, crystalline structure, and surface dislocations of cement grains, especially alite [17]. After the initial dissolution [18], the rate of reaction decreases rapidly to the point at which the induction period (Stage 2) begins.

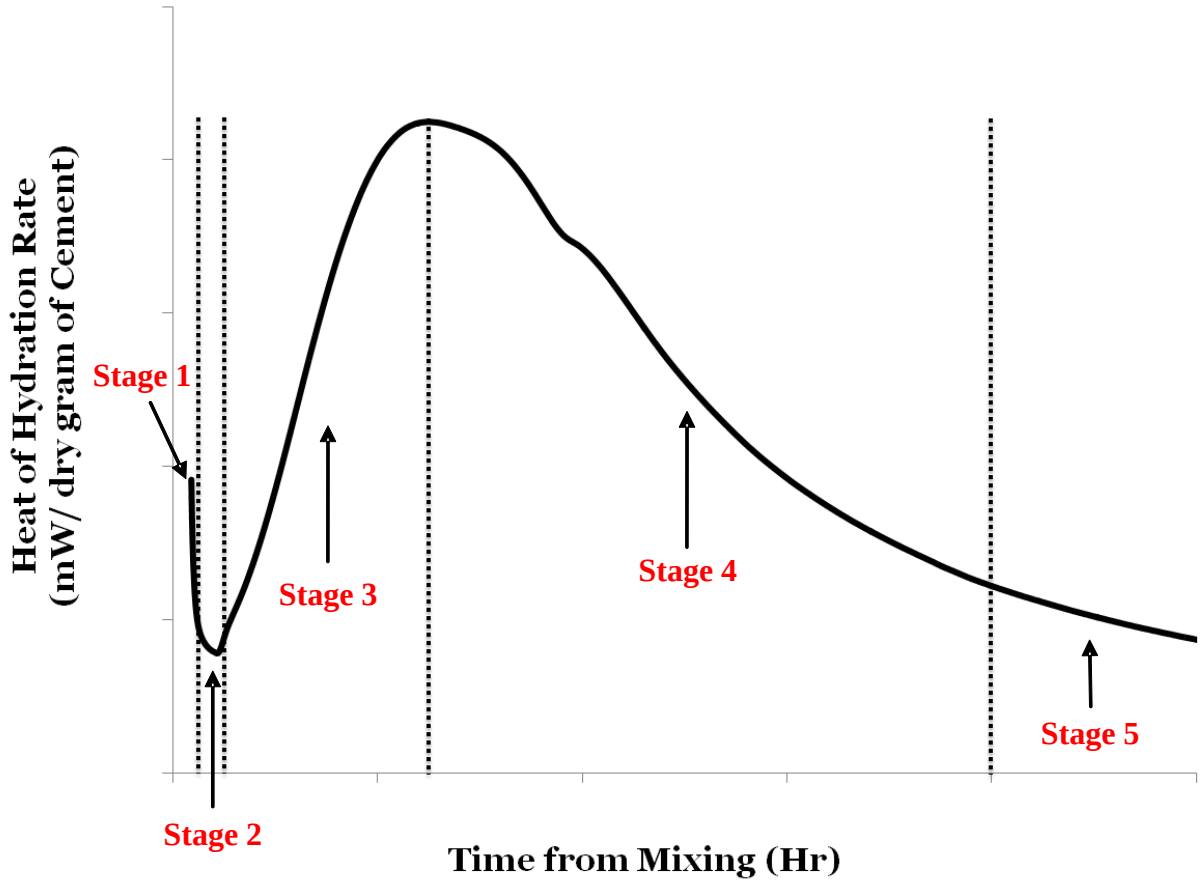

Figure 2.1 Hydration heat curve of portland cement paste

During the induction period, the cement dissolution is greatly slowed, reducing the reaction rate. This very slow reaction period allows for concrete transportation, placement, and finishing [17]. Many theories have been proposed with consequent studies performed to investigate the mechanisms for the ending of the induction period. One of the first hypotheses for the end of the induction period is the *Metastable Protective Membrane* theory which was developed by Stein [19,20]. This theory assumes that a rapid formation of hydration products from C_3S hydration creates a thin layer of C-S-H, named C-S-H (m) by Gartner [21], on the surface of the cement grains making it hard to water to reach unhydrated C_3S and continue hydration. This limits ion diffusion from the surface of unreacted C_3S, greatly slowing down

the reaction rate [18]. Another theory explaining the induction period is the *Slow Dissolution Step* theory which was developed by Nonat et al. [22-24]. According to this theory, the induction period begins when there is a steady state between slow dissolution of C_3S and initial nucleation and growth of C-S-H. When concentration of calcium hydroxide (CH) increases, the rate of C_3S dissolution decreases dramatically. Although many aspects of this theory have been studied [25-27], the main problem is the theory cannot well explain the time-dependent dissolution rate of silica concentration at the very beginning of hydration [18]. An alternative hypothesis is the *Double Layer Theory* which states that the induction period is the result of inhibiting further hydration of C_3S by ions released during the initial reaction [20]. Even though this mechanism is well-understood in surface-solution interfaces, Tadros et al. [28] showed that this mechanism needs a required phenomenon called incongruent dissolution, which is not necessarily happens during cement hydration. The *Poisoning Effect theory* is another commonly discussed theory which theorizes that the silicates poison CH crystals and prevent them from growing further [28]. According to this theory, if the supersaturation level of CH is capable of overcoming the poisoning effect, the induction period will end. A positive point of this mechanism is that Young et al. [29] showed that the ending of the induction period needs the calcium concentration in solution is at a maximum. However, other study [30] has cast doubt on this theory by claiming that the beginning of C-S-H formation happens much earlier that CH precipitation. One of the most widely accepted hypothesis for the induction period is *Nucleation and Growth of C-S-H*. Barret and Menetrier [31] and Garrault and Nonat [23] showed that nucleation and growth of C-S-H is the major factor dominating the reaction rate in induction period. This means that the induction period is the result of very slow nucleation and growth of C-S-H. Despite high acceptance of this theory among researchers,

this mechanism is not capable of clarifying the reason for the quick slowdown after the first couple of minutes of hydration [9]. Although there are several theories available that have some evidence as to their validity, the exact mechanisms of the onset of induction period are still unclear.

Following the induction period [17] is the acceleration period (Stage 3). During this stage, the reaction rate increases rapidly. The onset of the acceleration period could be related to thermodynamic or mechanical instability of the protective membrane [16]. Some of the possible reasons by which the acceleration period begins are: ageing and phase transformation destroying C-S-H (m), osmotic pressure, slow consumption of C-S-H (m) layer by more stable form of C-S-H, increase in suppersaturation level of CH in order to cope with poisoning effect, and large, accelerated and heterogeneous of nucleation and growth of C-S-H on C_3S [18,32-35]. This period, which is considered the hardening process [14], continues until the first peak (i.e. C_3S peak) in the hydration rate is reached [17]. The time needed to reach this peak is typically 6 to 12 hours at laboratory temperatures [14].

After the acceleration period, the hydration rate decreases quickly, beginning the deceleration period. Although it was assumed that the deceleration period is mainly dominated by diffusion, Biernacki [36] has showed that diffusion-controlled would not be a likely mechanism for deceleration period. He found that C-S-H has low density at the beginning of Zone 5, reflecting that the deceleration period is the start of moving towards diffusion controlled process [17]. Some of the other plausible reasons for the deceleration period are: reduction in space available to accommodate more hydration products as previously formed products have impinged into each other, reduced water availability for more hydration in the

case of low water-cementitious material ratio (w/cm) concrete, and the remaining unreacted particles are large and react much more slowly because of the low surface-volume ratio [18].

The last stage of cement hydration is transition-diffusion controlled or the steady state period. The steady state period is dominated by a diffusion-controlled mechanism since the surfaces of all reactants are covered by hydration products, silica hardly diffuses through hydration products to dissolve, and water hardly penetrates through hydration products to react with unreacted materials [37]. Bishnoi and Scrivener [38,39] have come up with a new theory, known as two-step volume filling and densification, which explains the shifting from acceleration period to deceleration period and from deceleration period to steady state period. This theory states that in the first step low density C-S-H is formed to fill out the pores and in the second step C-S-H will be densified at a lower reaction rate. Kirby and Biernacki [16] believed that if Bishnoi and Scrivener's theory accurately works increase in released heat should be seen since more space available among particles. However, they showed that almost no changes seen in total released heat even if w/cm varies. Kirby and Biernacki [16] showed that even Bishnoi and Scrivener's theory cannot fully explain the mechanisms behind stages 3, 4, and 5, and should be revised for hydration of calcium silicate-based cement.

In spite of extensive studies on the cement hydration, the exact mechanisms governing some of the changes in reaction rates during hydration are not fully understood. This is an ongoing area of continued work by many researchers, with more theories closer to the reality are expected in the near future.

Factors Affecting Hydration Rate

Hydration rate varies for different cementitious materials, mixture properties, and conditions. Chemical compositions of cementitious materials, w/cm, applied pressure, particle sizes of cementitious materials, and curing temperature can all affect the rate of hydration of cementitious materials [15]. In the case of portland cement, different amounts of C_3S, C_2S, C_3A, and C_4AF result in different hydration heat (Table 2.2). C_3S and C_3A have the highest rate of reaction and produce the greatest amount of heat per unit quantity in the cement [40].

Table 2.2 Amount of heat produced per gram of each phase

Phases	Hydration heat (J/g)
C_3S	500
C_2S	260
C_3A	866
C_4AF	420

Another important factor is w/cm ratio which not only affects the hydration rate, but also influences the degree of hydration (DOH) and strength gain of concrete. Higher w/cm ratios enhance the cement rate of hydration during the acceleration period [41,42]. A study of the impact of applied pressure on cement hydration [43] showed that hydration rate of cement will increase when higher pressure is used. This is a significant factor to consider for oil well cements that are used in the high temperature and pressure conditions found in oil wells. Another study showed that hydrostatic pressure increases the hydration rate and did have a significant influence on hydration product density [44]. Since this study focuses on the effect of curing temperatures and particle sizes on the reaction rate of cementitious systems, the last two contributing factors are more of interest to this study.

Particle size plays an important role in hydration rate. As general rule, smaller particle sizes of cementitious systems and finer cement can increase the rate of hydration [40,45-47]. Finer cementitious materials have higher specific surface providing more available area to water and causing higher hydration rate. Higher surface area of cementitious system has been found to produce thinner hydration product resulting in higher final degree of hydration [15].

Influence of curing temperatures of the reaction rate of cementitious materials can be surveyed from two aspects. First of all, elevated curing temperatures can enhance the rate of hydration [48,49]. However, higher curing temperatures can cause rapid formation of hydration products which means that the hydration gradually shifts to a diffusion-controlled mechanism. This phenomenon makes it hard for water to access unreacted cementitious materials and results in a lower rate of reaction at later ages and lower ultimate hydration degree [15,50]. It should be kept in mind that although most studies have addressed the hydration behavior of the materials below 60°C, there are few experimental studies available on the effect of curing temperatures on isothermal hydration rate of cementitious materials beyond 60°C. [51,52].

Supplementary cementitious Materials (SCM)

Cement production is an energy-intensive process and responsible for 5-8% of global man-made CO_2 emissions [53]. These CO_2 emissions come from calcination of limestone and fuel combustion in the kiln [53]. One of the most effective ways to reduce greenhouse gas emission and consumed energy from the cement industry is to partially substitute cement by other siliceous and aluminosiliceous material, known as Supplementary Cementitious Materials (SCM) [14,53]. Since most SCMs are by-products of different industries, using

SCMs not only reduces CO_2 emission and consumed energy, but also prevents industrial by-products from accumulating in landfills [14,54]. In addition to ecological benefits, using SCM improves fresh and hardened concrete properties. Some SCMs can benefit the fresh concrete by enhancing the workability, delaying setting time which is beneficial in hot weather, and reducing bleeding [55]. SCMs can also improve the properties of hardened concrete containing SCMs through the pozzolanic reaction. The pozzolanic reaction occurs when the CH reacts with amorphous silica of SCMs and water to create more C-S-H gel. A typical form of the pozzolanic reaction can be expressed as Eq. (2.5):

$$Ca(OH)_2 + SiO_2 + H_2O \rightarrow (CaO)(SiO_2)(H_2O) \qquad \text{Eq. (2.5)}$$

The most widely used SCM is fly ash. Fly ash is a byproduct of combustion of pulverized coal in electric power generating plants. Fly ash can increase workability and finishability and decrease required water, air content, and heat of hydration. Slag is another commonly-used SCM which is obtained from blast furnaces for iron production. Slag enhances workability and finishability and lowers required water, and heat of hydration. Silica fume (SF) is a byproduct of silicon metal and the ferrosilicon alloy industry. Although concrete containing SF has a low workability, is difficult to finish, has higher plastic shrinkage propensity, and it shows significantly higher compressive strength compared to concrete containing other types of SCMs. In addition to the aforementioned SCMs, metakaolin and natural pozzolans, which are governed by ASTM C618, have become more popular in recent years [56].

From a mechanical point of view, SCMs can increase the concrete ultimate compressive strength. Many of them however lower the initial strength because they generally react slower than portland cement. From a durability standpoint, some SCMs such as Class F fly ash can

decrease the amount of heat evolved during hydration which can lower the risk of thermal cracking. SCMs can also reduce water permeability and decrease expansion propensity from alkali-silica reaction (ASR) and sulfate attack [55].

Lothenbach et al. [54] have shown that SCMs can improve concrete microstructure through changes in C-S-H composition and changes in the porosity. The changes in the C-S-H composition however depend on the SCM composition. SCMs can change the pore solution chemistry and reduce pH by consuming calcium hydroxide and increase early-age hydration rate of cement by a dilution effect. The dilution effect is a reduction in cement content in the concrete mixture when it is partially replaced by an SCM. Since the water-cementitious material ratio used depends on the total cementitious material ratio, this consequently causes an increase in the effective water-to-cement ratio [6-397]. The influences of SCM particle size, chemical compositions of SCMs, and curing temperatures on SCM reactivity are very important [5,57-59].

One material which has been studied for potential use as an SCM in concrete is waste glass cullet. Since glass cullet is a rich source of homogenous and amorphous silica, it can be used as an ideal model system to investigate the effect of particle sizes, glass types, and curing temperatures on reaction rate, microstructural properties, and mechanical properties of cementitious systems containing finely ground glass cullet.

Glass Cullet in Concrete

Millions of tons of glass cullet are landfilled throughout the world every year. In 2009, approximately 11.7 million tons of landfilled municipal solid waste (MSW) was glass cullet in the United States [60]. However, an increasing tendency for recycling glass has recently

emerged, possibly caused by concerns regarding landfilling of glass, i.e., limited capacity and environmental issues [2]. In 2011, more than three million tons of waste glass were recovered for recycling [61]. When waste glass is collected, different color glass is often intermixed. Mixed color glass cannot be recycled, however, because a mixing of coloring agents results in an unpredictable and uncontrollable color in the new glass [4]. Machines are capable of using optical sensors to efficiently sort large glass pieces by color; however, sorting small glass pieces is not economical and much of this unrecyclable glass cullet is then landfilled. Additionally, waste glass is often concentrated in locations in higher amounts than local demand can sustain for recycling. Consequently, unrecyclable glass is landfilled. For example, nine million tons of non-recyclable waste glass was landfilled in 2009 in the United States [62]. As the economic and environmental consequences of landfilling rise, the incentive to reuse glass cullet has grown. The concrete industry is one of the potential ways of reusing millions of tons of glass cullet per year either as aggregate or SCM [63].

Most research on crushed glass has focused on the use of glass as fine aggregates in concrete. However, alkali-silica reaction (ASR) occurring between alkalis from the cement and the amorphous silica from the glass have restricted the use of glass as aggregate in concrete [61,61,65]. Although Rajabipour et al. [66] have shown that if glass aggregates are crushed into smaller than 0.6 mm the risk of ASR would be minimal and no remedial action would need to be taken, there is much concern over its use as a an aggregate because of the risk of ASR.

Several studies have shown that glass behaves pozzolanically if ground finely enough, with a surface area of more than 300 m^2/kg [7-11,67,68]. Most studies on the effect of glass cullet on cementitious mixtures as an SCM focused on mechanical and durability properties.

Increases in long term compressive strength, flexural strength, resistance to ASR and sulfate attack, and reduction in water sorptivity of concrete containing finely ground glass powder have been found [69,70]. Moreover, some studies showed that finely ground glass powder had comparable or slightly better mechanical properties at later ages than fly ash and slag, but much less than silica fume (SF) [71,72]. Despite all of the aforementioned results, few studies have aimed to connect the microstructural properties of cementitious mixture containing glass powder to performance characteristics of the glass mixtures. Federico [73] performed an extensive study on the influence of glass powder on reaction kinetics and performance properties of cementitious mixtures. According to the results, glass powder smaller than 100 μm can be used up to 10% replacement by mass of cement to attain higher rate of reaction and pozzolanic reaction, and prevent ASR expansion. She also found that agglomeration of finely ground glass could provide an ideal area for ASR to be initiated if it is not dispersed properly. However, the effect of curing temperatures on glass cullet reaction kinetics and performance properties has not been addressed.

Temperature is one of the most pivotal parameters which affect cement or cementitious material hydration. Concrete temperature can change due to weather, heat curing applied, and heat of hydration. Elevated temperatures can increase the rate of hydration and early-age strength gain, change hydration products formed, change density of the formed products, and accelerate activation of pozzolanic activity [68]. However, high temperatures can also lower ultimate strength, increase permeability and drying shrinkage, and in some cases, cause delayed ettringite formation (DEF) [14,74]. Additionally, curing temperature plays an important role in the rate of hydration of SCMs.

One of the other important factors affecting glass cullet reactivity and performance properties of concrete containing glass powder is glass particle size ranges and glass types. Pereira-de-Oliveira et al. performed an experimental study to investigate the effect of narrow particle size ranges and different types of glass powder on compressive strength and ASR expansion of concrete containing glass powder [10]. They showed that 30% green glass with the size range of 45-75 μm can be used as cement replacement without having a concern about ASR. Shao et al. [2] found that replacement of cement by 30% glass powder smaller than 38 μm would enhance glass pozzolanic reaction and minimize the risk of ASR. They also showed that smaller particle sizes result in higher reactivity of glass, higher compressive strength, and lower ASR expansion. Federico [73] showed that mean particle sizes of 16.5 μm and more do not have pozzolanic behavior, while mean sizes of 6.6 μm to 16.5 μm do have pozzolanic reactivity. One of the possible reasons for the obvious discrepancies between the aforementioned results is that the particle used for different size ranges are not uniform. A review of the aforementioned studies showed that the size ranges selected for the studies did not contain uniform particle sizes. For example in the size range of 45-75 μm of Pereira-de-Oliveira et al.'s study [10], a large amount of particles smaller than 45 μm were observed to be present. These smaller particles can have higher reactivity, and therefore the test results cannot be contributed to the 45-75 μm, as they might be (with high probability) affected by smaller particles actions. Thus to investigate the accurate influence of particle sizes and types of glass cullet on hydration rate and performance properties, uniform particle in each narrow ranges is required.

The next topic related to the use of glass powder as an SCM in concrete which has not been extensively addressed is using combined glass types and size ranges in cementitious

systems. Mayer et al. [63] investigated the influences of combined types of waste glass as aggregate in concrete. Tagnit-Hamou and Bengougam [67] have studied the effect of combined finely ground glass as cement replacement on mechanical properties of concrete through field trials. They showed that using 20-30% of waste glass powder as cement replacement can improve workability, increase concrete ultimate strength, and enhance concrete durability by reducing water permeability and making concrete more resistant to chloride intrusion and freeze-thaw damage. Nonetheless, studies are needed to understand the kinetics and microstructure of using mixed glass types and sizes on hydration behavior and performance properties of concrete containing combined glass as SCM.

Background of Microstructural Modeling

Single Particle Model

The Single Particle Model was developed based on growing hydration products in layers on single spherical particles by Kondo and Kodama in 1967 [75]. This model suggested that the first layer of hydration products creates a protective layer, making dissolution harder and ending the induction period. This layer is then consumed and acceleration period begins. Clifton et al. [76] proposed a diffusion-based single particle model for C_3S which has similar fundamentals to the Kondo and Kodama's model [75]; but has stronger mathematical bases. The strong point of this model is its ability to account for the continuous integrity of products layers through the boundaries. In addition to the mathematical models, some single-particle-based empirical models have been developed. Parrot and Killoh [77] performed an X-ray diffraction (XRD) analysis to extract a dissolution model considering cement types and sizes, w/cm, and relative humidity (RH). Tomosawa [78] proposed an empirical model which is

similar to Parro and Killoh's [77], and takes into account the effect of fineness of cement particles and w/cm on cement reaction kinetics. Both of these empirical models are effective with spherical shapes and easy to be executed. However, these empirical models are just valid for the property ranges used to develop the models and need to be calibrated for other materials properties. The major drawbacks of the single particle model are that the models are not able to consider interaction between particles and cannot evaluate total cement reaction kinetic for different size ranges.

Nucleation and Growth Models

C-S-H nucleation and growth are consider and modeled as one process using Nucleation and Growth models, despite they are two different mechanisms. The first type of Nucleation and Growth model is *Early Nucleation and Growth* considering two main cases: site saturation and continuous nucleation [75]. Site saturation happens when nucleation is very quick at the beginning of hydration but suddenly stops. Continuous nucleation occurs when nucleation sites are not fully consumed. The simplest and the most widely used nucleation and growth model is *Johnson and Mehl, Avrami, and Kolmogorov (JMAK)* model typically used for C_3S modeling. This model utilizes mathematical rules to explain hydration products overlapping. The JMAK model however, is not capable of providing physically meaningful parameters, is just valid in isothermal conditions, and is not able to take into account the impact of cement surface area as an important criterion of particle sizes on reaction rate. Regardless of these limitations, many researchers have implemented the JMAK model to study different aspects of cement hydration. The first application of the JMAK model is dated back to 40 years ago when Tenatousse and de Donder [79] used the model to find out that the nucleation and

growth process is not limited to the acceleration period and can be considered as a contributing process during the deceleration period. Models proposed by Brown et al. [80] and Gartner and Gaidis [81] are the other examples of using JMAK model. The model by Brown et al. did not show conclusive results. The model by Gartner and Gaidis tried to cast doubt on spatial nucleation hypothesis in the JMAK model but it was not accepted. One of the other approaches in nucleation and growth modeling is the *Mathematical Boundary Nucleation and Growth (BNG)* model originally developed by Chan in 1956 [82]. This model assumes that C-S-H nucleation occurs merely on arbitrarily oriented and dispersed planar borders. A recent study [83] showed that BNG models can deliver more significant and realistic results compared to the JMAK models. On the other hand, the BNG model is just an estimation which means that the exact boundary condition would not be evaluated and hydration of C_3S is only accounted for. Additionally, the BNG model is developed for a fixed surface area which is not true in real world.

Hydration Simulation Model

It should be noted that this type of models has a significant difference with those mentioned above. The single particle and nucleation and growth models are mathematical models based on scientific theory, whereas simulation models are the visualized applications of those principals. Currently, advances in computer technologies have paved the way for researchers to study complicated hydration of cementitious materials accurately and in more details [75]. The first simulation model was developed by Frohnsdorff et al. [84]. Although this model did not broad application until next 20 years, it could be fairly successful in simulating hydration kinetics and formation of microstructure. The first published simulation

model was in 1986 called the *Jennings and Johnson Microstructure Simulation* model. They developed a 3D platform which utilized an off-Lattice (Vector) approach to simulated cement hydration. Off-Lattice is a method of presenting different shapes using their properties. Cement particles were simulated by spherical particles randomly distributed in the paste cube. Hydration was also simulated through the decrease in radius of reactant particles as hydration progresses, and an increase in thickness of hydration products on the reactants' surface. This proposed simulation model was capable of taking into account many complicated mechanisms such as different particle sizes, overlapping phenomenon, and position and quantity of CH crystals. However, the model had restricted computational abilities making it not broadly advanced and implemented. Another simulation model developed is the *HymoStruc (HYdration, Morphology, and STRUCtural development)* model developed by Van Breugel [85]. This model utilizes a 3D platform for modeling, is traceable from computational point of view, and uses the same principal as Jennings and Johnson's for cement hydration. Though the model had many shortcomings such as the model was able to simulated just one product, did not explain the influence of pore solution, did not calculate overlapping phenomenon, and the reaction rate was a function of particle size only. One of the fairly successful simulation models was *CEMHYD3D Digital Hydration* model developed by Bentz and Garboczi [86]. This model uses a 3D lattice-based platform on digital images. The discrete element approach was implemented in this model. The model operates quickly, and is able to simulate non-spherical cement particles. Additionally, the simulation model incorporates a broad range of phenomena such as hydration heat, porosity, chemical shrinkage, setting time, and the effect of environmental conditions on microstructural development. Not having a physical time scale and thermodynamic information, as well as necessity of calibration of time scale and not being

numerically convergent are of the foremost drawbacks of the CEMHYD3D model. In order to solve some of drawbacks of previous simulation models like restrictions of kinetics, limited implementation of different materials, and deficiency of CEMHYD3D regarding convergence a series of probabilistic rules were used by Bullard [87] to develop a stochastic simulation model known as *HydratiCA Simulation* model. This model is capable of simulating dissolution, nucleation, growth, and diffusion processes, as well as complicated reactions that happen in pore solutions. The two biggest advantages of this model are: the ability of the model to deliver an accurate prediction of hydration kinetics based on chemistry of solutions and temperatures, and user does not need to make any modifications in parameters during simulation. The main drawback of this model is that the model is cumbersome and computationally expensive, as several required inputs are needed to be specified at the beginning of simulation. The last simulation model discussed in this study is the multi-scale finite element-based model, called *DuCom Hydration* model which was developed by University of Tokyo. This semi-empirical model was used to predict structures' durability. This model was a constructional model rather than a microstructural one. The main disadvantages of this model were its dependency on merely empirical relations and using single particle approach to simulate hydration [17].

Although many researches have carried out on microstructural modeling of cement hydration, more work is still needed to obtain an accurate and comprehensive model which is able to evaluate field performance of concrete, address material-related problems, and simulate new cementitious materials.

µic the Model

The principles of the µic (reads mike) were obtained from the approach outlined by Navi and Pignat [88]. µic has been designed in a way that it can be improved as our knowledge of cement progresses. µic is a customizable modeling platform that enables users to model new cementitious materials and reaction algorithm, to extensively develop in the future, to easily interact with a friendly environment, to simulate a wide range of particles sizes as an influential factor in cement hydration, and to use the model in regular computers. µic utilizes a fast and resolution-free approach called "Vector Approach". Vector approach, versus discrete approach, is a widely accepted method using locations and sizes of objects to define objects' geometry and to simulate multi-scale materials like cement. However, since vector approach is expensive from computational aspect some simplifying suppositions have been taken into account like spherical approximation, statistical homogeneity, and reduced particle size distribution. Among these three suppositions, spherical approximation has been executed for µic to make the model faster, as the sphere is the most regular shape and has fastest computation time. Object-oriented programming in Java also has been utilized in µic, as the most effective method for cement hydration to make µic operate faster. This is achieved by storing information in diverse assemblies without noticeable increases in required memory. µic simulates cement grains as spherical particles with determined radius and initial coordination in a virtual computational cube. Cement hydration is then simulated through decrease in radius of reacting particles, and simultaneous formation of hydration products in different layers on available surface of unreacted phases or in porosities. In addition to nucleation and growth of hydration products and by-products, overlapping of hydration products is also included.

Chapter 3 - Experimental Program - Materials

Introduction

This chapter explains the material properties for the cement, glass, aggregates, and water used in this study. It also explains the approach used to obtain glass cullet with very narrow particle size distributions. Additionally, mix proportions of cement paste and mortar samples are presented.

Materials

Cement and Water

An ASTM C150 [89] Type I/II ordinary portland cement (OPC) was used in this study. Table 3.1 shows the cement chemical composition as determined by X-ray fluorescence (XRF) analysis. Potential primary cement components used in this study, calculated by Bogue equations [89] and Rietveld analysis of XRD are summarized in Table 3.2. Distilled water was also used as mixing water for this study.

Table 3.1 Chemical components of cementitious materials

Cementitious Materials	Chemical Components							
	SiO_2 (%)	Al_2O_3 (%)	CaO (%)	Na_2O (%)	K_2O (%)	Cr_2O_3 (%)	Fe_2O_3 (%)	$CaCO_3$ (%)
OPC	19.66	4.71	62.74	0.12	0.56	-	3.26	2.2
Clear Glass	73.50	0.06	9.02	12.65	0.02	0.02	0.28	-
Green Glass	73.10	1.65	10.55	12.34	0.58	0.24	0.44	-

Table 3.2 Potential composition of cement based on Bogue equations and Rietveld analysis

Bogue equations				Rietveld Analysis						
C_3S (%)	C_2S (%)	C_3A (%)	C_4AF (%)	Alite (%)	Belite (%)	Aluminate (%)	Ferrite (%)	Lime (%)	Calcite (%)	Gypsum (%)
58	11	7	10	64.1	14.6	4.36	10.01	0.40	2.54	4.03

Glass Cullet

Three narrow particle size ranges, 63-75 µm, 25-38 µm and smaller than 25 µm, of green and clear glass were used in this study. Clear and green glass was used in this study because clear glass is the most commonly available type of glass, and green glass has the highest pozzolanic reaction [10]. To color the glass, small quantities of doping agents are added as coloring agents in glass production. These coloring agents change the glass composition and structure along with the color. The source of clear glass was waste window glass collected from a recycling company in Kansas City, Kan., and the source of green glass was bottle glass from the same bottle manufacturer and bottle type collected from a recycling center in Manhattan, Kan.. Table 3.1 shows the glass cullet chemical composition obtained by XRF analysis. Table 3.3 shows the density and Blaine surface area of cement and glass particles.

Table 3.3 Density and Blaine surface area of cementitious materials

Materials	**Density (Kg/m^3)**	**Blaine Surface Area (m^2/Kg)**
Type I/II portland cement	3,150	395
Clear Glass 63-75 µm	2,477	53
Clear Glass 25-38 µm	2,483	126
Clear Glass < 25 µm	2,483	433
Green Glass 63-75 µm	2,501	53
Green Glass 25-38 µm	2,501	126
Green Glass < 25 µm	2,501	476

To obtain the desired size ranges, 63 to 75 µm, 25 to 38 µm, and smaller than 25 µm, six steps were followed. These steps include: washing, crushing, milling, dry sieving, wet sieving, and sedimentation. The glass was washed and dried before crushing to remove any surface residues. After crushing to smaller than 1.18 mm (No. 16 sieve), glass particles were milled in a laboratory ball mill. The next step was wet and dry sieving, which was the most

important step for providing glass powder in different size ranges. Dry sieving was performed only for the large particle size (63 to 75 µm) because for finer size ranges, the screen openings would clog. After dry sieving, the glass was wet-sieved with isopropanol using sieves with 63 µm, 38 µm, and 25 µm openings. The final step was to use sedimentation with the 63 to 75 µm and 25 to 38 µm glass particles obtained from wet sieving. This step, which is based on Stokes' Law, was used to remove all finer-than-desired particles. Thirty to 50 grams of glass powder was poured in 200 mL of isoproponal. The mixture was then completely stirred so that the glass particles were suspended. After a couple of seconds, a visible layer of coarser sized particles would settle down to the bottom of the container. At that time, the alcohol containing fine glass powder was taken out by pipette. Repetition of the sedimentation step depended on the uniformity and amount of finer particles in the final powder. Table 3.4 summarizes the processing steps used to prepare the narrow particle size range glass powders used in this study.

Table 3.4 Sieving strategy for collection of glass powder with different size ranges

Size Ranges	Dry Sieving	Wet Sieving	No. of Times Sedimentation was Repeated
63 – 75 µm	√	√	2 – 4
25 – 38 µm	–	√	4 – 6
< 25 µm	–	√	–

Glass powder uniformity and amount of finer particles were controlled by a series of quality control measures, including optical microscopy, measurement of the particle size distribution through laser diffraction, and scanning electron microscopy (SEM). Particle sizes distributions of the glass powder and cement particle used are shown in Figure 3.1. The particle size distribution of the finest fraction of glass powder used is similar to the cement particle size distribution. Figure 3.2 shows scanning electron microscope images of the cement and glass particles after preparation. Of particular note in Figure 3.2 is the absence of very fine

particles in 63 to 75 µm or 25 to 38 µm size glass powders that normally adhere to the larger particles. In addition to individual glass particles, four combinations of glass types and size ranges were used for this study. Table 3.5 summarizes the quantities and combinations of glass used in the four mixtures.

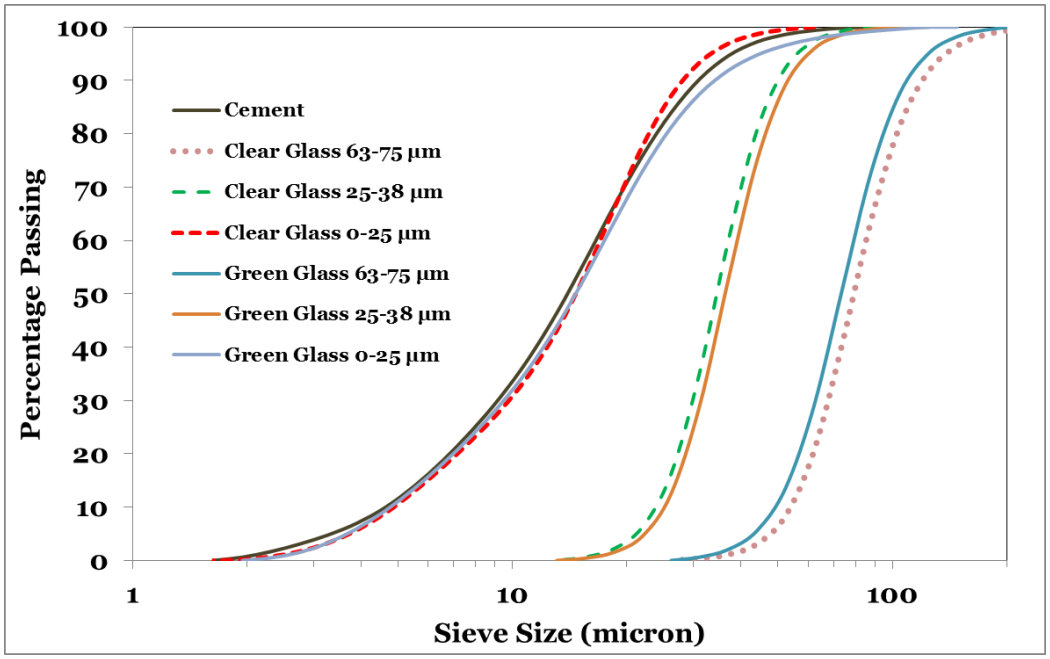

Figure 3.1 Gradation of cementitious materials

The main reason of using the multistage process for collecting glass cullet was to obtain uniform particle size in a desired range to study the effect of particle size on performance and mechanical properties of cementitious system. To collect glass cullet as an SCM in commercial scale, large ball mill and crushing operations are used followed by air classification to control powder fineness.

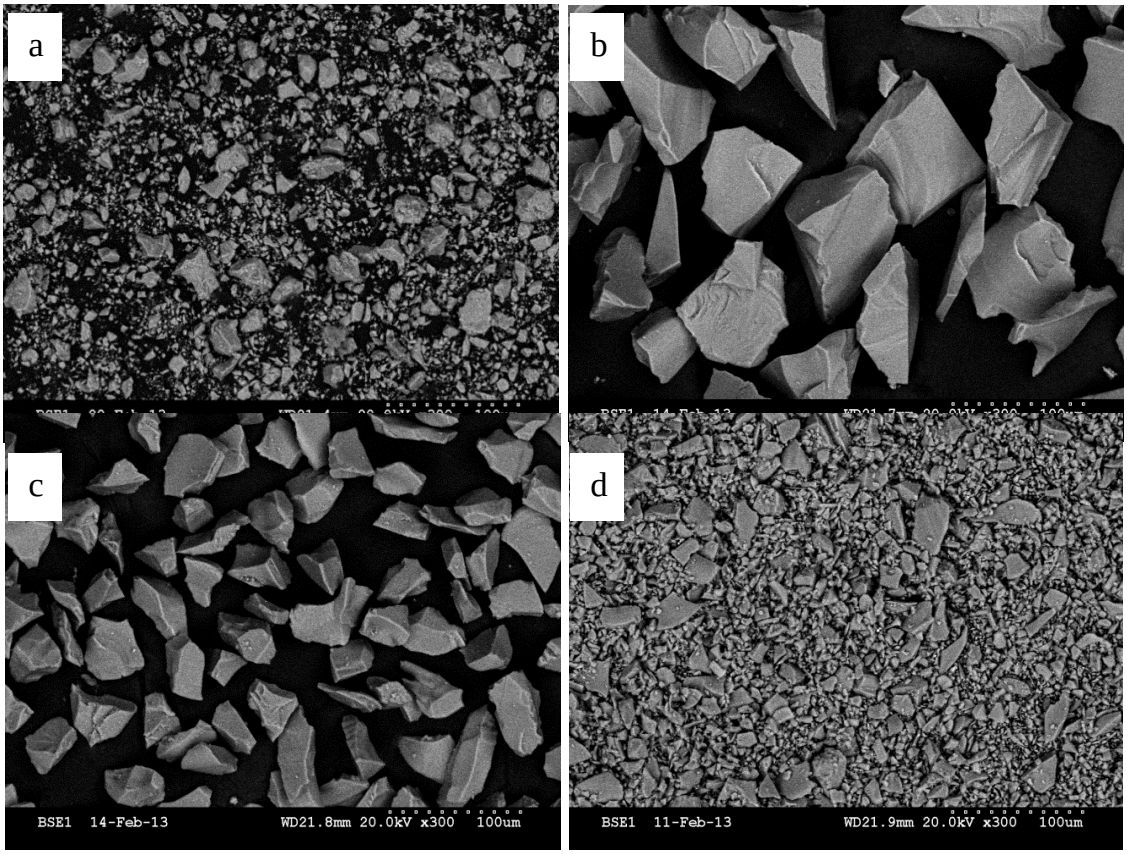

Figure 3.2 SEM Images of: a. Cement grains, b. Green glass 63-75 µm, c. Green glass 25-38 µm, d. Green glass < 25 µm

Table 3.5 Density and Blaine surface area of cementitious materials

Mix #	Constituents	Density (Kg/m^3)	Blaine Surface Area (m^2/Kg)
Mix 1	Green 63-75 µm + Green < 25 µm	2,501	264.5
Mix 2	Green < 25 µm + Clear < 25 µm	2,492	454.5
Mix 3	Clear 63-75 µm + Clear < 25 µm	2,480	243
Mix 4	Green 63-75 µm + Clear < 25 µm	2,489	53

Cement Paste

Cement paste samples were made with a water-cementitious materials ratio (w/cm) of 0.35, using a 25% replacement by mass of portland cement with individual clear or green glass powder as well as combined types and sizes of glass cullet, as recommended by other studies [67].

Cement Mortar

All mortar mixtures used in this study were made with a w/cm of 0.485 and sand-cementitious material of 2.75 specified by ASTM C109 [90]. Standard graded silica sand was used. The w/cm of mortar samples is different from that for the paste samples because of bleeding issues found in paste samples at high w/cm ratio and workability problems in mortar samples with lower w/cm.

Chapter 4 - Experimental Program - Methodology

Introduction

In this chapter, preparation procedure and curing conditions of cement paste and mortar samples are explained. Test methods used to measure reaction rate and pozzolanic reactivity glass powder, quantify cement and glass cullet degree of hydration, and correlate performance properties and mechanical properties of cementitious mixture containing glass cullet are discussed as well.

Sample Preparation

Paste Samples

All paste raw materials were preconditioned at target temperatures (10°C, 23°C, and 50°C) before mixing. Water and cementitious materials were stirred at slow speed (500 rpm) for three minutes, followed by two minutes rest, and then high speed (2,000 rpm) for two minutes [91]. After mixing, paste samples for thermogravimetric analysis (TGA), SEM, and XRD were casted in a polystyrene vials with diameter of 17 mm and height of 50 mm. Paste samples with or without the glass powder were wet-cured beginning at six hours after casting at three curing temperatures in a temperature-controlled chamber.

Mortar Samples

All materials and molds were precooled and preheated to 10°C and 50°C, respectively for one day before casting. Mortar samples were made with and without single-particle and combined glass powders using a 25% cement replacement by mass. All mortar specimens were then kept in the mold for 24 hours during which they were maintained in a temperature-controlled chamber at 10°C, 23°C and 50°C. After demolding, mortar samples were cured at

10°C (Control, Clear < 25 µm, and Green < 25 µm), 23°C (all samples), and 50°C (all samples).

Bottle Leaching of Glass Cullet

Bottle leaching experiments were carried out to measure the concentration of aluminum and silica ions that leach out into alkaline solutions at different pH values at 23°C and 50°C. In the bottle leaching experiments, five grams of glass powder was mixed into 50 grams of potassium hydroxide (KOH) solution with pH varying from 12 to 14.5. This variation in pH of KOH solution was obtained by adding different amounts of KOH to ultrapure water until the target pH was obtained. The solution was rotated at 30±1 rpm for 24 hours and filtered. Inductively Coupled Plasma (ICP) Spectrometry was used to measure the ion concentration in solution.

Cement Paste Experiments

Isothermal Calorimetry

The hydration rate and total heat of hydration of cementitious system containing single particles and combined-glass cullet were measured using an eight-channel isothermal calorimeter. Approximately 30 g of paste samples were placed in the sample containers, weighed, and placed into the calorimeter. The time between initial contact of water and cementitious materials and placing samples into the calorimeter was less than 15 min in all cases. The influence of glass type and curing temperature on hydration kinetics could be observed as the change in heat of hydration when the calorimetry results were normalized by the mass of dry portland cement used in the paste. This change in heat of hydration is likely from the dilution effect providing additional space for hydration product formation and glass

powder providing nucleation platform for calcium silicate hydrate (C-S-H) and glass hydration [92,93].

The apparent activation energy concept describes the temperature sensitivity of physical and chemical properties of different cementitious mixtures [72]. For cementitious systems where multiple chemical reactions occur simultaneously, the Arrhenius concept does not yield the true activation energy but provides a parameter that represents the temperature sensitivity of the overall reaction rate useful for modeling [94]. Eq. (4.1) shows the mathematical form of the apparent activation energy [95]:

$$K(T) = A\, e^{-Ea/RT} \qquad \text{Eq. (4.1)}$$

Where K(T) is the rate constant, T is absolute temperature, A is proportionality constant, E_a is apparent activation energy of concrete (J/mol), and R is universal gas constant (8.314 J/mol K). The hydration rate can then be presented by Eq. (4.2) [95]:

$$\frac{d\alpha}{dt} = g(\alpha) \times K(T) \qquad \text{Eq. (4.2)}$$

Where α is degree of hydration, and g(α) is the function of the degree of hydration. The apparent activation energy was also calculated based on the Arrhenius plot according to the procedure described by Poole et al. [94]. This method is based on drawing an Arrhenius plot, followed by multiplying the universal gas constant R (8.314 J/mol/K) by the slope of the best line fit to the data. Figure 4.1 shows a typical Arrhenius plot for three curing temperatures.

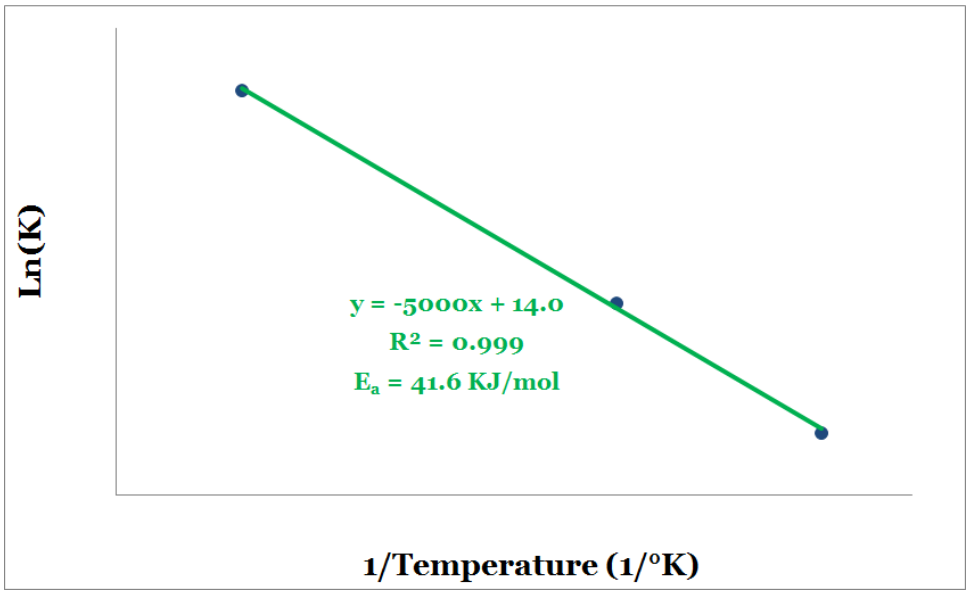

Figure 4.1 Typical Arrhenius plot for three curing temparatures

Chemical Shrinkage

When cementitious material hydrates, the hydration products have less volume than initial reactants (cementitious material and water). This difference in volume is known as chemical shrinkage. Chemical shrinkage, also considered as a complementary method to calorimetry, indirectly measures the reaction rate of the cementitious system long after the hydration heat measurement is below the sensitivity of the isothermal calorimeter. Chemical shrinkage measurements were carried out according to ASTM C1608 [96]. In this method, approximately six grams of cement paste were placed in a plastic vial. Distilled water was carefully added to the top of the paste taking care not to mix the added water with the paste. The sample vials were sealed by a rubber stopper with a graduated pipette placed through the center of the stopper. The pipette was filled with distilled water with a drop of red immiscible oil on top of the water raised through a pipette. Time lapse pictures of the red liquid in the pipette were taken, showing hydration progress and volume change of the cementitious system. Chemical shrinkage was measured through image analysis (IA) taken from the downward

movement of the oil drop at regular intervals. The software for image analysis was developed by Bishnoi [97].

Thermogravimetric Analysis (TGA)

To study the pozzolanic reactivity of glass powder, the calcium hydroxide (CH) content of cement paste samples was measured by the thermogravimetric analysis (TGA) using the approach outlined by Marsh [98]. Paste samples with or without the single particle and combined glass powder were wet-cured starting at six hours after casting at three curing temperatures. At 1, 7, 28, and 91 days after casting, hydration was stopped by solvent exchange with isopropanol. Paste samples were cut from the 17-mm diameter samples into 2 mm thick discs and placed in isopropanol for seven days. The samples were then dried in a vacuum for at least four days. To minimize the risk of carbonation during casting, drying, and testing, high level of care was taken. Finally, 30-50 mg of dried paste samples were ground and heated at a rate of 20°C/min to 1,000°C in nitrogen atmosphere.

Scanning Electron Microscopy (SEM)

Analysis of images captured by scanning electron microscope (SEM) in backscattered electron (BSE) mode of cut, epoxy impregnated, and polished paste samples was used to directly quantify glass cullet degree of hydration at a given curing age and curing temperatures. This was achieved by detecting glass in images, measuring glass pixel percentage of image, dividing the glass area percentage by the initial percentage of glass volume of the total material volume, and finally subtracting the quotient from one. In backscattered mode (BS) of SEM, image brightness is a function of the material average atomic number and can be used to differentiate between different phases in the image [38], and to calculate the relative density

of C-S-H as a criterion of the effect of curing temperature on reaction product [17] using the method outlined by Zhang [99]. SEM analysis was performed on paste samples containing single particles of Clear smaller than 25 µm, Clear 63-75 µm, Green smaller than 25 µm, and Green 63-75 µm as well as two series of combined-glass mixtures, i.e. Mix 2 and Mix 4.

X-Ray Diffraction Analysis (XRD)

Quantitative X-ray diffraction (QXRD)/Rietveld analysis was used to quantify crystalline phases in and perform hydration analysis of cementitious system. The hydrated cementitious samples were scanned using a Rigaku MiniFlex II Desktop X-ray diffractometer from 5 – 70° 2θ (CuKα) with increments of 0.02° over a 6 second step-time. The samples used for QXRD were obtained through the method already explained in the TGA section. A small piece of dried paste sample was ground and homogenously mixed with Rutile (TiO_2) as internal standard in the mass ratio of 10:1. Rutile was selected because the cementitious system contains no rutile. In order to measure cement degree of hydration Rietveld refinement was performed using Topas.

Cement Mortar Samples

Compressive Strength Test

Glass powder pozzolanicity was determined by evaluating compressive strength with time [100]. Compressive strength was measured on 50×50×50 mm mortar cubes at 1, 7, 28, and 91 days after casting in accordance with ASTM C109M [90]. This test, which could be used to correlate performance characteristics of samples containing glass powder to reactivity properties of the glass powders, was done on mortar samples containing individual and combined glass type and size at different curing ages and temperatures. The average

compressive strength results of three mortar cubes was reported as the compressive strength value at each curing age.

Water Sorptivity

Durability of concrete is strongly impacted by mixing water and ion transport properties. A comparison between strength and water sorptivity of mortar provides information in regards to pore connectivity and tortuosity because compressive strength is a function of pore volume [68]. Water sorptivity is also dependent on pore volume but additionally dependent on pore size distribution, connectivity, and tortuosity. Cylinders with 75 mm diameter by 150 mm height were casted for water sorptivity tests. Water sorptivity, originally based on the method developed by Hall [101], was measured using the procedure outlined by ASTM C1585 and modified by Zhang [99,102]. Samples were sawcut at the same ages as compressive strength testing to 30-mm thick for use in a water sorptivity test. After sawcutting, three samples for each age were immersed in isopropanol for seven days to stop hydration by solvent exchange. After immersion in isopropanol, the discs were dried in a vacuum desiccator for an additional seven days. The mortar discs were weighed followed by sealing the sides and top of the sample by plastic sheets and waterproof tape. The samples were reweighed and then left in water so that 2±1 mm of the bottom of the discs (exposed surface) was in contact with water. After removal from the water, the sample bottom was blotted with a paper towel to remove free surface water and weighed in order to measure weight gain of the sample due to water uptake of capillary pores. This process was repeated at 1, 5, 10, 20, 30, 60, 120, 180, 240, 300, and 360 min from the time the sample was placed in the water. The weighing procedure was repeated once a day for eight days.

Chapter 5 - Effect of Curing Temperature and Glass Type on the Pozzolanic Reactivity of Glass Powder

Introduction

This chapter focuses on quantifying the kinetic reactivity of very finely ground glass particles of different types (finer than 25 μm) in concrete as partial cement replacement at different isothermal temperatures, namely 10°C, 23°C, and 50°C with performance measured by strength and sorptivity.

Bottle Leaching

Based on the bottle leaching test (Figure 5.1), green glass has more silica and aluminum ion in solution at higher pH (i.e. more than 12.5), meaning that changes in green glass microstructure, which was caused by adding impurities to give color to glass, as well as breakdown of silica framework by high pH resulted in higher dissolution rate of green glass. Thus, green glass may react faster because aluminum and silica of the green glass are more quickly dissolved in the cement matrix [103].

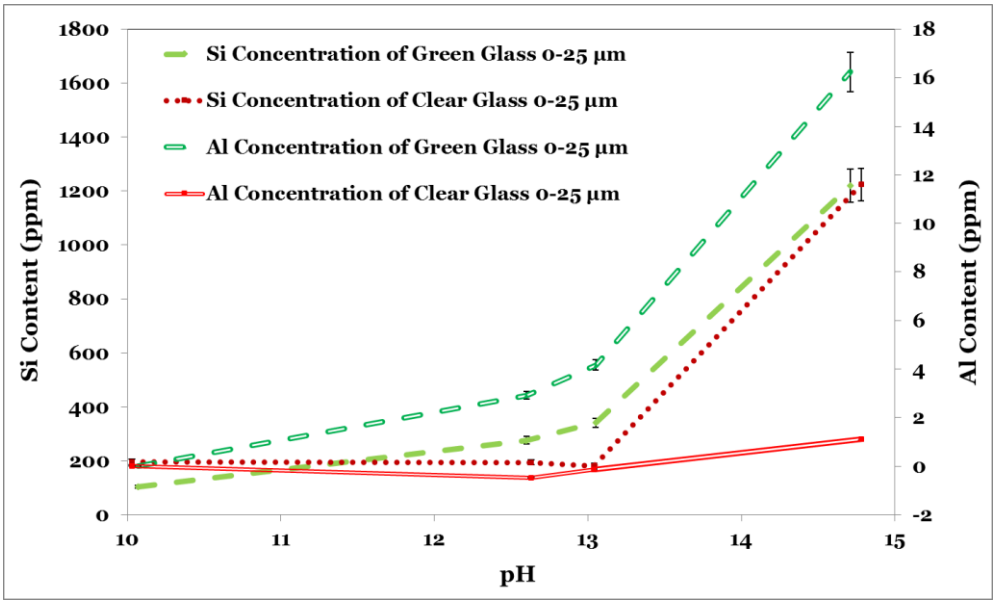

Figure 5.1 Al and Si concentrations at different pH (ICP test)

Isothermal calorimetry

Figure 5.2 shows total heat of hydration for control samples and samples containing clear and green glass of smaller than 25 µm hydrated at 10°C, 23°C, and 50°C. As seen in the figure, the total heat of hydration at 96 hours at 10°C and 23°C is similar for both types of glass, meaning the degree of cement hydration at 96 hours is similar for both clear and green glass samples. At 50°C, green glass showed 10% higher total heat of hydration compared to clear glass, reflecting the higher reactivity of green glass at elevated temperatures. However, glass samples show slightly higher total heat of hydration than control samples at all temperature (i.e. 12%, 13.5%, and 20% at 10°C, 23°C, and 50°C, respectively). At lower temperature, i.e. 10°C and 23°C, the increase in heat of hydration rate of samples containing glass particles is most likely due to the of greater space availability from increased effective w/cm. While at 50°C, the increase in hydration rate is mostly caused by a combination of

higher effective w/cm and glass particle pozzolanic reaction, which was evidenced by the higher reaction rate of green glass compared to clear glass at 50°C.

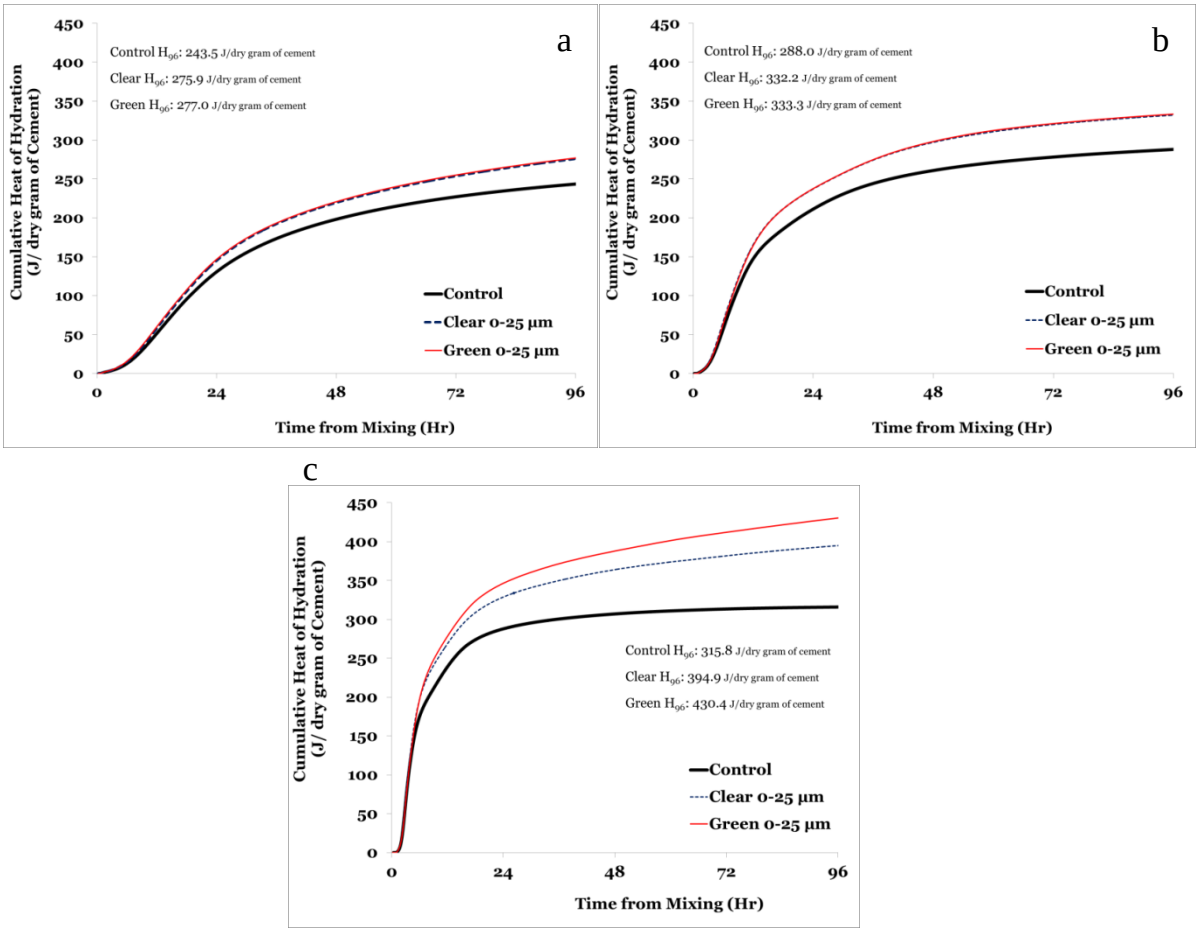

Figure 5.2 Total heat of hydration of paste samples; a. at 10°C, b. at 23°C, c. at 50°C

The Arrhenius plot of control samples and samples containing glass powder is shown in Figure 5.3. While control samples and clear glass samples have similar apparent activation energy (E_a) (i.e. 38.2 and 37.0 KJ/mol, respectively), the green glass sample has slightly higher E_a (i.e. 9% – 12%) than the other two mixtures [94]. This indicates that green glass is more sensitive to temperature and more reactive at elevated temperature than clear glass.

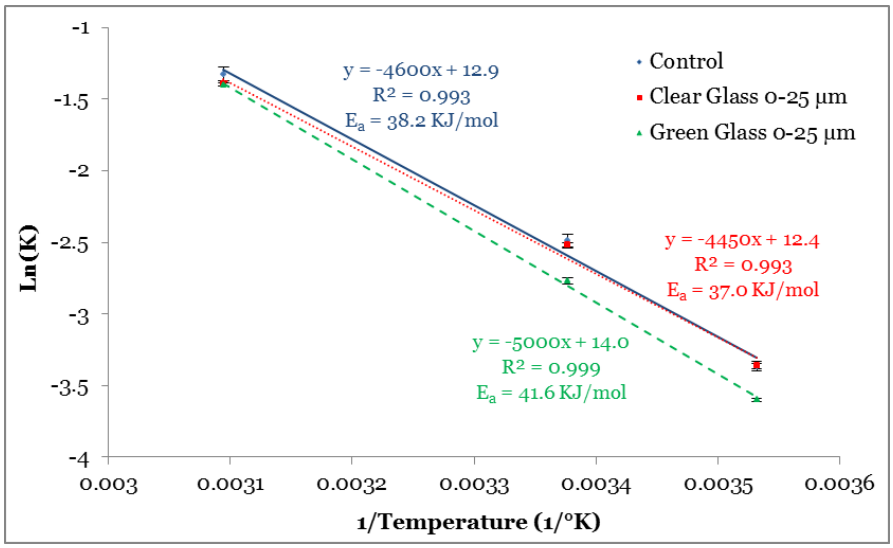

Figure 5.3 Arrhenius plot of cementitious samples

Chemical shrinkage

Figure 5.4 depicts chemical shrinkage results through 28 days of hydration for control samples and samples containing glass powder at 10°C, 23°C, and 50°C. As was seen in heat of hydration measurements, increased temperature greatly increased reaction rate, as measured by chemical shrinkage. Furthermore, pastes made with clear and green glass show different reactivity at all temperatures, unlike the calorimetry results. At 10°C, clear glass sample showed 31% higher chemical shrinkage than control samples at 28 days, while green glass powder showed a 48% increase in reactivity at 28 days compared to the control samples. Increases in reactivity at 50°C compared to 10°C are 14.5%, 46%, and 22.5% for control, clear glass, and green glass samples, respectively. These results not only reveal that green glass is likely more reactive than the clear glass, but the effect of curing temperature could also be taken into account. Higher chemical shrinkage measurements, which show a higher amount of reaction at 50°C, shows the influence of elevated temperature on cement and glass hydration.

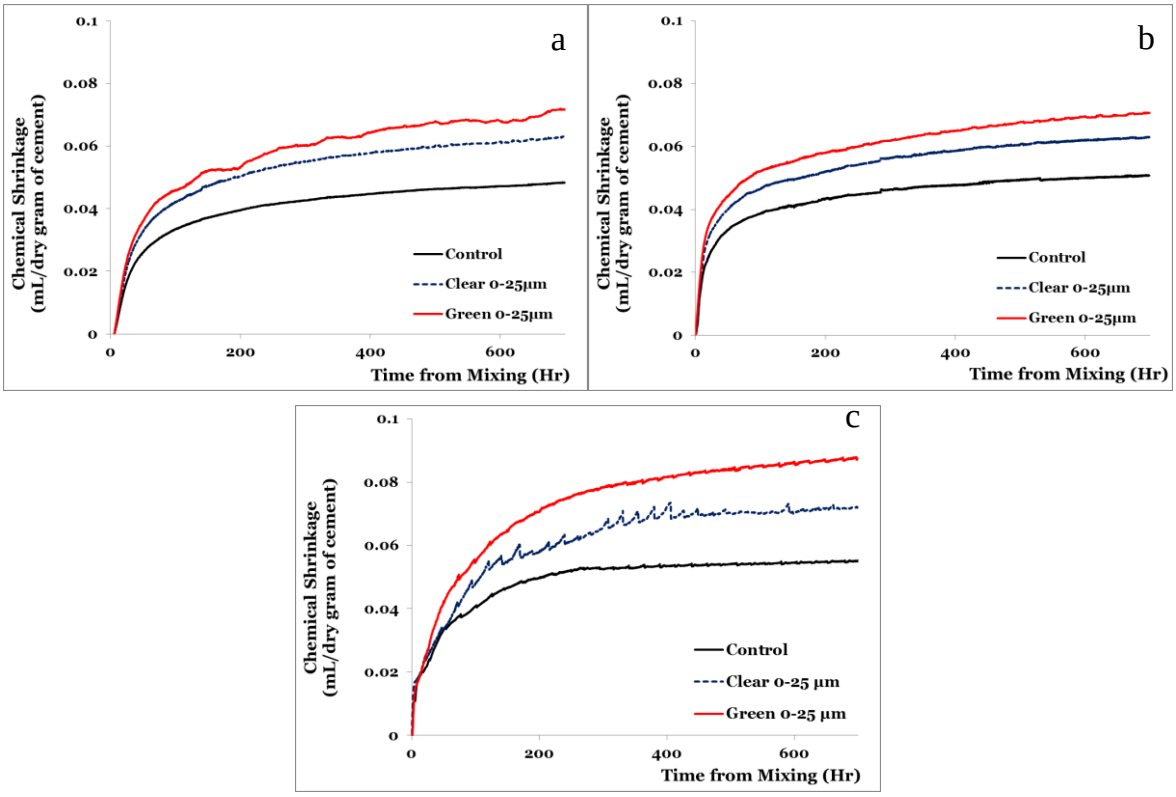

Figure 5.4 Chemical shrinkage of paste samples; a. at 10°C, b. at 23°C, c. at 50°C

Thermogravimetric Analysis (TGA)

To measure CH content mass loss in paste sample at around 400-500°C was used. Figure 5.5 shows TGA curve of 1-day hydrated control paste sample at 50°C. Change in CH content with time and curing temperature in cement paste samples is shown in Figure 5.6. At low temperature (10°C), the decrease in CH seen with time as an indication of the pozzolanic reaction was not seen to be significant. However, at 23°C, samples with green glass powder had about 13%, 18%, and 19% lower CH than control samples at 7, 28, and 91 days, respectively. Glass powder showed significant long-term CH reduction at 50°C: samples with clear and green glass of smaller than 25 µm showed 9% reduction in CH even at one day. At seven days, clear and green glasses showed CH reduction of 13% and 23%, respectively. At 28 and 91 days, clear and green glass samples behaved similarly since both can lower CH

content by approximately 34%, confirming that elevated temperature can accelerate the glass hydration reaction.

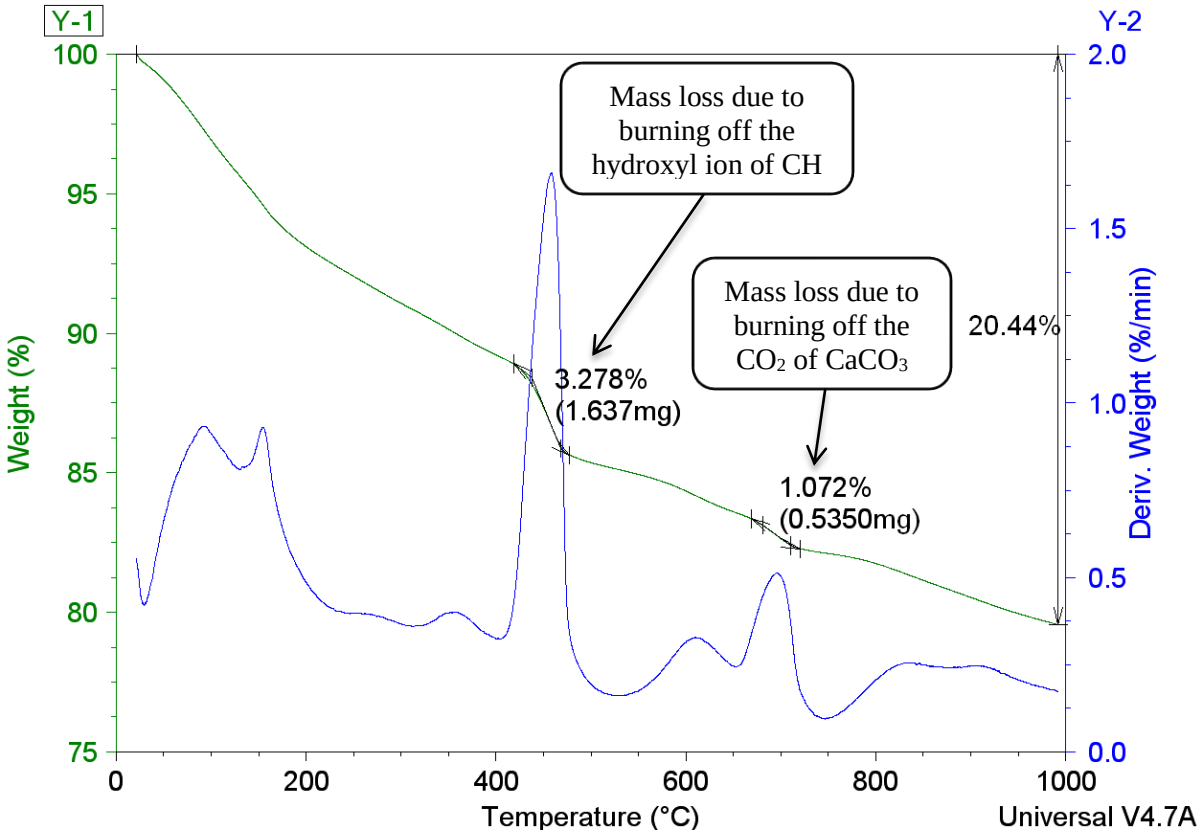

Figure 5.5 TGA curve of 1-day hydrated control paste sample at 50°C

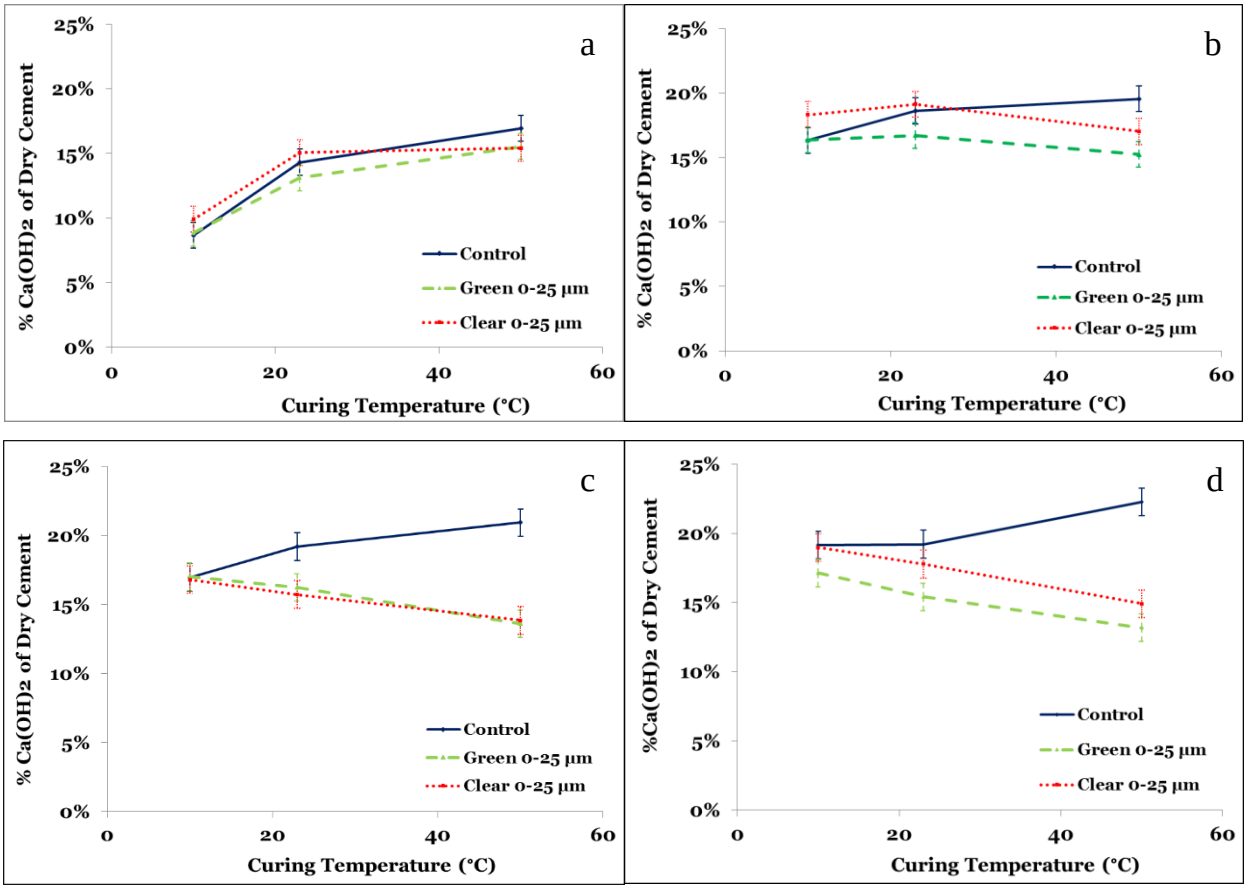

Figure 5.6 CH content of paste samples; a. at 1 day, b. at 7 days, c. at 28 days, d. at 91 days

Another interesting point is that the calcium carbonate ($CaCO_3$) content was lower at lower temperature. The source of calcium carbonate is the limestone added to the cement as a processing addition, which is 2.2% for the cement used for this research. As shown in Figure 5.7, paste samples had lower $CaCO_3$ at 10°C than 23°C and 50°C, possibly because CO_2 from $CaCO_3$ reacts to form calcium monocarboaluminate phases (AF_m) faster at lower temperatures. This faster reaction reduces calcium carbonate concentration and creates additional driving force for $CaCO_3$ dissolution. At 28 and 91 days, calcium carbonate contents were lower in paste samples containing glass powder than control.

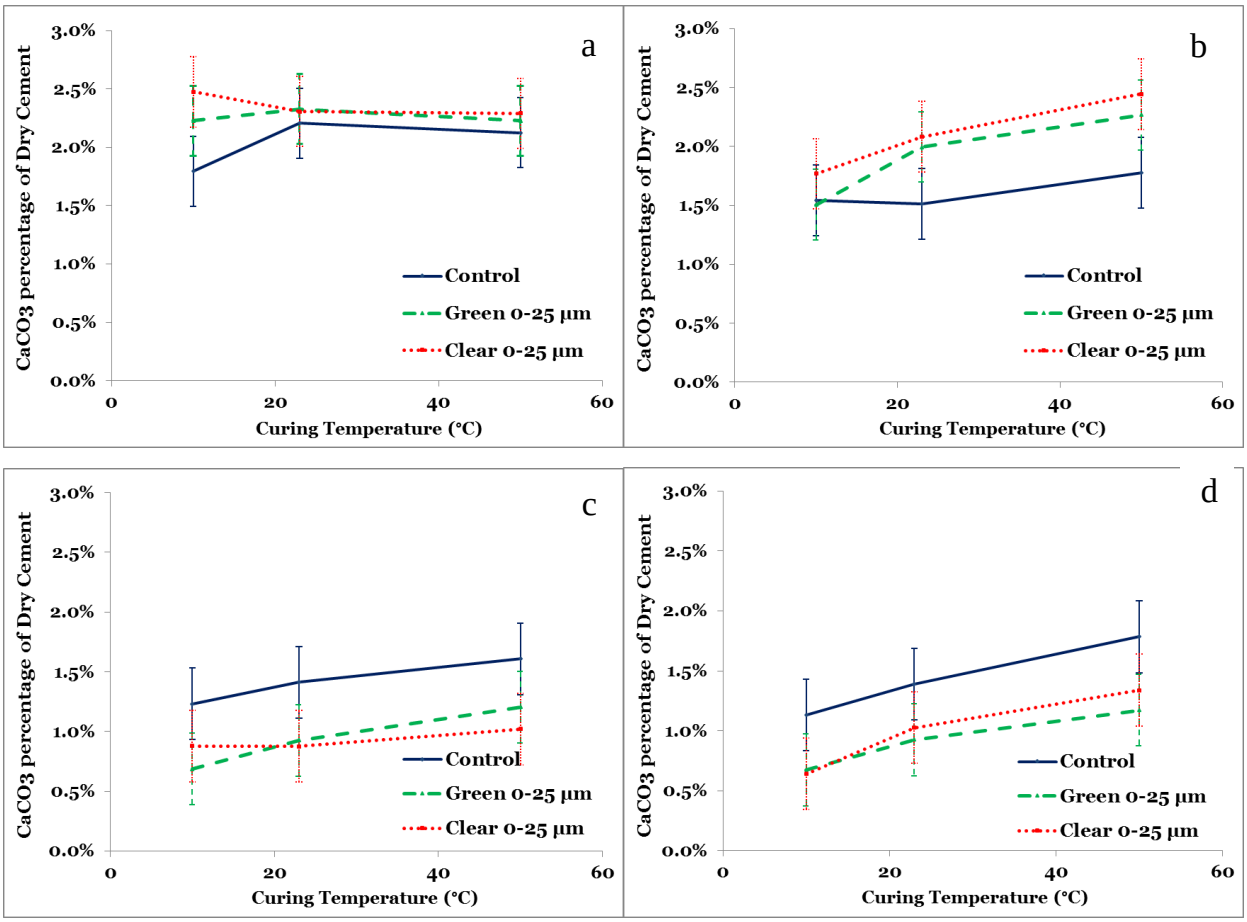

Figure 5.7 Calcium Carbonate content of paste samples; a. at 1 day, b. at 7 days, c. at 28 days, d. at 91 days

Scanning Electron microscope (SEM)

Figure 5.8 shows SEM images of paste sample containing clear glass powder at seven and 180 days. To investigate the effects of glass powder and curing temperature on reactivity, relative density of inner C-S-H around cement grains was calculated. At seven days and 23°C, inner C-S-H relative density around the cement grain in paste samples containing green glass was 2.48, while higher density was noted at seven days and 50°C (inner C-S-H density of 2.50); meaning hydration products are produced more significantly at elevated temperatures. At 180 days and 23°C, the calculated density was 2.51 and at 50°C was 2.54, reflecting that the C-S-H density at initial ages and lower curing temperature is less than later ages and

elevated temperatures as density of C-S-H is increased while time passed and the temperature is increased.

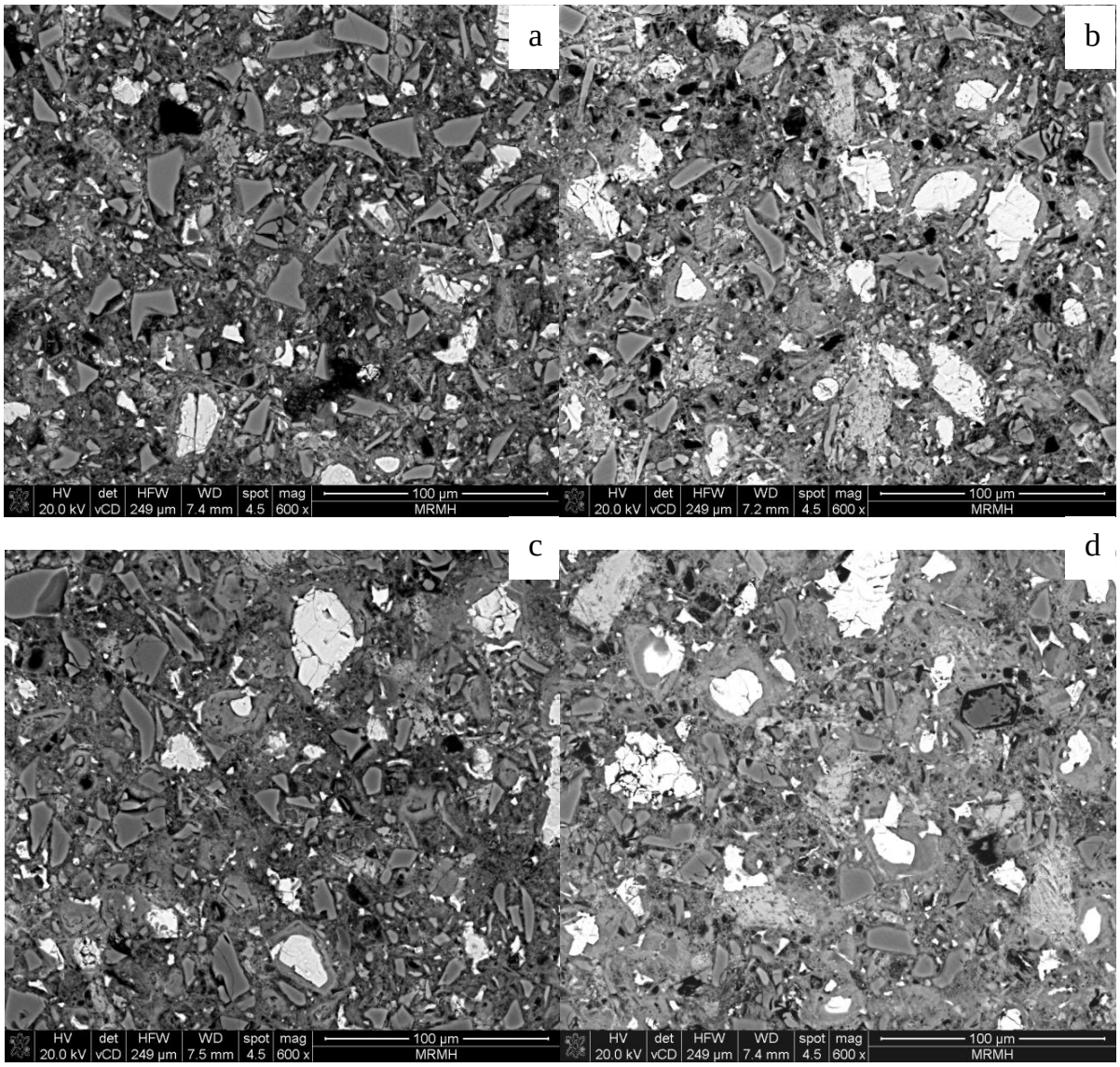

Figure 5.8 SEM Images of paste samples containing clear glass cullet; a. at 23°C at 7 days, b. at 50°C at 7 days, c. at 23°C at 180 days, d. at 50°C at 180 days

X-Ray Diffraction (XRD) – Rietveld Analysis

Figure 5.9 shows XRD pattern for 1-day hydrated cement paste at 50°C. Result of Rietveld analysis on cementitious mixtures at 50°C (Figure 5.10) shows that degrees of hydration of cement are similar for mixtures with and without glass cullet smaller than 25 µm,

especially at 28 days. This finding reflects that higher 28-day chemical shrinkage of mixtures containing clear smaller than 25 µm and green smaller than 25 µm at 50°C might be attributed to glass pozzolanic reaction, which could be verified by the CH content results.

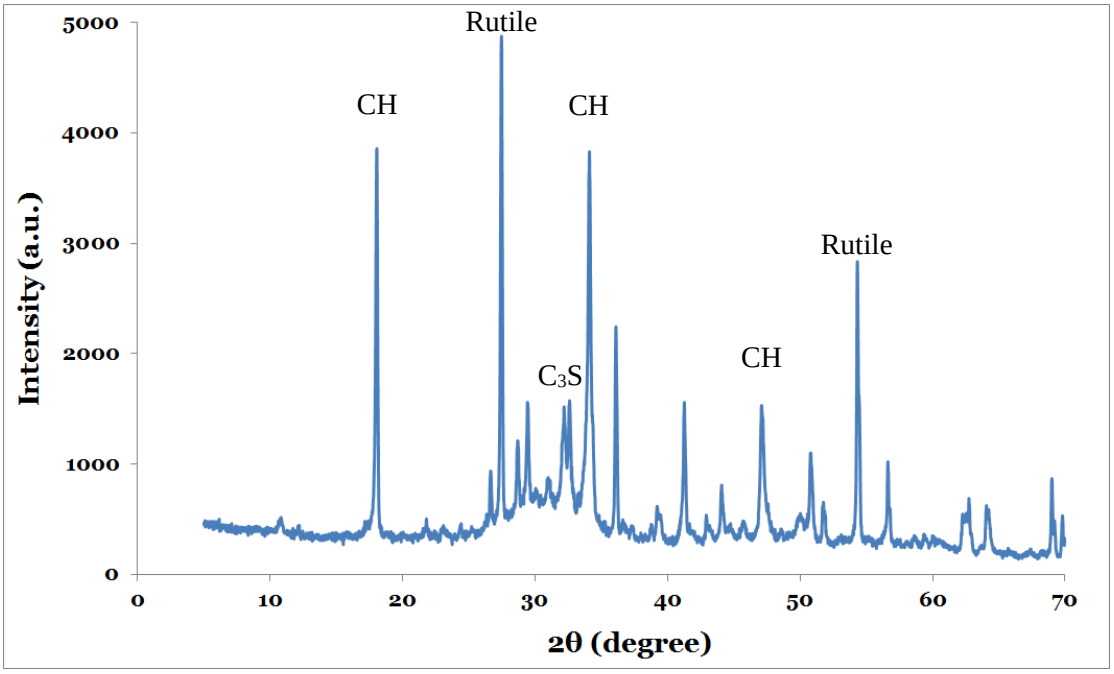

Figure 5.9 XRD pattern for 1-day hydrated cement paste at 50°C

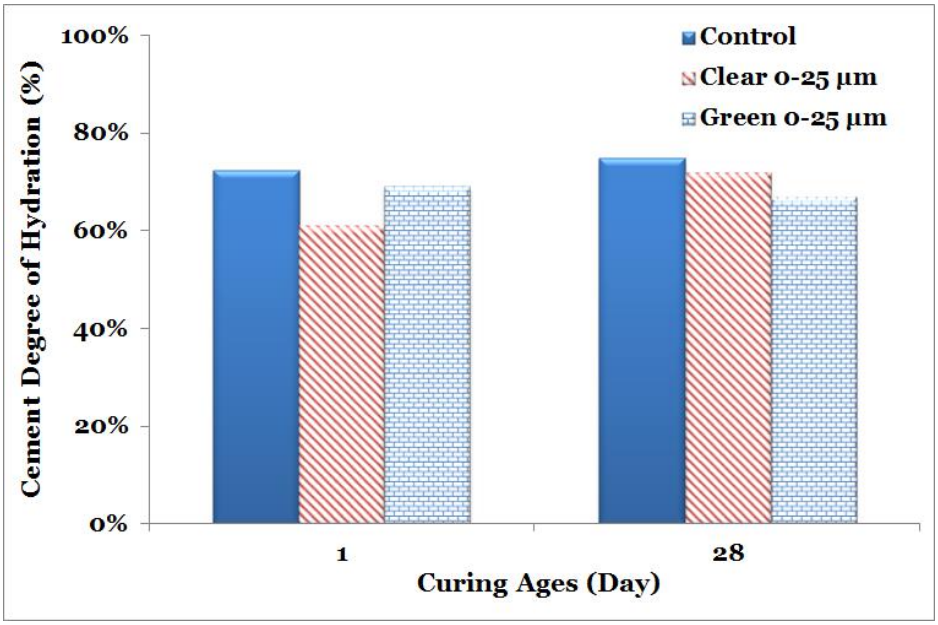

Figure 5.10 Cement degree of hydration of cementitious mixtures at 50°C obtained by Rietveld analysis

Compressive strength

Evolution of compressive strength of mortar samples with and without 25% cement replacement by glass powder is illustrated in Figure 5.11. The control samples were seen to have higher strength than those containing glass powders at all curing ages tested up to 90 days and at 10°C and 23°C. The lower strength of samples containing glass can be attributed to the increase in effective w/c ratio and from the lower glass reaction level at lower temperatures. However, as glass reaction increased at later ages, compressive strength of mortar increased and approached the strength of the control samples. At 50°C and after seven days, control and clear glass samples exhibited lower strength than green glass samples. After 28 days, clear glass showed some pozzolanic reaction, reflected by slightly higher compressive strength than control sample. Results indicate that green glass is significantly more reactive than clear glass because high pH cementitious matrix breaks down the silica structure of the glass and silica and aluminum could dissolve more and participate in the pozzolanic reaction. Higher silica and aluminum dissolution seen in the green glass during the bottle leaching experiment correlate with the higher pozzolanic reaction and lower CH and higher compressive strength. This is likely due to change in the glass structure from the addition of coloring agent. Additionally, the effect of elevated temperature on strength gain is observed in Figure 5.11. At 28 days, neither clear nor green glass powders showed significant pozzolanic reaction at 23°C. Although TGA results showed some pozzolanic reaction at 23°C, that pozzolanic reaction was not enough to overcome a decrease in compressive strength at 28 days caused by the higher effective water-to-cement ratio. However, at 50°C compressive strength increased 30% at 28 days, which was in well agreement with the TGA results.

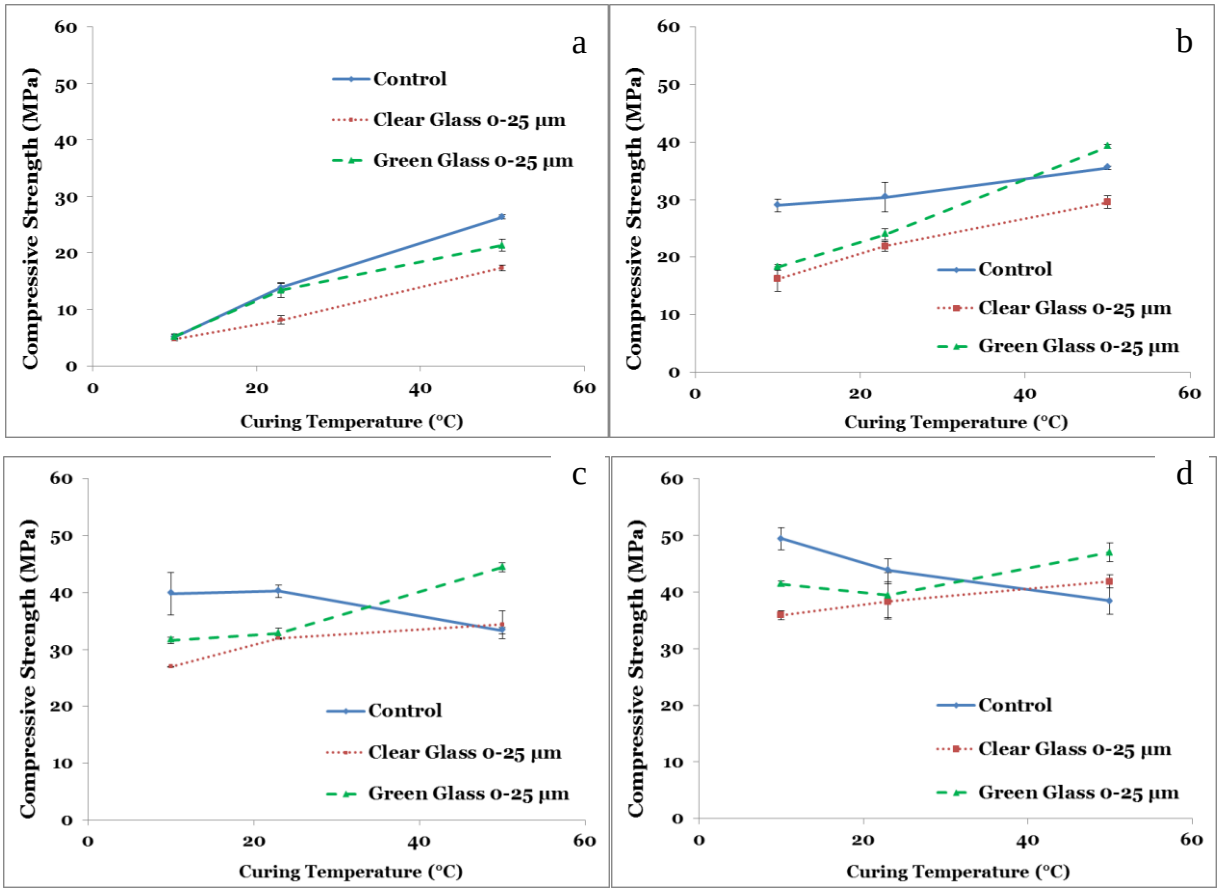

Figure 5.11 Compressive strength of mortar samples; a. at 1 day, b. at 7 days, c. at 28 days, d. at 91 days

Water Sorptivity

Figure 5.12 shows water sorptivity of mortar discs with and without glass powder. All samples had considerable absorption at early ages (i.e., one day), especially at 10°C. At 50°C, water absorption was reduced up to 30% because of accelerated hydration and the creation of more hydration products. This phenomenon indicates that at early ages, elevated temperature decreases concrete porosity by producing denser hydration products, already observed in inner C-S-H relative density results from the SEM images, especially, due to the existence of adequate space to accommodate quickly-formed hydration products. At later ages, water sorptivity of the control sample at 50°C was much higher than that at 10°C (cross-over effect). Although reaction products of control samples are denser at later ages at 50°C, there is more

porosity which is the reason for higher water sorptivity of control samples. On the other hand, glass cullet which reacts slower than the cement is better able to fill in higher porosity from denser cement hydration products at later ages at elevated temperature eliminating the cross-over effect as seen in Figure 5.12. An explanation may be because no additional space for hydration products existed (diffusion controlled stage) and the overall structure was already set. In addition, green glass is able to reduce water absorption to some extent more than clear glass, as green glass has a higher tendency to participate in the pozzolanic reaction.

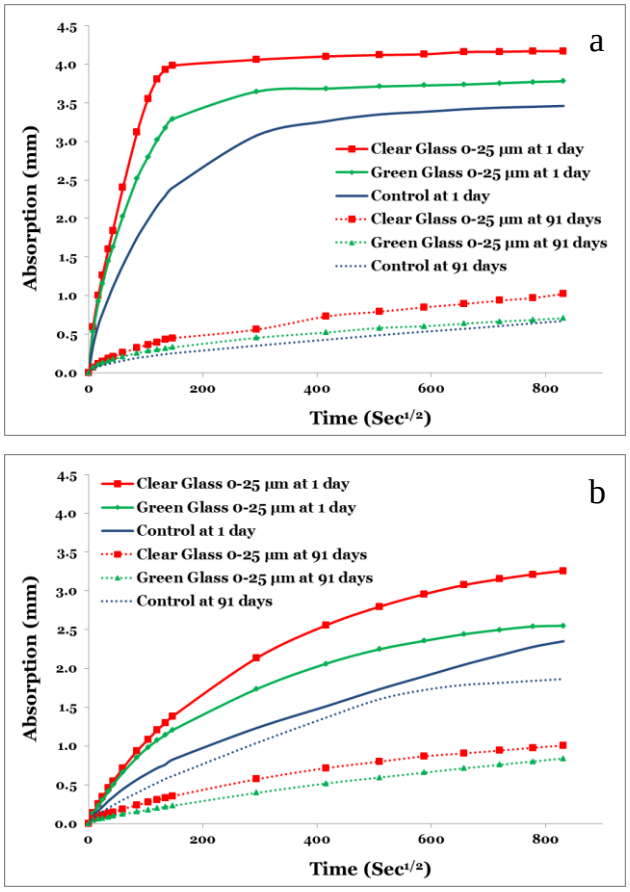

Figure 5.12 Water absorption of mortar samples; a. at 10°C, b. 50°C

Chapter 6 - Influence of Different Particle Sizes on Reactivity of Finely Ground Glass as New Supplementary Cementitious Material (SCM)

Introduction

This chapter investigates the pozzolanic behavior of varying glass size ranges in concrete, with a specific focus on microstructural as well as mechanical properties. The uniform composition of glass particles also makes it an ideal model system for examining the effects of particle size for glassy SCMs in general. The influence of three size ranges of very finely ground glass particles (63 to 75 μm, 25 to 38 μm, and smaller than 25 μm) on reaction kinetics, mechanical and water absorption properties have been studied. In addition, the apparent activation energy concept has been used to describe temperature sensitivity of the three size ranges in order to quantify reaction rate changes while curing temperatures vary [94].

Bottle Leaching

ICP leaching test results showed that smaller than 25 μm had much higher silica and aluminum ion in solution than two other particle sizes at pH greater than 12.5 (Figure 6.1).

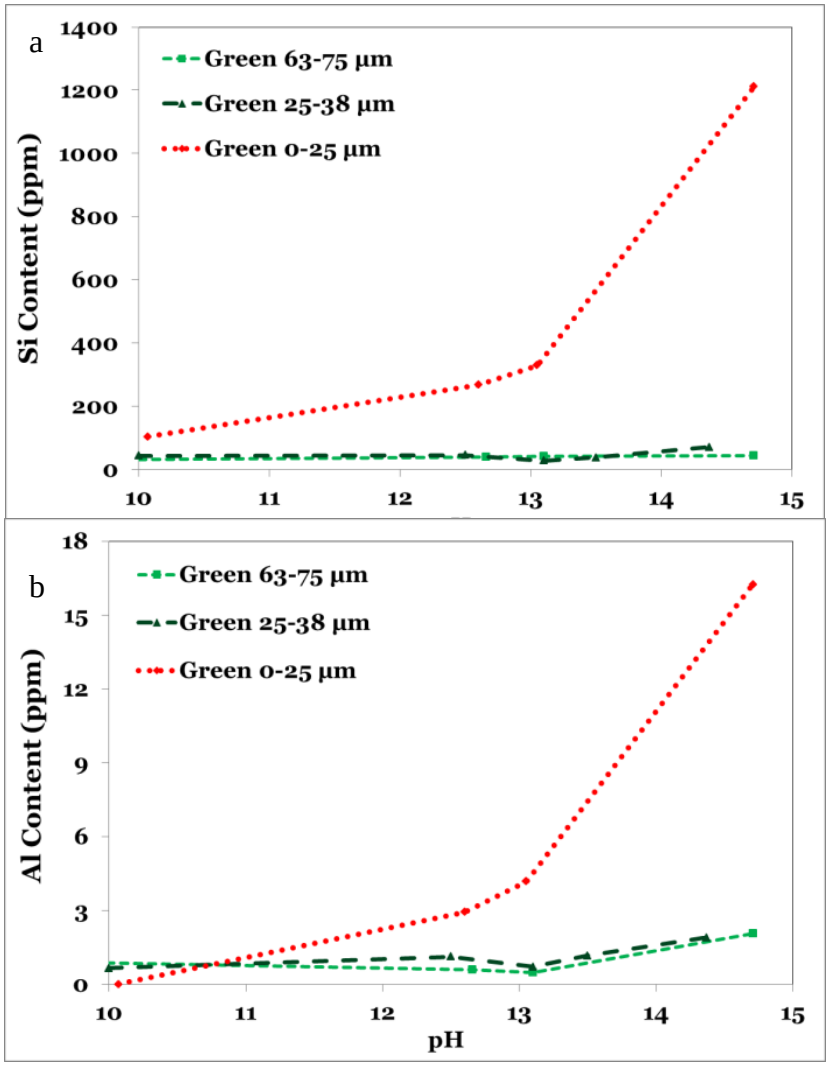

Figure 6.1 ICP test results at different pH: a. Si concentrations, b. Al concentrations

Conversely, 63-75 µm and 25-38 µm had almost identical ion content. These findings revealed that, while reactivity of 63-75 µm and 25-38 µm were similar, smaller than 25 µm was considerably more reactive in order to create more calcium aluminate hydrate (C-A-H) or calcium aluminate silicate hydrate (C-A-S-H) since it can more easily be dissolved in a cement matrix. This can also be attributed to the surface area of the particles, as could be seen in Figure 6.2. This figure shows that the dissolution of silica and aluminum could be linearly affected

by the surface area. Since smaller than 25 µm has significantly higher surface area compared to 63-75 µm and 25-38 µm, it showed higher reactivity.

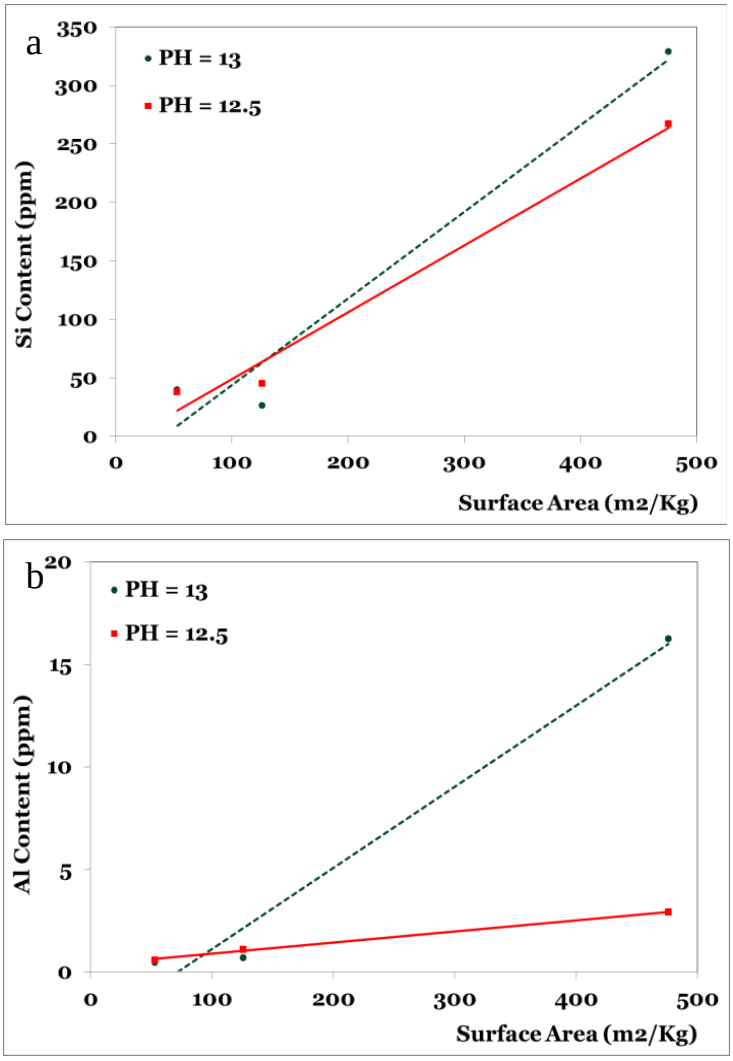

Figure 6.2 Effect of particle surface area on ions dissolution: a. Si concentrations, b. Al concentrations

Isothermal Calorimetry

Total differential heat of hydration between paste samples containing green glass cullet of 63-75 µm, 25-38 µm, and smaller than 25 µm and control samples at three curing temperatures are shown in Figure 6.3. At 10°C and 23°C at 96 hours, the total higher hydration heats of paste samples containing glass samples of 63-75 µm and 25-38 µm were similar. This showed that the larger glass particles had little reaction at that point in time. While smaller

than 25 µm glass samples have slightly higher total heat of hydration than other size ranges at 10°C and 23°C, at 50°C green glass samples showed significantly higher reaction kinetics than the control samples. This higher total hydration heat is caused by increased cement degree of hydration because more space is available due to increased effective water-to-cement ratio with glass particles serving as nucleation sites for C-S-H and glass hydration [92,93].

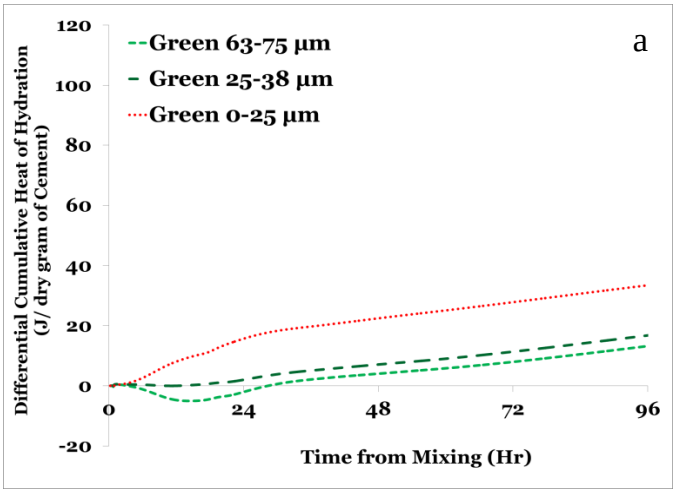

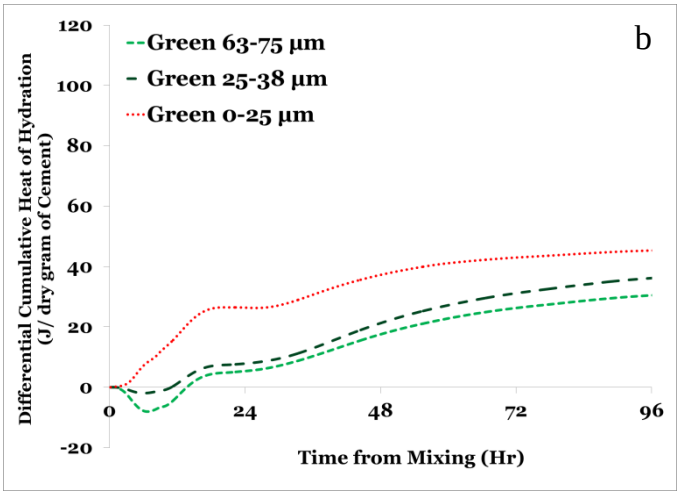

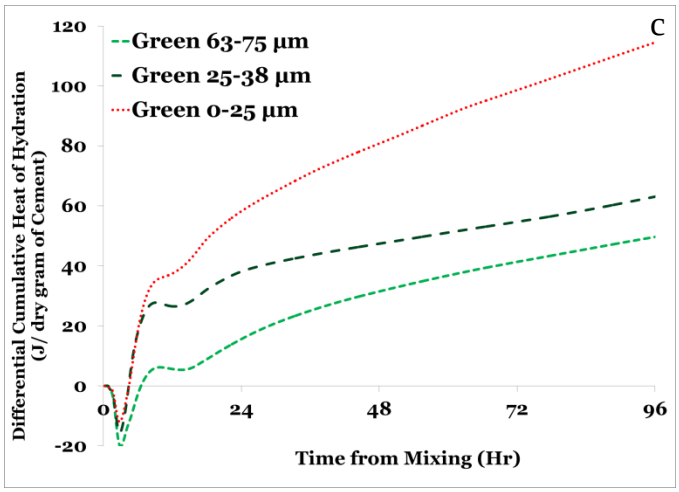

Figure 6.3 Total differential heat of hydration of paste samples: a. at 10°C, b. at 23°C, c. at 50°C

Figure 6.4 shows the Arrhenius plot of control samples and samples containing glass powder, and Table 6.1 lists calculated apparent activation energy (E_a) of control and glass samples. The smaller than 25 µm glass particles had the highest E_a, followed by 25-38 µm and 63-75 µm glass samples.

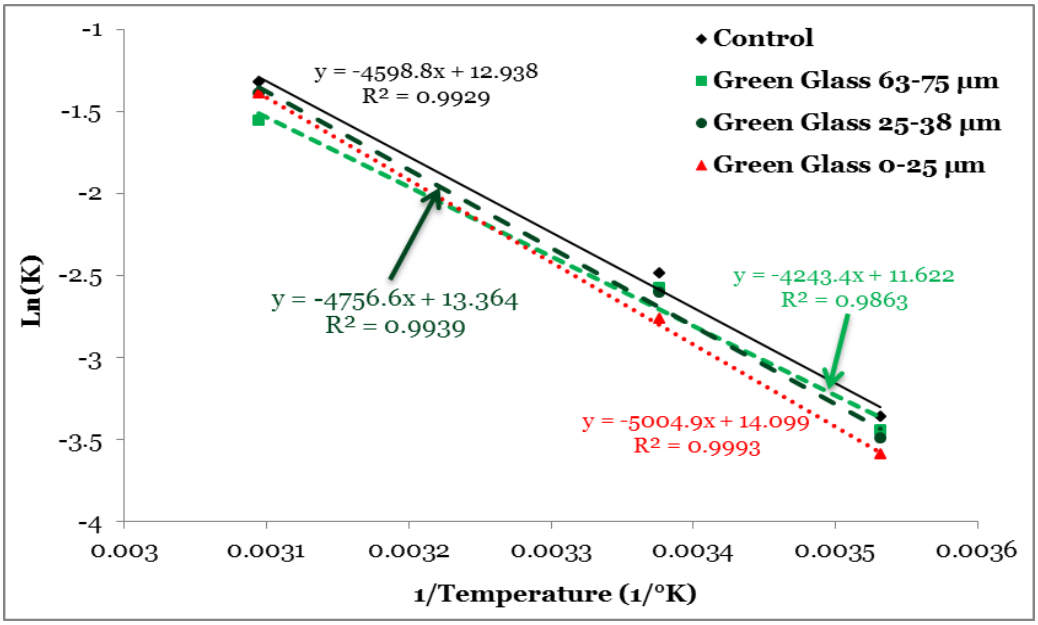

Figure 6.4 Arrhenius plot of cementitious samples

Table 6.1 Activation Energy of Cementitious Samples

Sample	Activation Energy (KJ/mol)
Control	38.2
Green Glass 63-75 µm	35.3
Green Glass 25-38 µm	39.5
Green Glass < 25 µm	41.6

The effect of surface area of glass particles on the differential reaction rate is also shown in Figure 6.5. The interesting point is that the increase in reaction rate could be expressed as a linear function of surface area. The influence of curing temperatures on reaction rate could be investigated as well. The slope of the best-fit line could be used as a criterion for the effect of temperatures. While the best-fit lines had similar slopes at 10°C and 23°C, the slope of the best-fit line is significantly higher reflecting that the elevated temperatures could heighten the reaction kinetics. These results showed that smaller than 25 µm glass sample not only had higher reactivity than control samples and other size ranges, but it was also more sensitive to temperature and had higher reaction rate at elevated temperatures. Additionally, 63-75 µm glass samples showed the least propensity to pozzolanic reaction.

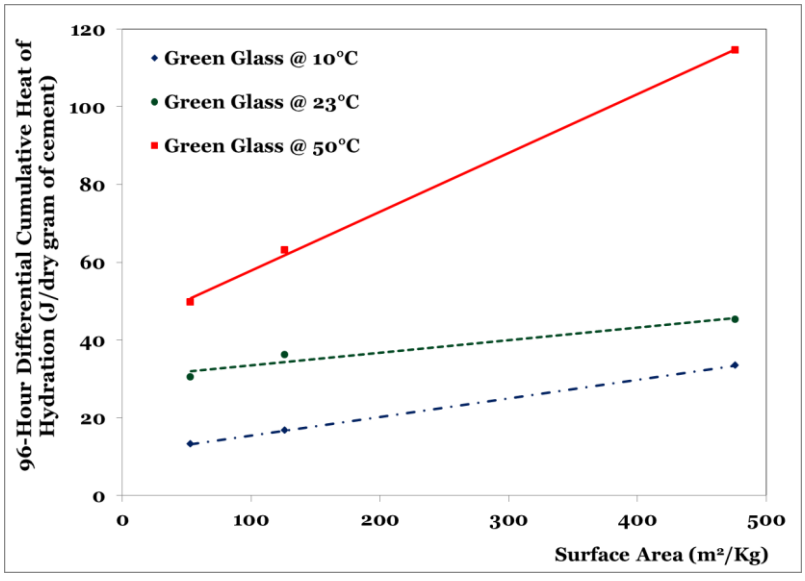

Figure 6.5 Relationship between particles surface area and differential reaction rate

Chemical Shrinkage

Paste chemical shrinkage experimental results for the three curing temperatures are shown in Figure 6.6. At all curing temperatures, paste samples containing glass powder showed increased chemical shrinkage. Among them, smaller than 25 μm samples had higher reactivity, followed by 25-38 μm and 63-75 μm samples. Furthermore, the effect of elevated curing temperature is significant. While chemical shrinkage measurements at 10°C and 23°C were very similar, increase in chemical shrinkage at 50°C was considerable. For example, smaller than 25 μm samples had 21% higher reactivity at 50°C than those at 10°C or/and 23°C. This example showed higher temperature dependency of glass powder as an SCM, evidenced previously by the apparent activation energy calculations.

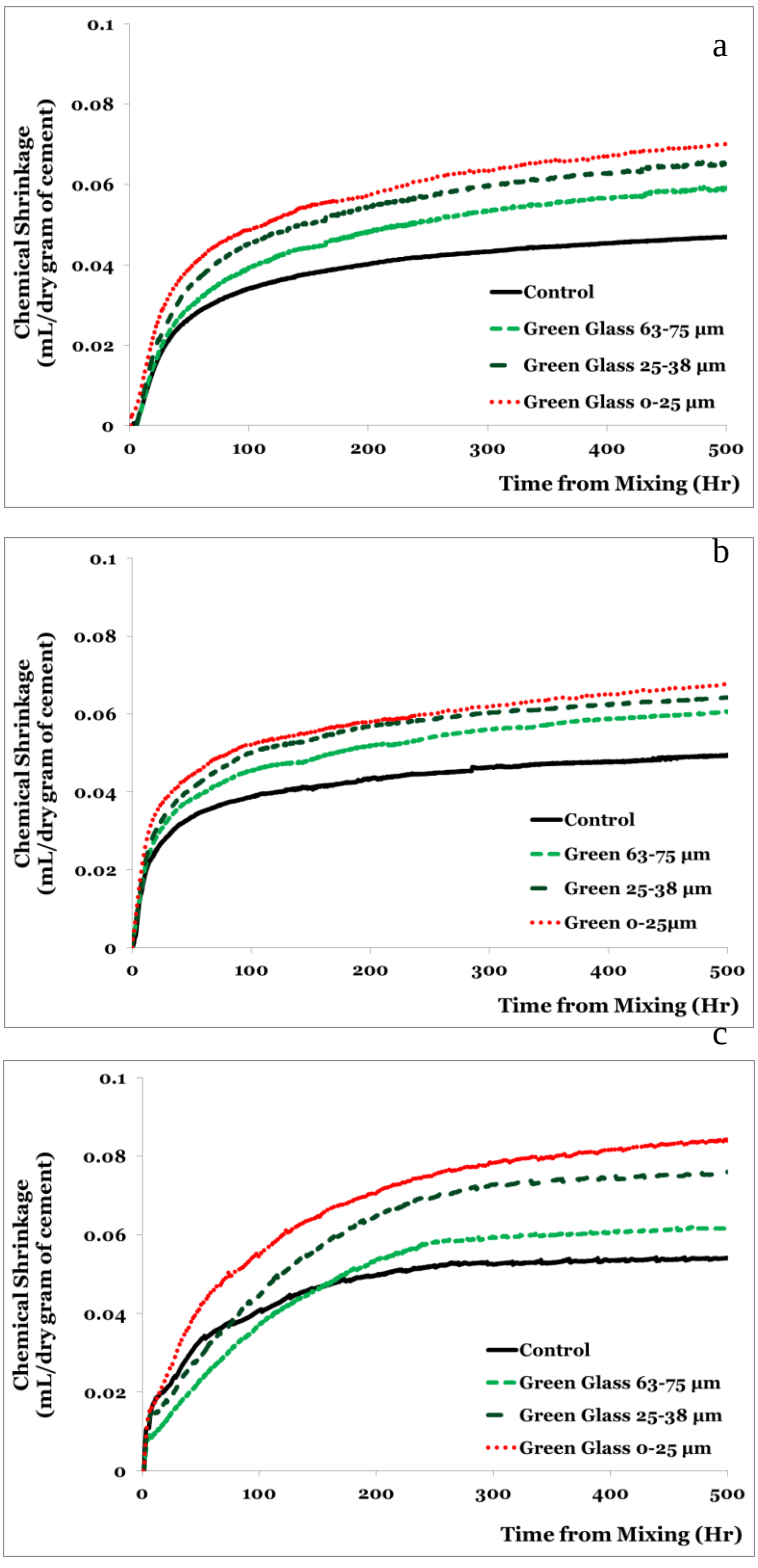

Figure 6.6 Chemical shrinkage of paste samples: a. at 10°C, b. at 23°C, c. at 50°C

Thermogravimetric Analysis (TGA)

Figure 6.7 shows variation of calcium hydroxide (CH or portlandite) content of paste samples containing various size ranges of glass powder versus curing temperature at different ages. The decrease in portlandite content of paste samples containing glass powder compared to the control is a measure of SCM pozzolanicity. Glass samples of 63-75 μm did not show pozzolanic reactivity at 10°C and 23°C until 91 days, while at 50°C, they had 17% and 30% lower portlandite content than the control mixture at 28 and 91 days, respectively. However, samples containing smaller size ranges began to show pozzolanic reaction even at 7 days, especially at 23°C and 50°C. Paste samples with smaller than 25 μm had the highest rate of pozzolanic reaction, because CH content was decreased by 1.5 times more than 25-38 μm and 2.3 times more than 63-75 μm at 50°C at 91 days. The effect of curing temperature on pozzolanic reaction of different size ranges was investigated as well. While CH content of smaller than 25 μm samples at 91 days is 25% lower than 28 days at 23°C, portlandite of smaller than 25 μm samples at 91 days is 30% lower than 28 days at 50°C.

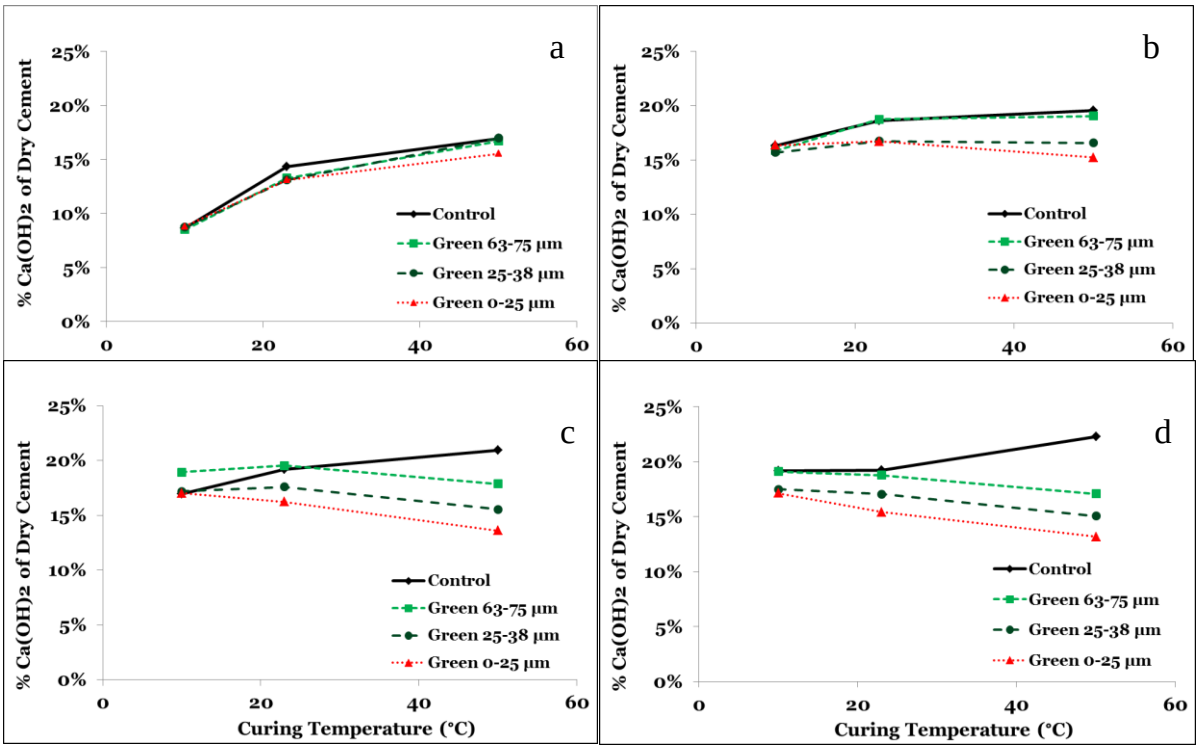

Figure 6.7 Portlandite content of paste samples: a. at 1 day, b. at 7 days, c. at 28 days, d. at 91 days

Figure 6.8 shows the relationship between chemical shrinkage and portlandite content of the paste samples with and without glass particles at three curing temperatures. At all temperatures, the CH content is linearly proportional to the reaction rate. Temperature sensitivity of glass powder could be also investigated from Figure 6.8. While portlandite content had an increasing trend versus increase in reaction rate at 10°C and 23°C, at 50°C calcium hydroxide content decreased as chemical shrinkage increased, showing glass is a temperature sensitive SCM. Additionally among different size distributions, samples containing smaller than 25 µm was the most temperature sensitive particles. This finding is in agreement with calorimetry results since glass samples were temperature sensitive and had higher reaction at elevated temperatures.

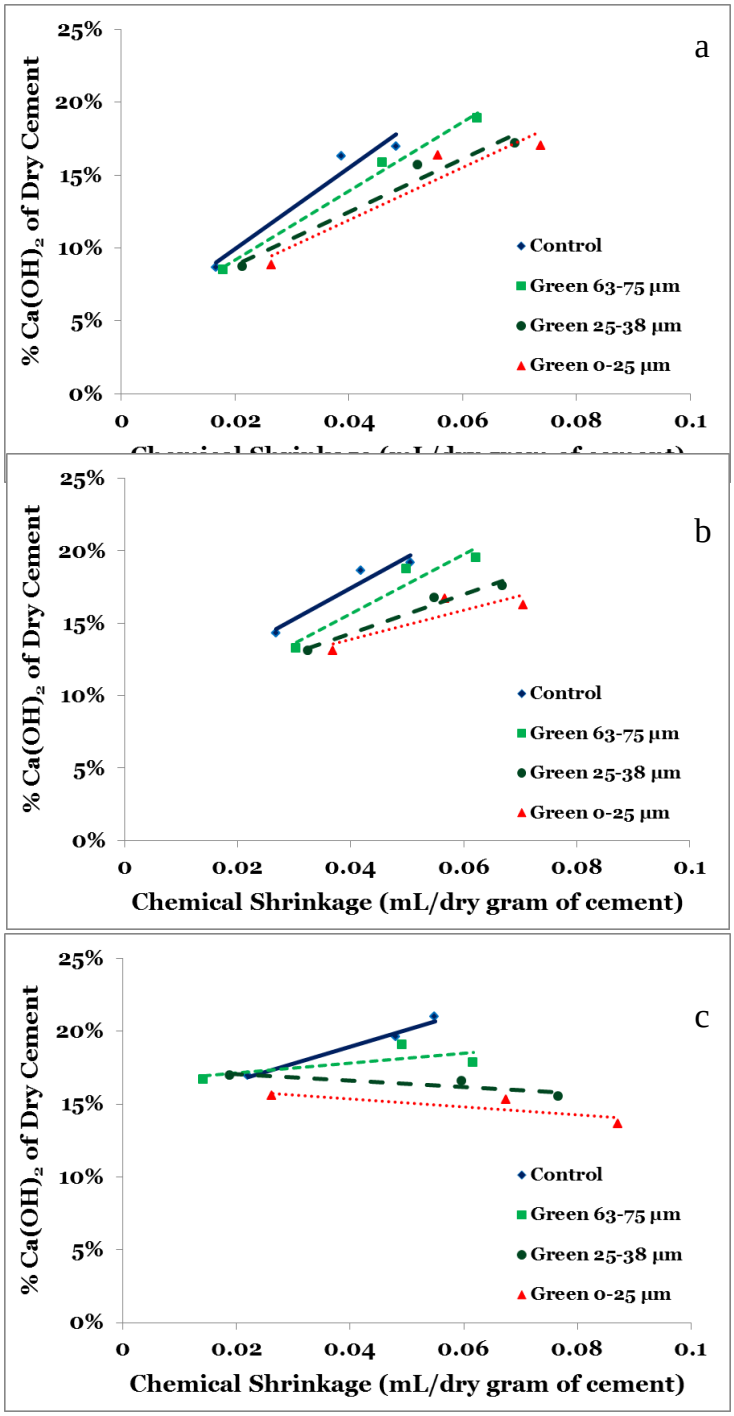

Figure 6.8 Relationship between chemical shrinkage of the paste samples and portlandite content: a. at 10°C, b. at 23°C, c. at 50°C

At 10°C, calcium carbonate ($CaCO_3$) showed a higher degree of reaction. This $CaCO_3$ originates from limestone added during cement production as processing additions. Figure 6.9

shows that, at 10°C, paste samples had lower $CaCO_3$ than 23°C and 50°C which could be from the higher tendency to form carbonate bearing monosulfoaluminate phases (AF_m) at the lower temperatures. Calcium carbonate contents were lower in glass samples than control, especially at 28 and 91 days, meaning additional aluminum content of glass powder was released and had reacted with the dissolved $CaCO_3$.

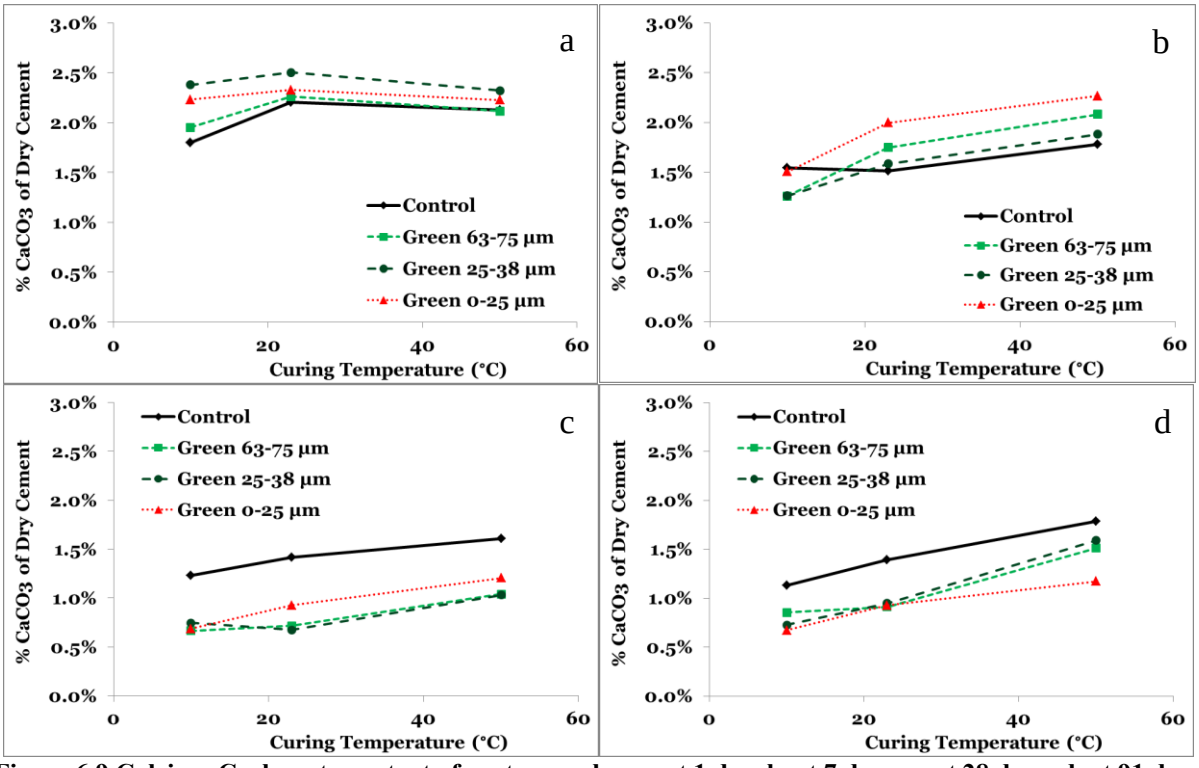

Figure 6.9 Calcium Carbonate content of paste samples: a. at 1 day, b. at 7 days, c. at 28 days, d. at 91 days

Scanning Electron Microscopy (SEM)

According to the findings based on SEM image analysis, degree of hydration of glass particles 63-75 µm and 25-38 µm at 23°C were negligible even at 91 days; however, smaller than 25 µm particles had a high degree of hydration, especially after 7 days. At elevated temperatures, all glass particles had degrees of higher hydration than at 23°C. 63-75 µm and 25-38 µm had similar hydration degrees, while smaller than 25 µm had much higher degree of hydration than the other two size ranges, indicating that the effect of size distribution combined

with curing temperature influence is considerable since higher hydration degree occurs for the finest particle sizes and higher curing temperatures. Figure 6.10 shows SEM BS images for the different particle sizes at 23°C and 50°C at 91 days. At a given curing age, criterion comparison of the C-S-H relative density for 23°C and 50°C could be made [99]. Calculated inner C-S-H relative density results demonstrated that inner C-S-H density at higher temperature is more than inner C-S-H density at lower ones since inner C-S-H density increases when curing temperature increases. As shown in Figure 6.11, the cement inner C-S-H density increases with decreasing glass particle size and increasing temperature, reflecting that some part of inner C-S-H density could be caused by the pozzolanic reaction of glass particles especially smaller than 25 μm.

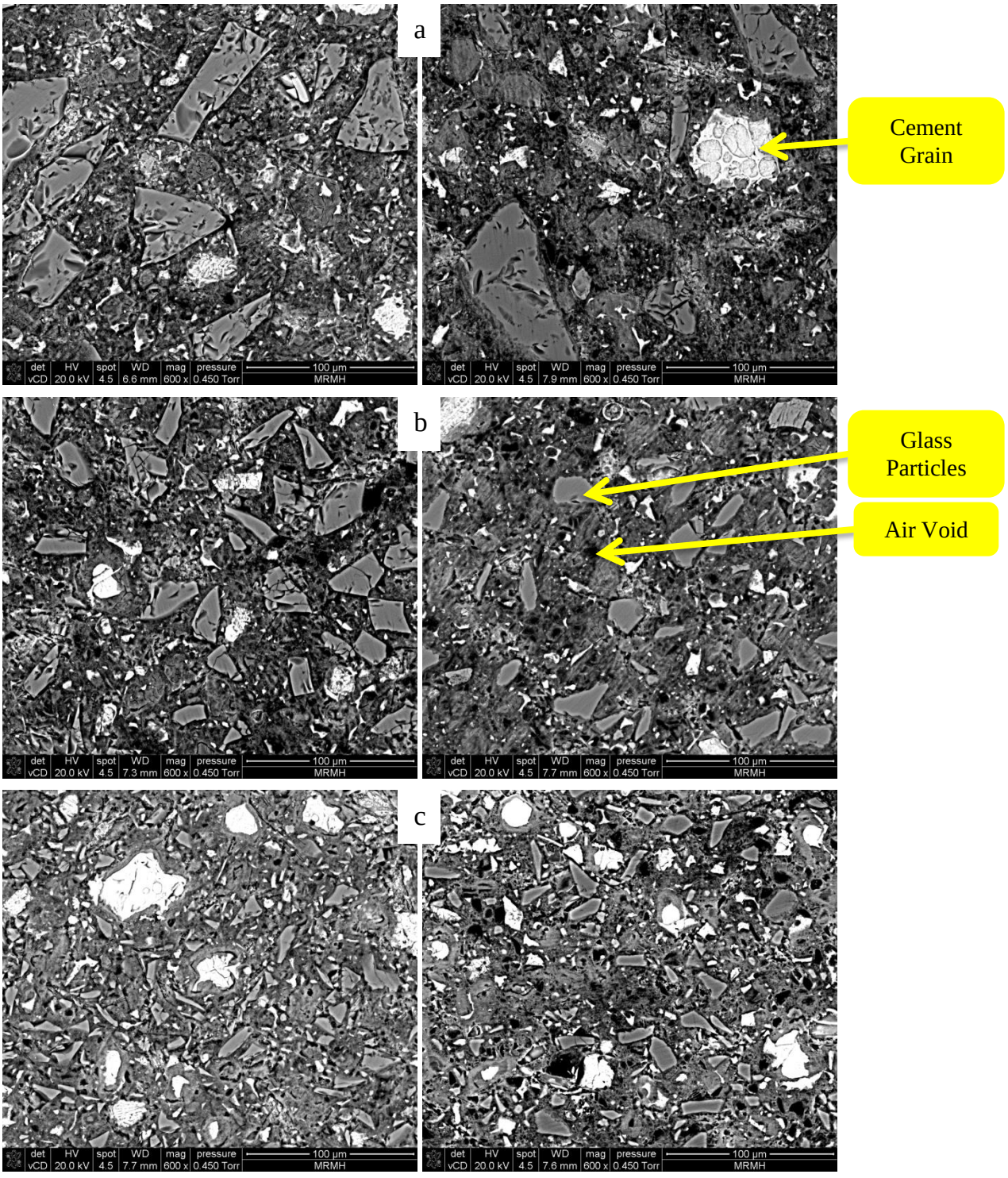

Figure 6.10 SEM Images of paste samples containing green glass cullet at 91 days curing age at 23°C (Left) and 50°C (Right): a. 63-75 µm, b. 25-38 µm, c. smaller than 25 µm

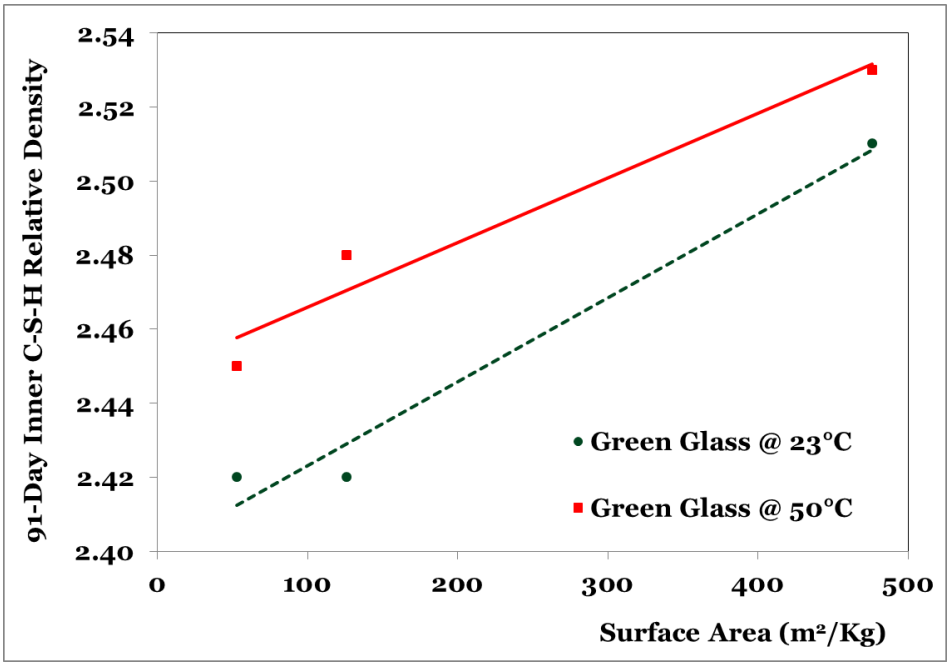

Figure 6.11 Relationship between surface area and 91-day relative density of cement inner CSH

X-Ray Diffraction (XRD) – Rietveld Analysis

Result of quantitative analysis on cementitious mixtures at 50°C is shown in Figure 6.12. At a curing age of 28 days cement DOH for control sample, and glass samples containing all three narrow sizes are very similar mirroring that the differences in hydration rate, illustrated as increase in chemical shrinkage of samples containing glass cullet compared to control, could be the result of glass cullet pozzolanic reaction. TGA results can also be used to further verify glass cullet pozzolanic reaction, as 28-day CH contents of samples containing glass at elevated temperature were significantly lower that CH content of control sample at the same curing age and temperature.

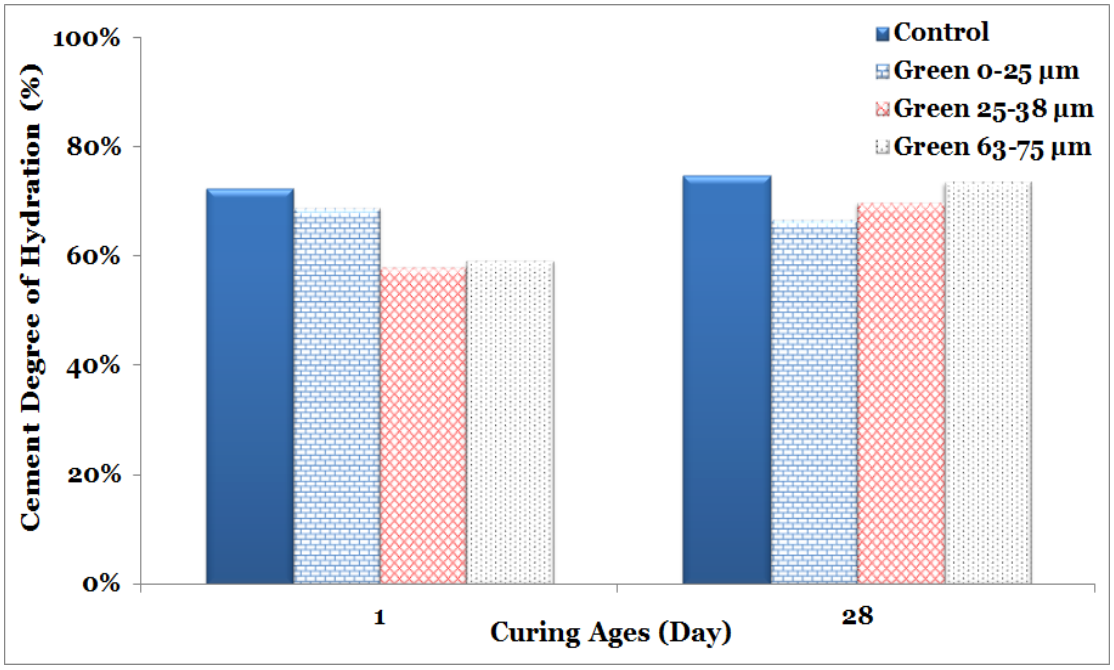

Figure 6.12 Cement degree of hydration of cementitious mixtures at 50°C obtained by Rietveld analysis

Compressive Strength

A comparison of mortar compressive strength of control and glass samples (25% cement replacement) is shown in Figure 6.13. At 23°C, mortar samples containing glass cullet have lower strength than control samples, even up to 91 days due to the increase in effective w/c ratio from the lower glass reaction level. Among different size glass particles, smaller than 25 µm samples had the highest strength and 63-75 µm samples had the lowest strength. At 50°C, while compressive strength of all glass samples are lower than control at 1 day, smaller than 25 µm samples show pozzolanic reaction after 7 days. After 28 days, 63-75 µm and 25-38 µm samples also began to show an increase in compressive strength.

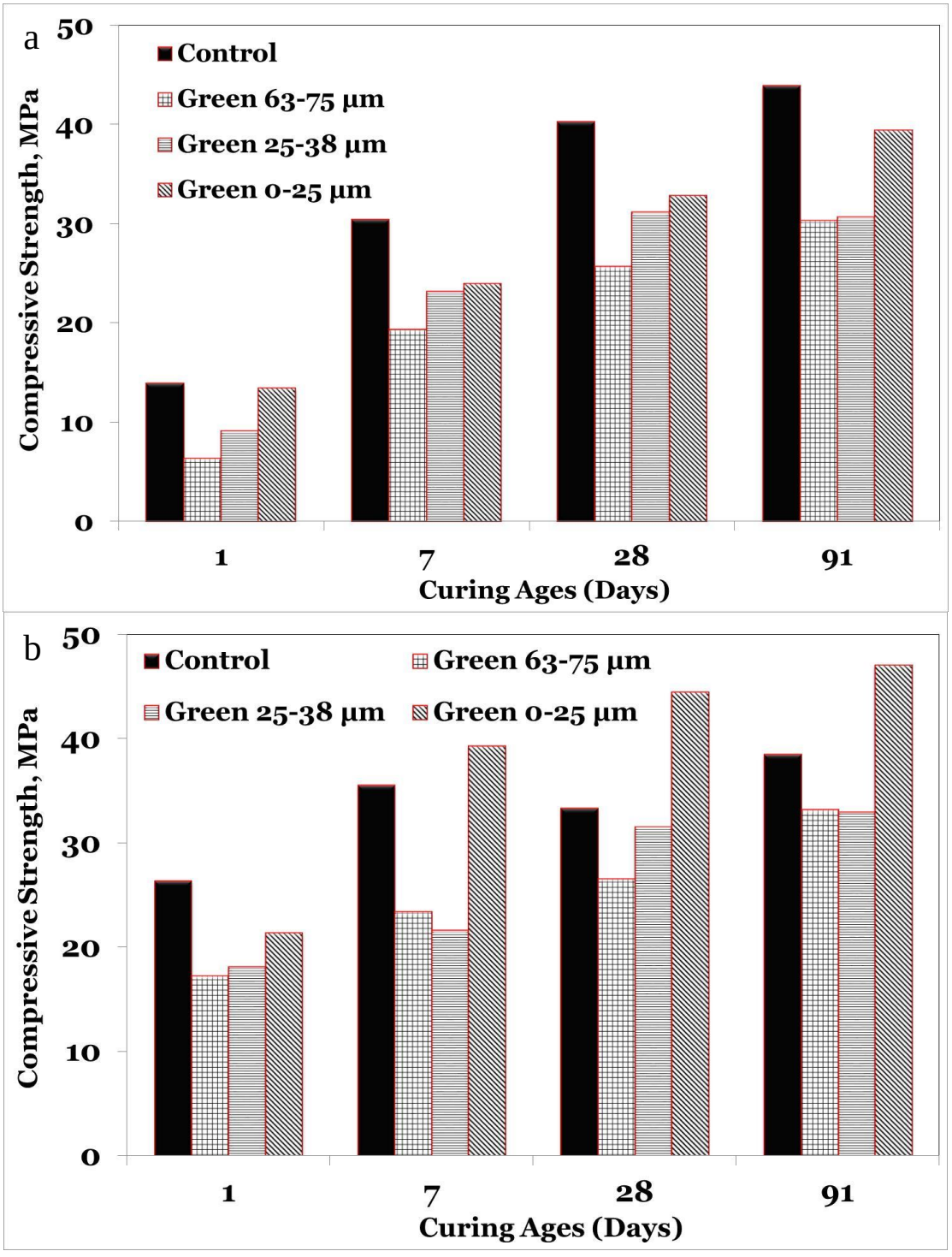

Figure 6.13 Compressive strength of mortar samples: a. at 23°C, b. at 50°C

Figure 6.14 shows the relationship between glass hydration degree from SEM and compressive strength, indicating that performance properties of concrete containing finely

ground glass powder as SCM were directly affected by degree of hydration and curing temperature. A comparison was made between performance and glass surface area.

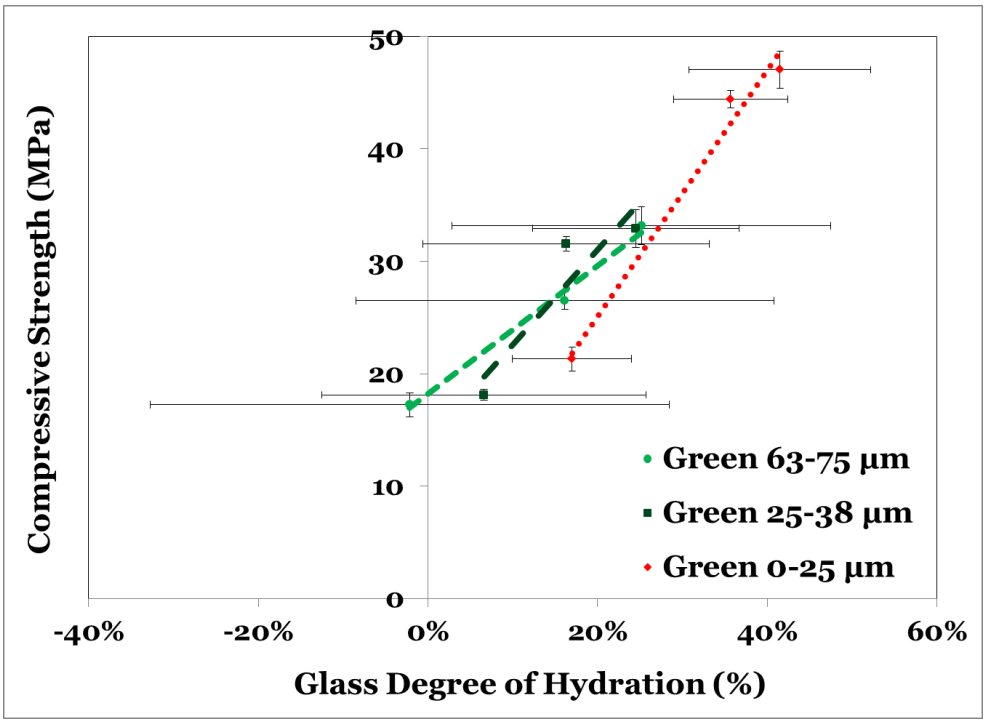

Figure 6.14 Relationship between degree of hydration of glass particles from SEM and compressive strength at 50°C

As shown in Figure 6.15, performance of cementitious mixture can be linearly proportional to the particles surface area. This direct correlation allows the effect of glass particle sizes on microstructural properties would be modeled by accounting for the particle surface area. Additionally, temperature sensitivity of glass powder is more pronounced using the slopes of the best-fit lines. Since the slopes of the best-fit lines at elevated temperatures are steeper than those at 23°C, glass powder might have more reactivity at elevated temperature, previously evidenced by the apparent activation energy concept, as well. However, although the reaction rate was higher at 50°C at 28 days compared to 23°C, the reaction rates at later ages were not significantly different.

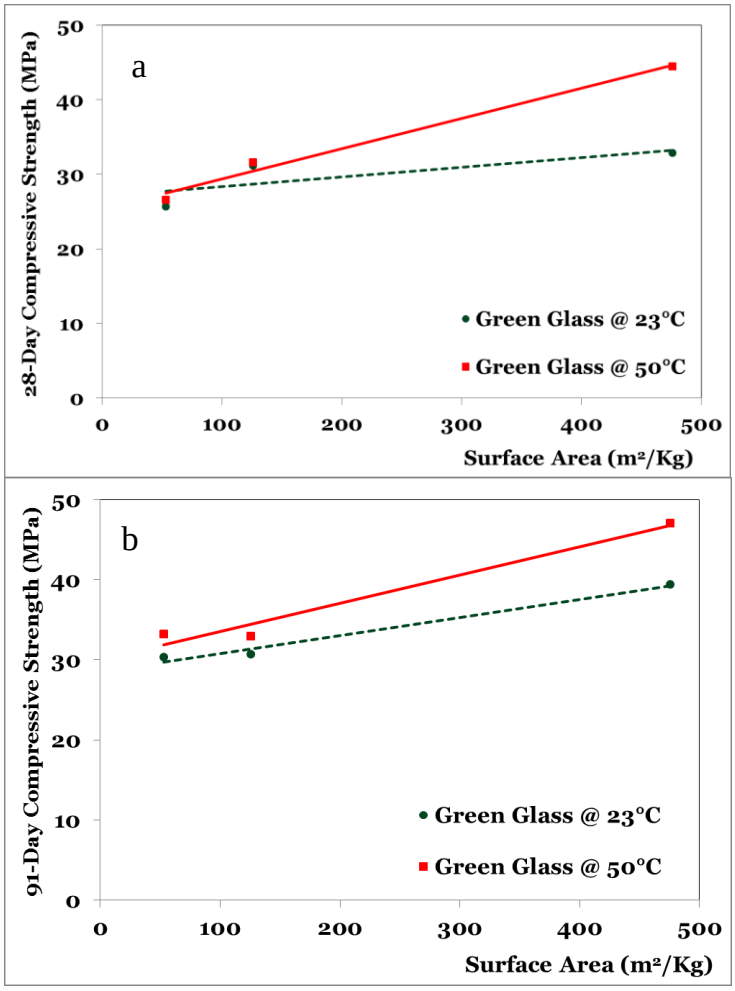

Figure 6.15 Relationship between surface area and compressive strength: a. at 28 days, b. at 91 days

Water Sorptivity

As shown in Figure 6.16, all mortar samples with or without glass powder had high water absorption at one day. However, smaller than 25 µm samples had lower absorption than other size ranges, attributed to the micro-filling effect in which voids among cement grains are filled by very fine glass particles [104]. At elevated curing temperatures, water sorptivity of mortar samples decreased by 2-10%, reflecting that at 50°C, quick formation of denser hydration products at early ages diminishes the porosity of concrete because enough room is available to accommodate those products. As hydration progressed, although the water absorption on the control samples hardly decreased with age. This can be considered as a cross-

over effect on water absorption. The pronounced effect of smaller sizes of glass in reduction of water sorptivity of all mortar samples containing glass cullet were seen, which can be ascribed to refining the pore size distribution and increasing the tortuosity of the pore network resulting from higher reaction rate of glass cullet. Samples containing smaller than 25 μm glass particles showed much higher reduction in absorption than the other two size ranges at two curing temperatures due to higher tendency to participate in pozzolanic reaction and create more hydration products.

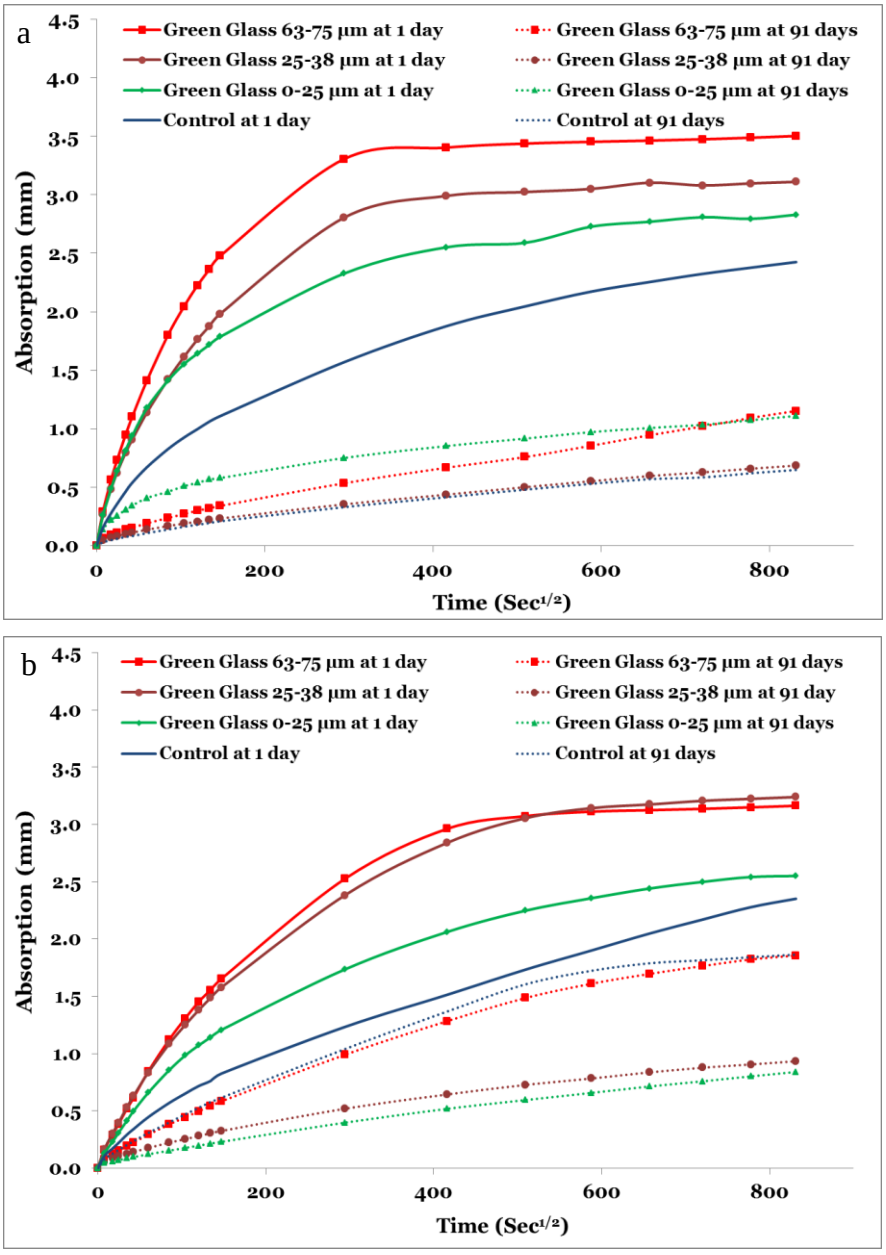

Figure 6.16 Water absorption of mortar samples: a. at 23°C, b. 50°C

Chapter 7 - Effect OF Combined Glass Particles on Hydration in Cementitious Systems

Introduction

This chapter investigates the pozzolanic behavior of combined glass particles types and size ranges in concrete, focusing on reaction kinetics, microstructural characteristics and mechanical properties. Glass particles can be tailored to have uniform composition, making them a good model system to study the influence of particle size ranges of other amorphous SCMs. This chapter studies the effects of four series of combined glass particle types and sizes on glass reaction rate, changes in reaction product and product density, and mechanical and water sorptivity characteristics of mortar samples containing finely ground glass cullet.

Bottle Leaching

Figure 7.1 shows results of ICP leaching test on single particles at 23°C and 50°C. Green glass cullet smaller than 25 µm had considerably higher aluminum contents in solution at pH greater than 13.5 compared to clear glass at 23°C and 50°C. Although clear glass smaller than 25 µm showed similar silica concentration in solution to green smaller than 25 µm at 23°C, clear glass showed higher silica concentration compared to green glass at elevated temperatures. At all pH levels, concentrations of silica and aluminum ions of coarser particles (i.e. 63-75 µm) were negligible. These findings indicate that finely ground glass, especially green cullet smaller than 25 µm, has higher solubility in cement matrix to create more calcium aluminate hydrate (C-A-H) or calcium aluminate silicate hydrate (C-A-S-H), especially at elevated temperatures since silica and alumina are, respectively, eight and three times more soluble at 50°C than 23°C.

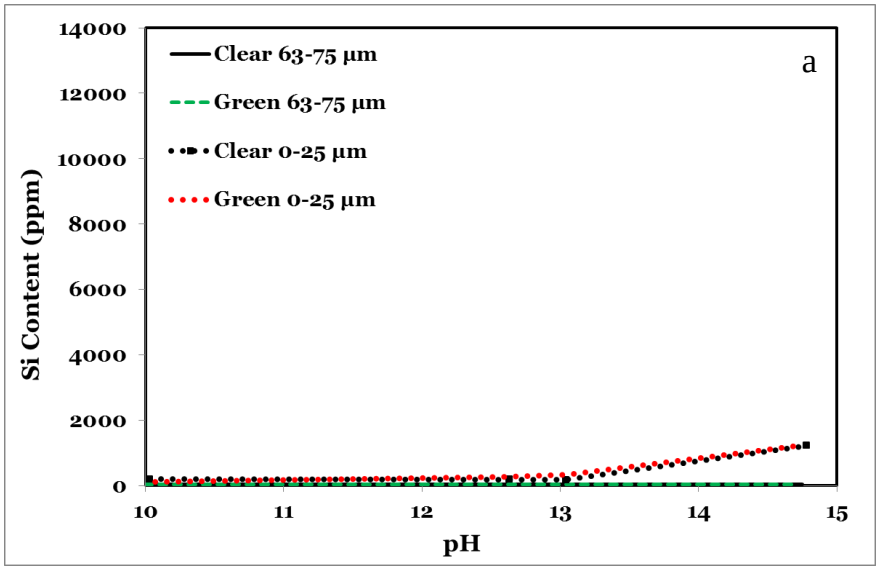
a
Clear 63-75 µm
Green 63-75 µm
Clear 0-25 µm
Green 0-25 µm
Si Content (ppm)
14000
12000
10000
8000
6000
4000
2000
0
10
11
12
13
14
15
pH

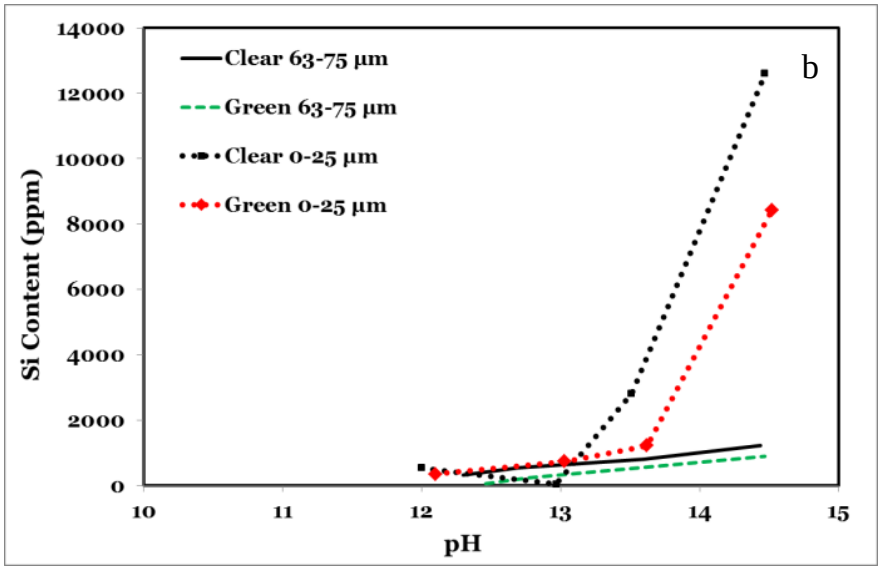
b
Clear 63-75 µm
Green 63-75 µm
Clear 0-25 µm
Green 0-25 µm
Si Content (ppm)
14000
12000
10000
8000
6000
4000
2000
0
10
11
12
13
14
15
pH

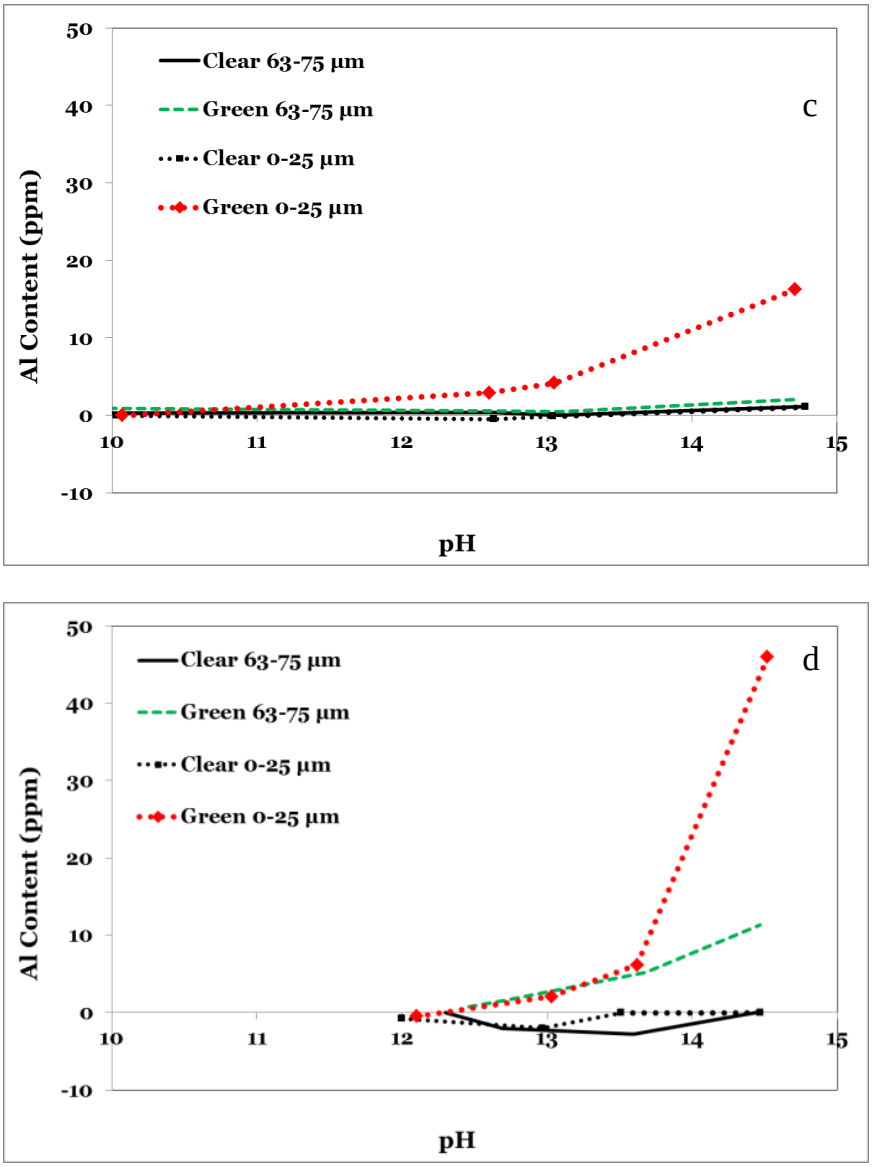

Figure 7.1 ICP test results at different pH: a. Si concentrations at 23°C, b. Si concentrations at 23°C, c. Al concentrations at 23°C, d. Al concentrations at 50°C

Isothermal Calorimetry

Figure 7.2 shows the total differential cumulative heat of hydration of mixed glass and control samples at 10°C, 23°C, and 50°C. At 10°C and 23°C, Mix 1 and Mix 3 were very similar, while Mix 2, which was the smallest combination of particle sizes, had a slightly higher reaction rate. Mix 4, the coarsest combination, had the lowest reaction rate, reflecting that mixtures containing 63-75 µm particles, clear or green, had very low reactivity even at

10°C and 23°C. At 50°C, Mix 2, Mix 1, Mix 3, and Mix 4 showed a higher reaction rate of 28.7%, 25.1%, 19.9%, and 14.3%, respectively. These results showed that cementitious samples containing finely ground mixed glass cullet, especially green glass smaller than 25 µm, have significantly higher reaction kinetics compared to control samples at elevated temperatures. This higher reaction rate includes the increased degree of hydration of the cement because of increased space available from the increased effective water-to-cement ratio (dilution effect), the glass particles serving as nucleation sites for C-S-H, and glass hydration [92,93]. The results also showed that the effect of curing temperatures on glass reactivity is very pronounced, since mixed cullet glass had a much higher reaction rate at 50°C than 23°C or 10°C.

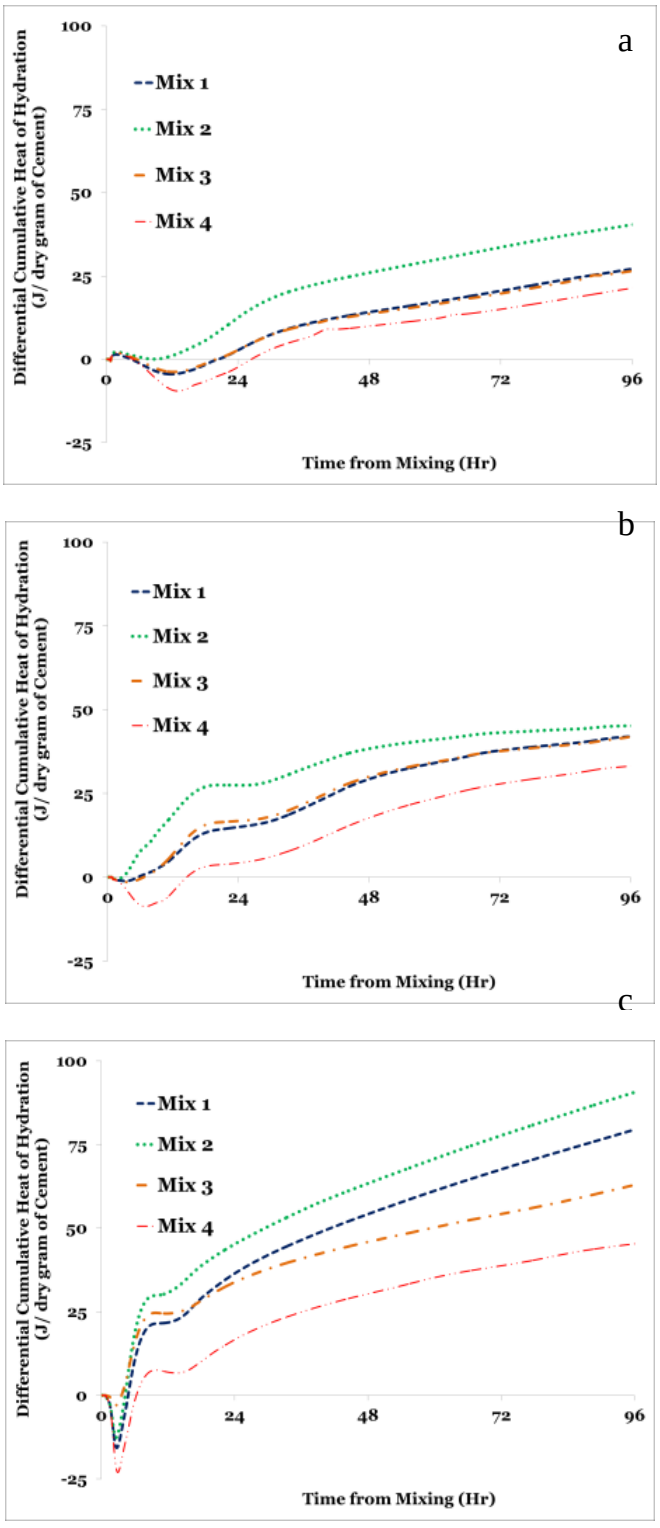

Figure 7.2 Total differential heat of hydration of paste samples: a. at 10°C, b. at 23°C, c. at 50°C

To further evaluate the mixed glass cullet temperature sensivity, Arrhenius plot of control samples and samples containing mixed glass powder were plotted (Figure 7.3), and apparent activation energy (E_a) of control and mixed glass samples were calculated (Table 7.1). Mix 1, Mix 2, Mix 3, and Mix 4 had similar E_a, meaning that the combined particle sizes had little effect on temperature sensitivity of cementitious systems containing combined glass cullet.

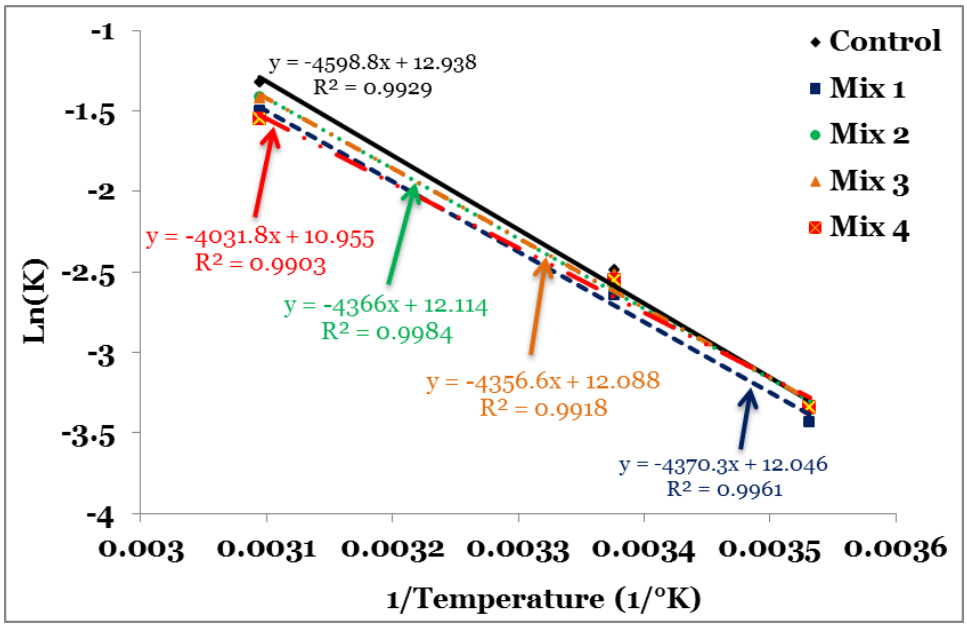

Figure 7.3 Arrhenius plot of cementitious samples

Table 7.1 Apparent Activation Energy of Cementitious Samples

Sample	Activation Energy (KJ/mol)
Control	38.2
Mix 1	36.3
Mix 2	36.3
Mix 3	36.2
Mix 4	33.5

In order to account for the simultaneous influences of size and type of glass cullet, a comparison was also made between calculated and measured cumulative heat of hydration (HOH) at 96 hours. Calculated 96-hour cumulative HOH was obtained by linear interpolation

of the measured cumulative HOH of single particles (i.e., 63-75 µm and smaller than 25 µm) of clear and green glass. As shown in Figure 7.4, the correlation between calculated and measured 96-hour cumulative HOH was linear, reflecting that the concurrent effect of size ranges and types of glass cullet on hydration reaction kinetics could be accounted for through linear addition.

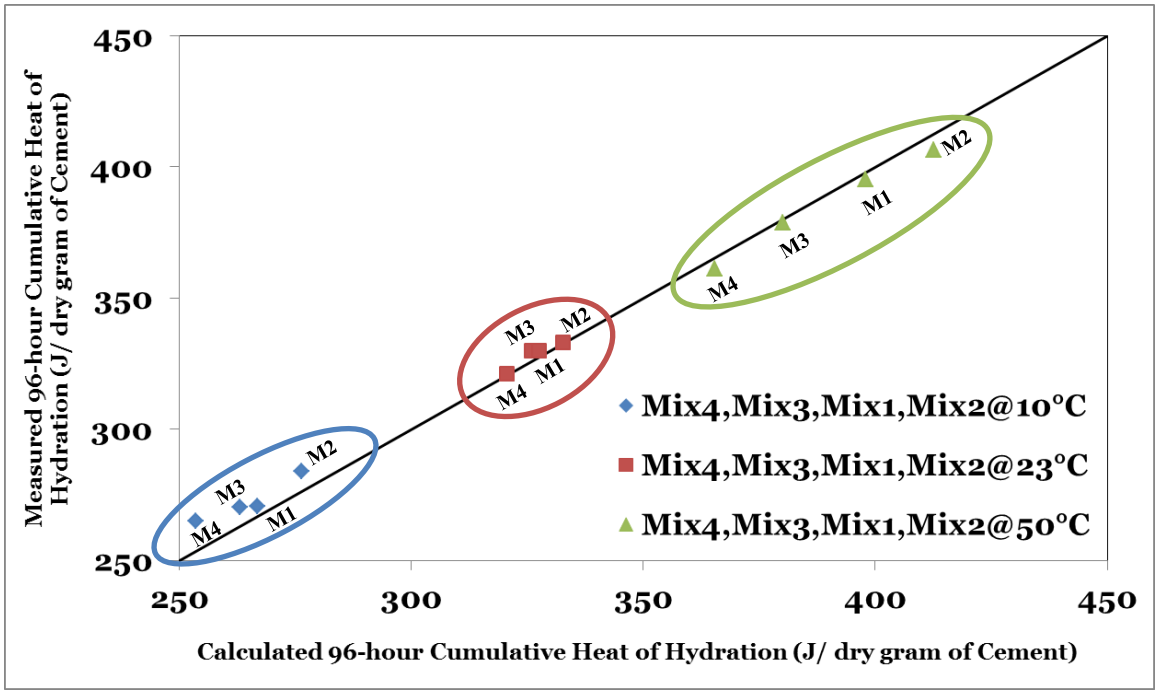

Figure 7.4 Relationship between calculated and measured 96-hr cumulative HOH

Chemical Shrinkage

The result of a chemical shrinkage test of paste samples with and without combined glass cullet at three curing temperatures is shown in Figure 7.5. At all curing temperatures, Mix 2, which was a combination of smaller than 25 µm of clear and green glass, had the highest chemical shrinkage, while Mix 4 had the lowest amount, reflecting the significant effect of particle size on glass reactivity. While 28-day chemical shrinkage of all samples at 10°C were slightly higher than samples at 23°C (except for Mix 1 which showed higher chemical

shrinkage at 23°C), all paste samples containing glass cullet showed lower 28-day chemical shrinkage at 50°C. This phenomenon could be explained by the fact that at elevated temperatures, paste samples had accelerated hydration, causing the microstructure to form faster. As shown in Figure 7.6, chemical shrinkage at elevated temperature slowly increased (i.e. 0–0.015 mL/dry gram of cement) up to HOH of 300 J/dry gram of cement while from HOH of 300 to 400 J/dry gram of cement chemical shrinkage increased dramatically (i.e. 0.015–0.04 mL/dry gram of cement). It can reflect that denser microstructure might make it harder for water to penetrate into the paste and create more hydration products while heat was formed due to dissolution process and hydration of different phases like C_3A. This phenomenon revealed that the glass powder had higher reactivity at elevated temperatures (i.e., higher temperature dependency).

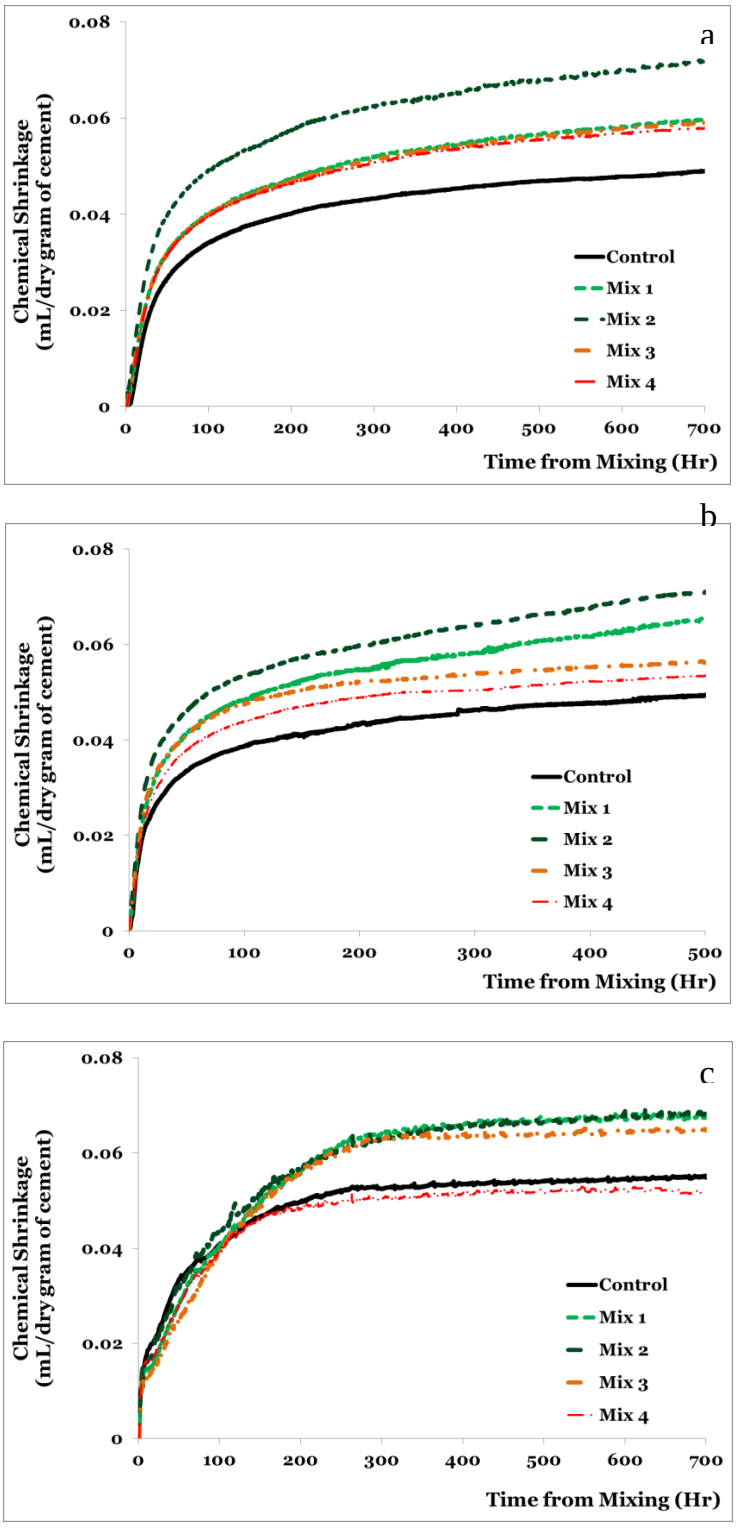

Figure 7.5 Chemical shrinkage of paste samples: a. at 10°C, b. at 23°C, c. at 50°C

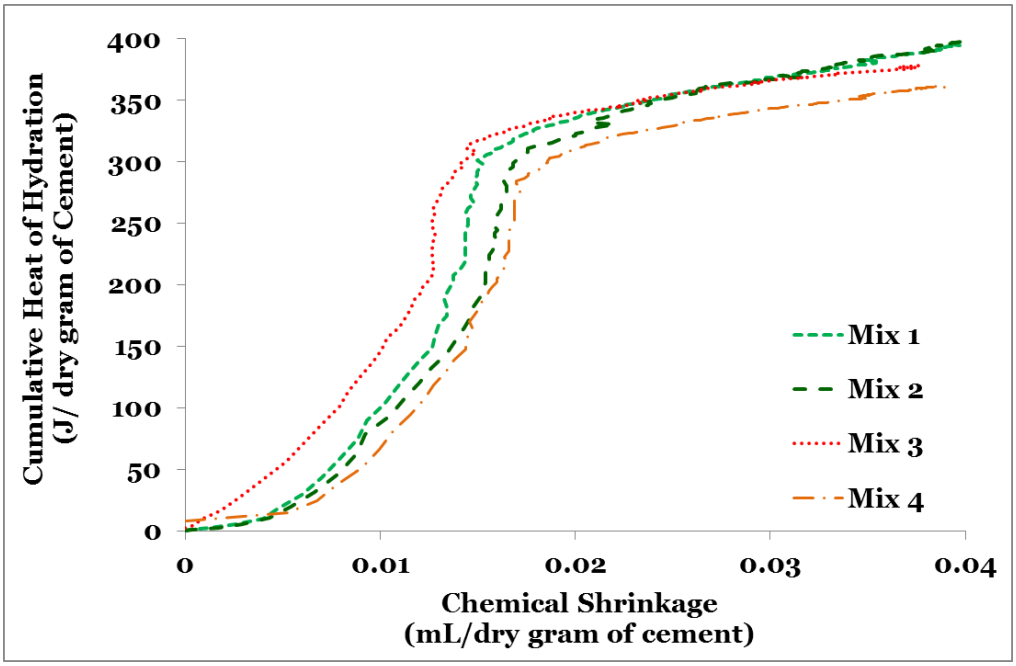

Figure 7.6 Relationship between chemical shrinkage and cumulative HOH of paste samples at 50°C up to 96 hs

Thermogravimetric Analysis (TGA)

Reduction in CH content of glass samples compared to control samples is commonly seen as an index of the pozzolanic reaction of glass powder. Variation in portlandite content of paste samples with and without combined glass cullet against three curing temperatures at different curing ages is shown in Figure 7.7. At one day, no pozzolanic reaction was observed at all three curing temperatures, while some reactions were observed after seven days at 50°C. At 28 days and 91 days, the combined glass particles did not show pozzolanic reaction at 10°C and 23°C; however, at 50°C, significant reductions in calcium hydroxide content were observed, i.e., 9.5% to 27% at 28 days and 21% to 29.5% at 91 days. Among the four mixed glass sets, Mix 2 had the highest pozzolanic reaction (27.2% decreases in CH at 50°C after 28 days), followed by Mix 1 and Mix 3, which are similar in behavior. The least reactivity belonged to Mix 4, with 9.5% CH reduction at 50°C after 28 days. This phenomenon could be

explained by the effect of surface area of the mixtures. Mix 2 had the highest surface area, reflecting higher propensity to participate in pozzolanic reaction. Conversely, Mix 1, Mix 3, and Mix 4 had lower surface areas and consequently showed lower reactivity. Mixed glass cullet is a slow-reactive SCM at low and moderate temperatures since almost no reduction in portlandite was observed at 10°C and 23°C, while mixed glass could be considered a moderate- to fast-reacting SCM at elevated temperatures.

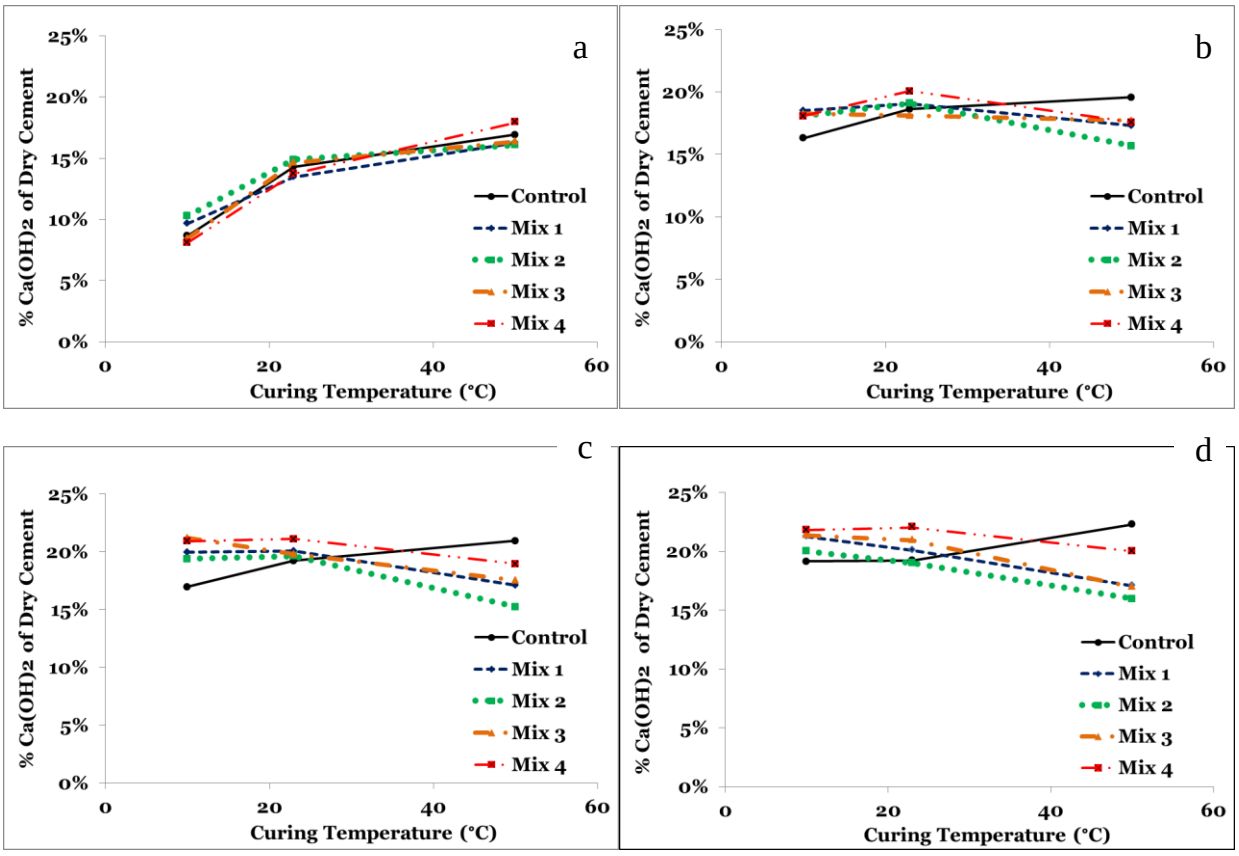

Figure 7.7 Portlandite content of paste samples: a. at 1 day, b. at 7 days, c. at 28 days, d. at 91 days

Variation in calcium carbonate ($CaCO_3$) content versus curing temperatures at different ages is another point of interest of this experiment (Figure 7.8). The source of $CaCO_3$ is the limestone added during cement production. At 10°C calcium carbonate content was lower compared to 23°C and 50°C, showing that $CaCO_3$ had higher reaction degree at lower curing

temperatures, explained by higher reaction propensity of AFm phases at low temperatures, resulting in a drop in calcium carbonate concentration. This decrease could cause more $CaCO_3$ to dissolve. Decrease in calcium carbonate contents of glass samples compared to control samples, especially at 28 and 91 days, could be caused by reaction between aluminum from the glass powder and dissolved $CaCO_3$.

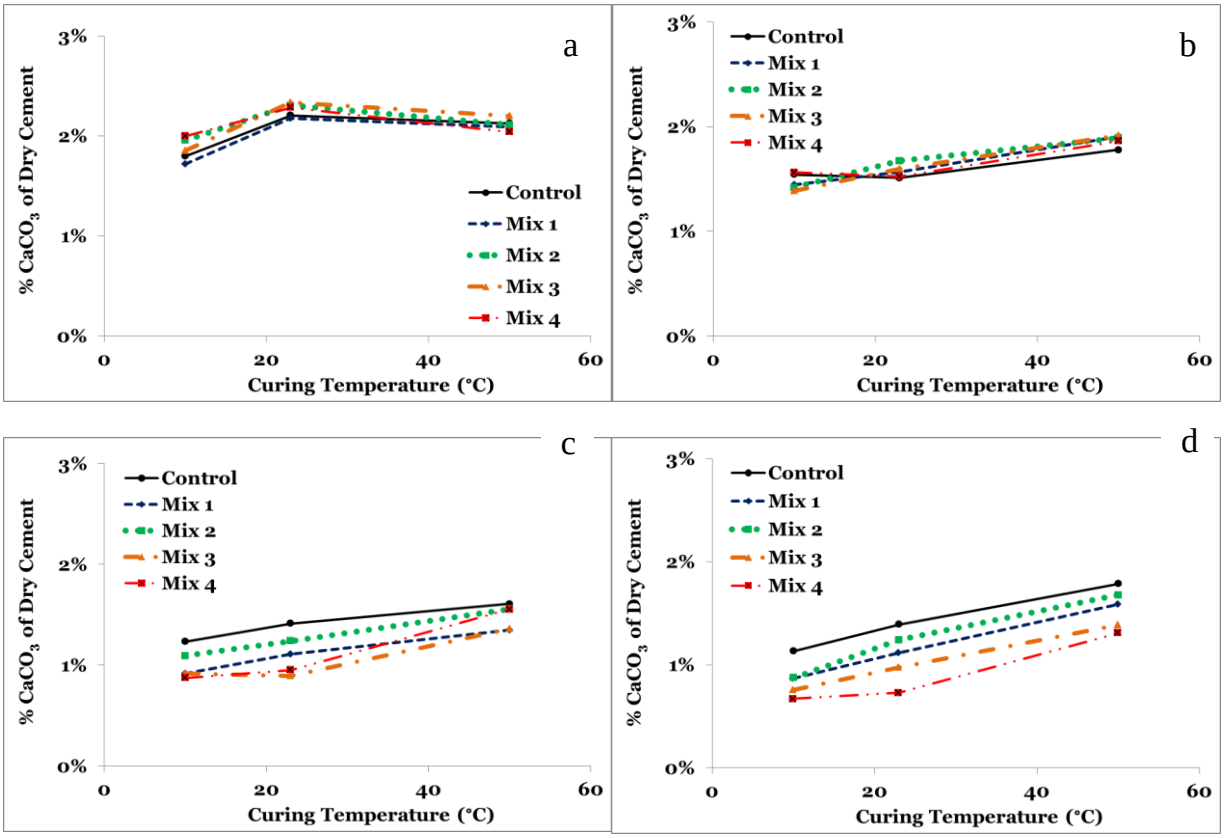

Figure 7.8 Calcium Carbonate content of paste samples: a. at 1 day, b. at 7 days, c. at 28 days, d. at 91 days

Scanning Electron Microscopy (SEM)

Figure 7.9 shows the hydration degree (based on SEM image analysis) of Mix 2 and Mix 4 of glass cullet versus time after casting for curing temperatures of 23°C and 50°C. Coarse glass particles had negligible hydration at 23°C even at 91 days, while Mix 2 had significantly higher hydration compared to Mix 4. No significant increase in hydration was

observed at 91 days compared to that seen at 28 days. Although Mix 4 did not demonstrate any hydration until 28 days at 50°C, it had almost 10% degree of hydration at 91 days. Mix 2 again showed a noticeably higher degree of hydration (DOH) than Mix 4, as well as an increasing trend of degree of hydration up to 91 days. These findings showed that the finer combined glass cullet has more reactivity compared to coarser combined glass cullet and verified the temperature dependency of glass cullet as an SCM since greater DOHs were observed at elevated curing temperatures.

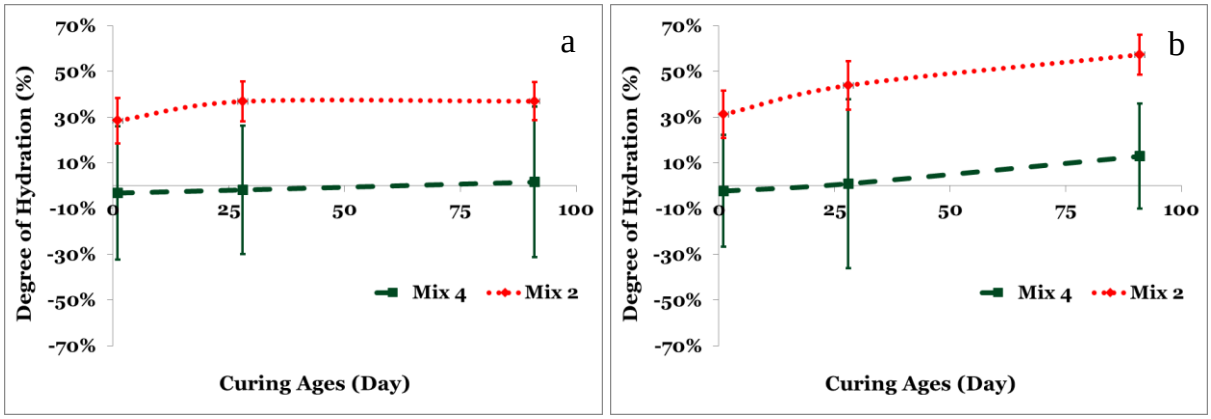

Figure 7.9 Degree of hydration of combined glass cullet obtained by SEM image analysis: a. at 23°C, b: at 50°C

Figure 7.10 illustrates the correlation between calculated and measured cement inner C-S-H density at 91 days at 23°C and 50°C. This comparison could explain the simultaneous effects of various glass cullet type and size on DOH. Calculated inner C-S-H densities were obtained by linear interpolation of inner C-S-H densities of individual particles. As shown, a linear correlation exists between two types of inner C-S-H densities, reflecting that the concurrent effects of type and size of glass powder could be accounted for through linear addition. This result was previously observed for the reaction rate of glass cullet according to isothermal calorimetry results. Moreover, cement inner C-S-H densities of mixed glass cullet

were higher when the curing temperature increased and particle size decreased, showing that increased cement inner C-S-H density partially originates from the pozzolanic reaction of combined smaller than 25 µm glass cullet at 50°C.

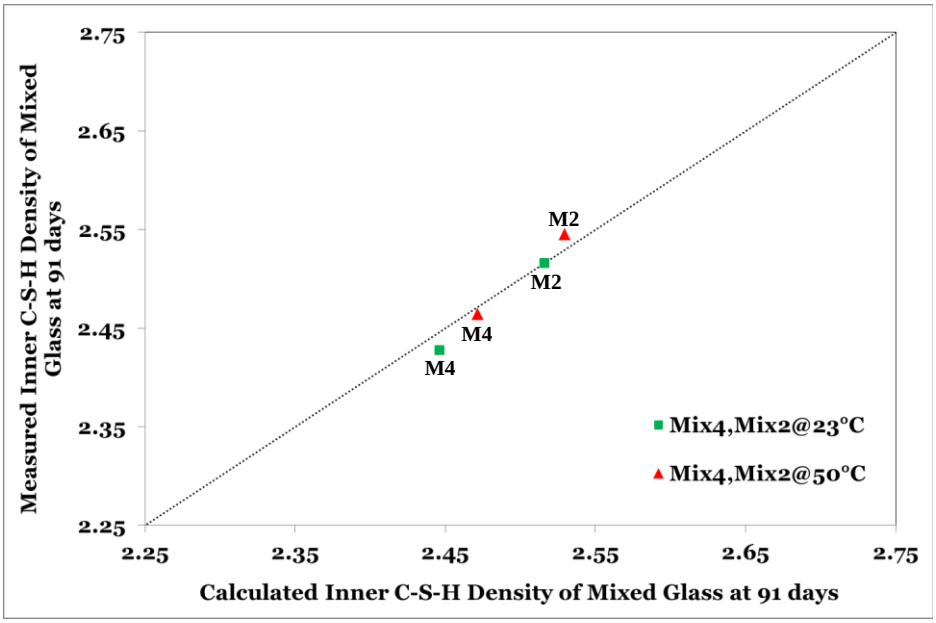

Figure 7.10 Relationship between calculated and measured 91-day relative density of cement inner CSH

X-Ray Diffraction (XRD) – Rietveld Analysis

As seen in Figure 7.11, results of Rietveld analysis on three cementitious mixtures at curing temperature of 50°C shows that all mixtures had similar degree of hydration of cement either at one day of curing age or especially at 28 days of curing age. This finding could provide valuable information about glass cullet reactivity. While DOH of cement is similar for control, Mix 2, and Mix 4 at 28 days, higher chemical shrinkage of Mix 2 at 28 days could be contributed to glass pozzolanic reaction. This pozzolanic reaction could be further evidenced by the TGA results: as at 50°C paste samples containing Mix 2 showed lower CH at 28 day. Additionally, the effect of particle size on pozzolanic reaction of blended glass was studied. Although Mix 2 and Mix 4 contained 25% amorphous glass content which was initially added to the mixtures, Mix 2 showed higher amorphous content compared to Mix 4 at 50°C either at 1 day or at 28 days (Figure 7.12).

This finding reflected that smaller particle sizes could have more pozzolanic reaction which results in a formation of more amorphous C-S-H.

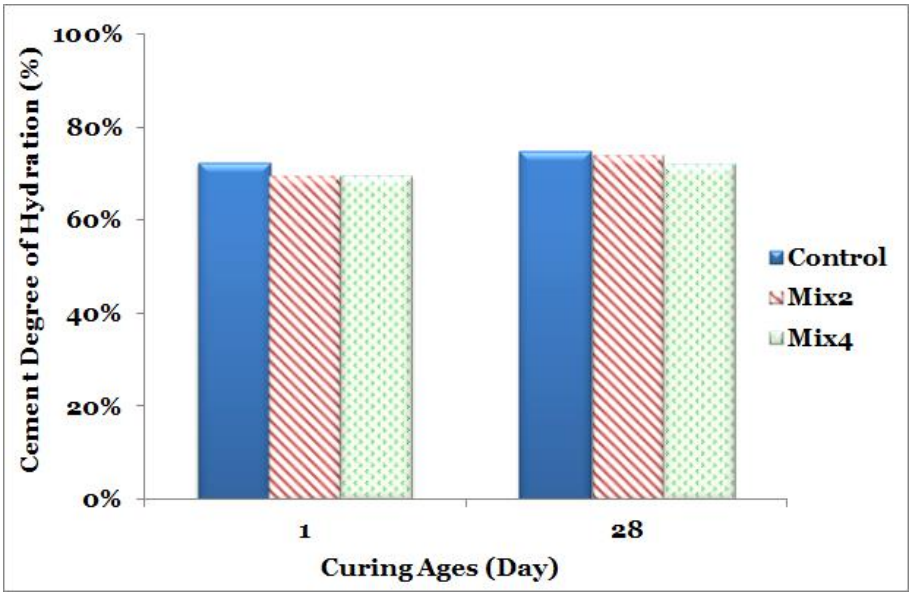

Figure 7.11 Cement degree of hydration of cementitious mixtures at 50°C obtained by Rietveld analysis

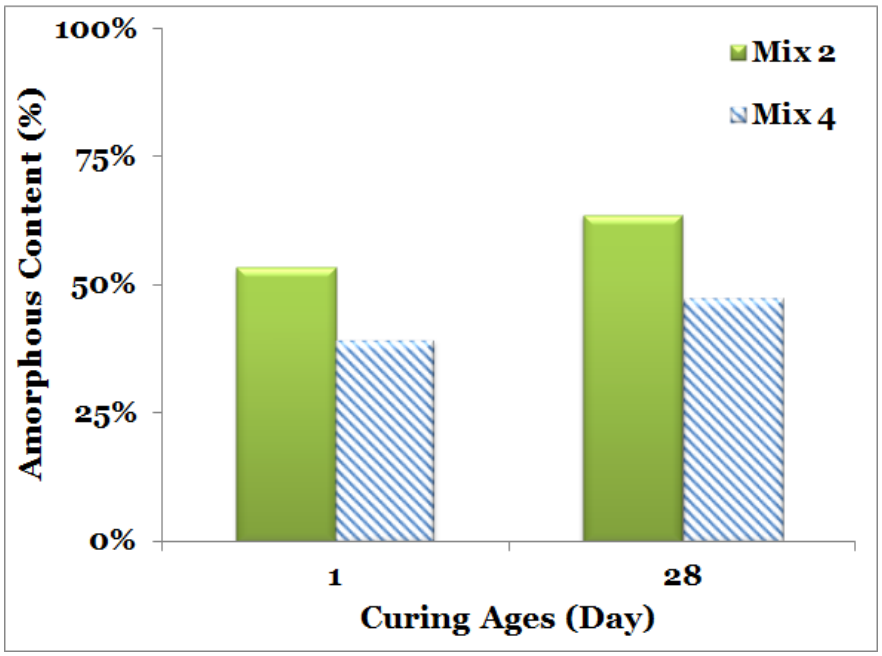

Figure 7.12 Amorphous content of cementitious mixtures containing combined glass at 50°C

Water Sorptivity

Figure 7.13 shows the water absorption of mortar samples with and without mixed glass powder at 23°C and 50°C. At 23°C, mortar samples showed similar water sorptivity after 1 day of curing, while Mix 2 mortar samples showed the lowest absorption, possibly explained by the particle packing effect in which the smaller than 25 μm particles give better particle packing among cement grains than the larger particles [104]. At 91 days, mortar samples, especially Mix 2, showed significant reductions in water sorptivity, which could be attributed to the progress in hydration. The effect of elevated temperatures could be investigated by results of absorption at 50°C. All mortar samples showed up to a 40% decrease in water sorptivity at 1 day. These reductions are the result of accelerated hydration and the creation of more and denser hydration products. While control samples showed higher water absorption at 91 days compared to 1 day (cross-over effect), mortar samples containing blended glass cullet, specifically samples with smaller than 25 μm glass cullet, had noticeably lower water sorptivity than 1 day. One possible explanation is pore size distribution refining, lower connectivity, and tortuosity increase of the pore network caused by higher reaction rate of glass cullet. Another point was the effect of mixed glass particle size on pore characteristics. Mix 4, which was the coarsest particle size, showed lower reduction in water sorptivity compared to other mixtures at 91 days than 1 day at 23°C and similar water sorptivity at 91 days than 1 day at 50°C, but mortar samples containing smaller than 25 μm showed considerable decrease in water absorption, reflecting that finer particle size has a higher tendency to participate in pozzolanic reaction and create more hydration products. A comparison between 91-day water absorption of mortar samples containing mixed glass at 23°C and 50°C showed that the mortar

samples, especially Mix 4, had higher water absorption at elevated temperature than 23°C. This could be explained by more and larger pores among hydration products at later ages.

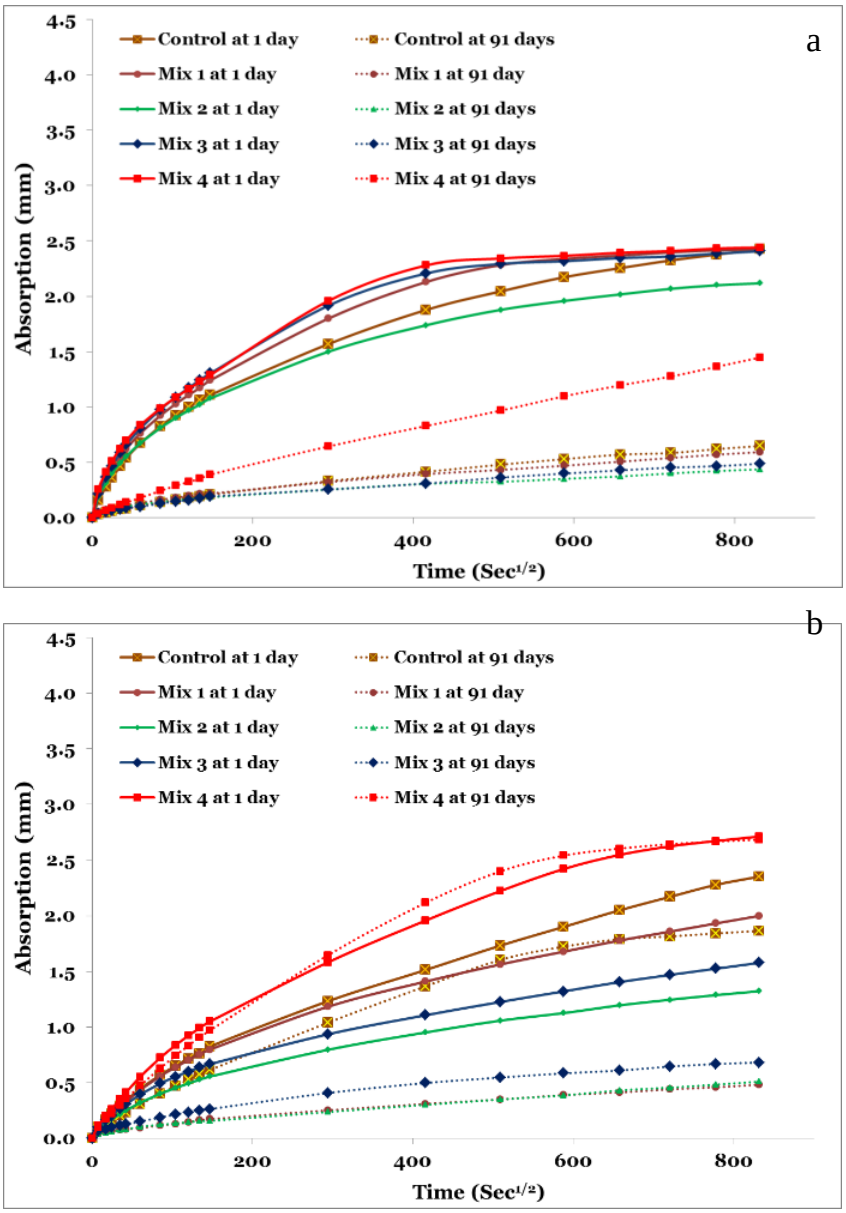

Figure 7.13 Water absorption of mortar samples; a. at 23°C, b. at 50°C

Compressive Strength

Comparison of calculated and measured compressive strength results is shown in Figure 7.14. The calculated compressive strength was obtained based on an average of compressive strength results of mixtures containing single glass particle sizes. At 23°C, a good agreement was seen

between calculated and measured compressive strength, reflecting that the effect of glass particle sizes and types on compressive strength of cementitious mixtures containing glass cullet can be accounted for through linear addition. At 50°C, however, a discrepancy was seen between calculated and measured compressive strength results. In all mixed glass mixtures the measured compressive strength followed the weaker side. In Mix 1, for example, the measured compressive strength was similar to green 63-75 µm which had lower compressive strength than green smaller than 25 µm. This finding was in contrast to the calorimetry results in which measured HOH was in well agreement with calculated results. This discrepancy could be due to pores sizes, distribution, and connectivity which is important factors affecting compressive strength. At elevated temperature, accelerated hydration provided rapid early-age hydration products which results in ineffectual decrease in larger pores among products (Figure 7.15), which could be the reason for higher secondary coefficient of absorption (S_s) of glass samples at 50°C than 23°C [99]. These pores might be accumulated in a way that a weak plane is created around larger particles (63-75 µm) and clear glass, which have lower and slower reactivity than smaller particles and green glass, and consequently result in lower compressive strengths (Figure 7.16).

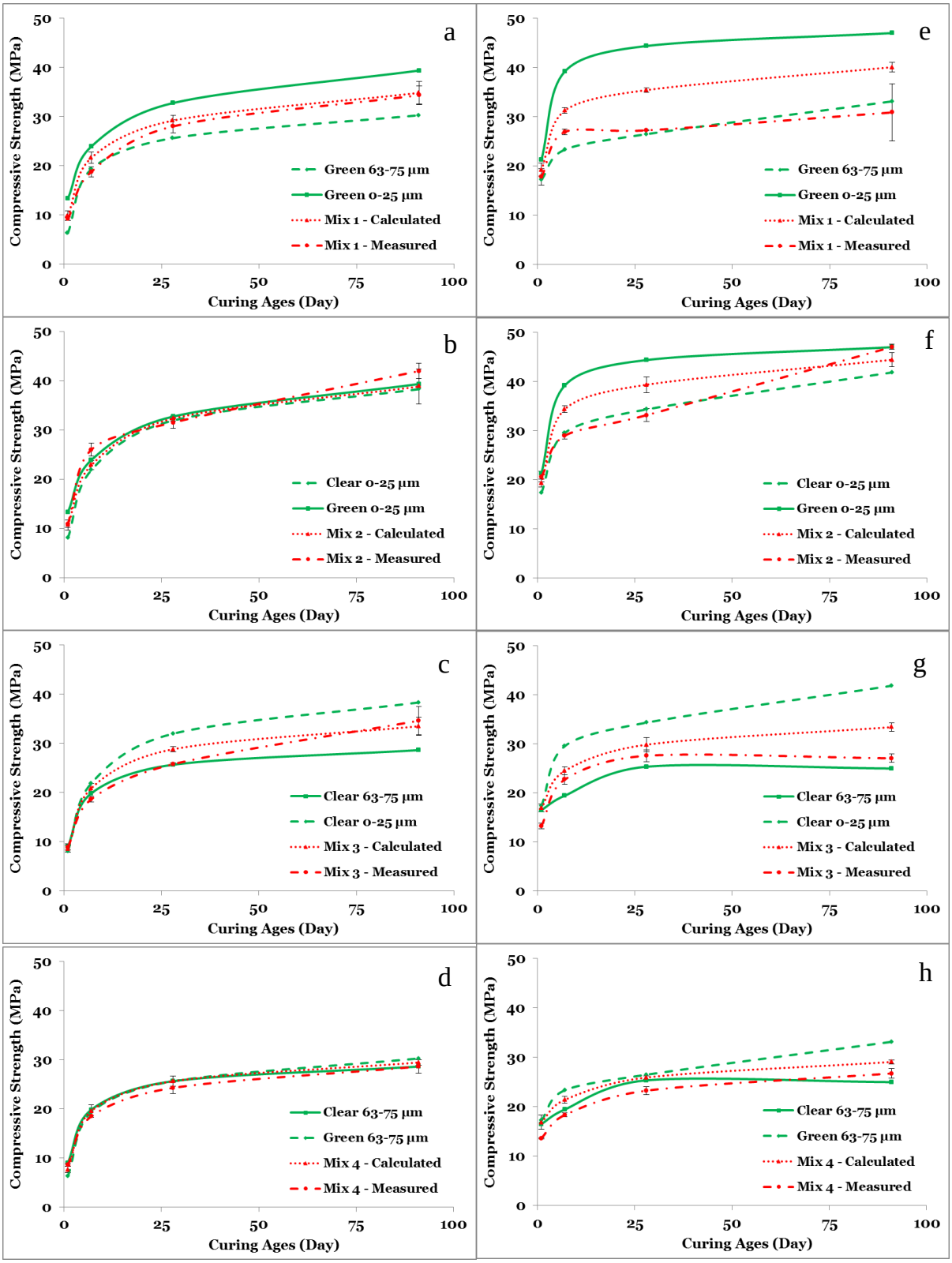

Figure 7.14 Comparison of calculated and measured compressive strength results of different mixed glass; a,b,c,d. at 23°C, e.f.g.h. at 50°C

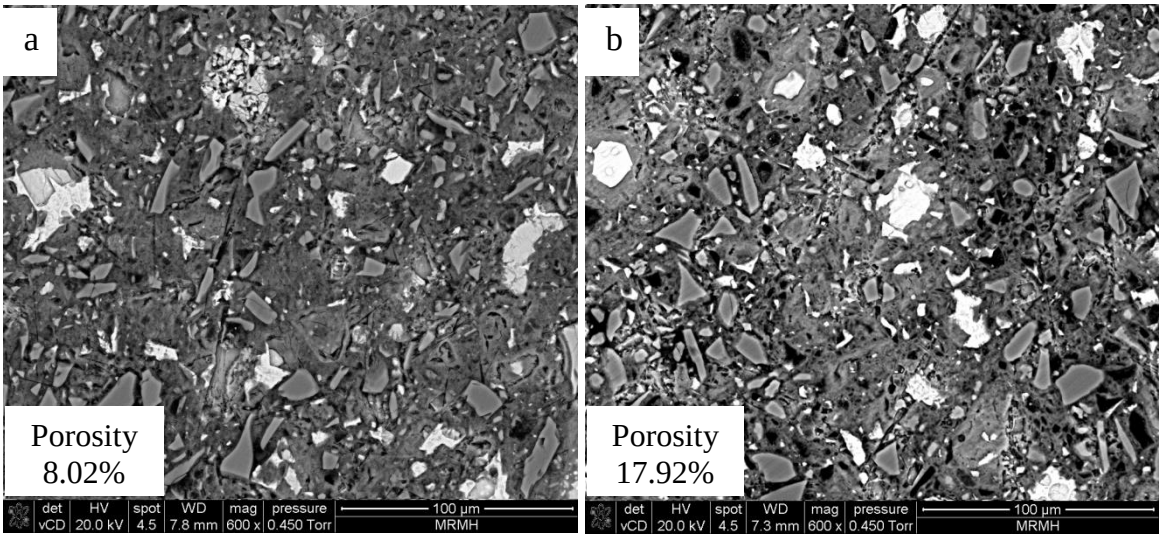

Figure 7.15 Effect of curing temperatures on porosity of paste samples; a. at 23°C, b. at 50°C

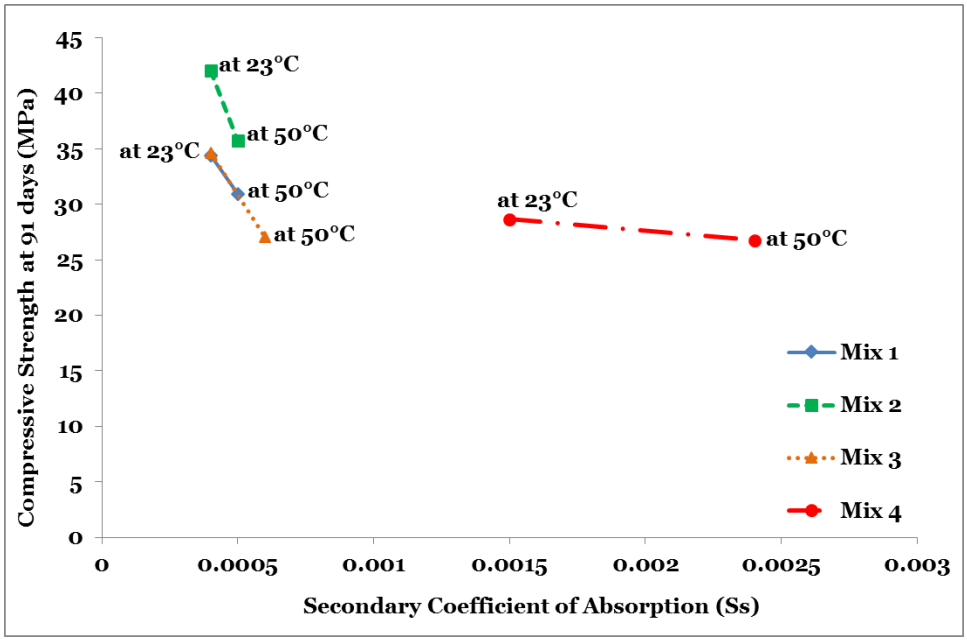

Figure 7.16 Correlation of pore sizes (S_s) and 91-day compressive strength

Chapter 8 - Microstructural Modeling of Glass Cullet Reaction

Introduction

Microstructural modeling is a helpful tool to obtain better understanding of cement hydration and microstructure development [17]. Mechanical and performance properties of concrete are directly related to the development of concrete microstructure, which is the consequence of progress in cement hydration [17,105]. Cement hydration is a complicated system making hydration difficult to model [106]. This complexity is the main reason for which there has not been developed a complete theory explaining cement hydration and chemical reaction, despite almost 200 years having passed from invention of cement [107]. Nevertheless, many efforts have been made during the past 40 years to microstructurally model hydration of cement and various cementitious materials such as fly ash, slag, and SF [106-112].

Modelling of Glass Cullet Reactivity using µic

The purpose of this study is to model the pozzolanic reaction of combined glass cullet by finding kinetics equation parameters. In this section, two single particles and two types, as well as one blended glass particles and type of very finely ground glass are simulated by means of µic.

Modeling of Cement Hydration

In order to simulate glass cullet reactivity, the cement hydration needs to be modeled by means of µic. Modelling cement hydration means to fit reaction kinetics equation parameters. For this study, the reaction kinetics equation used for cement hydration as well as glass reactivity is the Avrami equation. The Avrami equation is a nucleation and growth model

which was initially developed for metallic crystals. However, its S-shape is similar to the typical shape of cement hydration. Its implicity also helps make it one of the most popular reaction kinetics equations used for modeling cement hydration [17]. The Avrami equation can be expressed as Eq. (8.1) [113]:

$$-\ln(1-\alpha) = kt^n \qquad \text{Eq. (8.1)}$$

where α is cement degree of hydration, t is elapsed time from initial contact of water and cement, and k and n are Avrami parameters which depend on reaction rate and how crystals grow, respectively. The Avrami constant n is a function of three additional parameters as shown in Eq. (8.2):

$$n = (P/S) + Q \qquad \text{Eq. (8.2)}$$

where P is related to dimensions of products growths and can be 1, 2, or 3 for one-, two-, or three-dimensional growth, respectively. Parameter S is 1 for interface controlled and 2 for diffusion controlled mechanisms. Q is a function of rate of nucleation and can be 1 for continuous nucleation and 0 for only initial nucleation [80]. Respectively selecting 3, 1, and 1 for P, S, and Q, the value of n will be 4 for this study. Thus, the objective of modeling cement hydration is to find the Avrami parameter k by fitting degree of hydration results obtained from μic to those obtained from isothermal calorimetry.

The modeling in this study is done for three main compounds of cement, namely C_3S, C_2S, and C_3A, to attain more descriptive results. Having very complicated hydration products and known to be rather slow reacting, C_4AF has not been modeled in this study. Additionally, cement hydration and glass reactivity are simulated only at 50°C because experimental results showed that reaction rate of cement and pozzolanic reaction of glass cullet are more pronounced at 50°C compared to 10°C and 23°C.

Step 1 – Initial Settings

µic reads XML files that assign the hydration rate parameters and other inputs to the modeling engine. These XML input files can be created by a graphical user interface program or developed manually. From "File" tab in the command bar of the µic interface, "Load XML File" or "Create New Reactor" is selected. In this window the name of reactor, size of virtual paste cube, hydration time step, and some other initial settings such as pixel sizes and background color are determined. For this study, the size of the virtual paste cube is set to be a 100 x 100 x 100 voxel cube. Figure 6.1 shows a screen shot of the Reactor window.

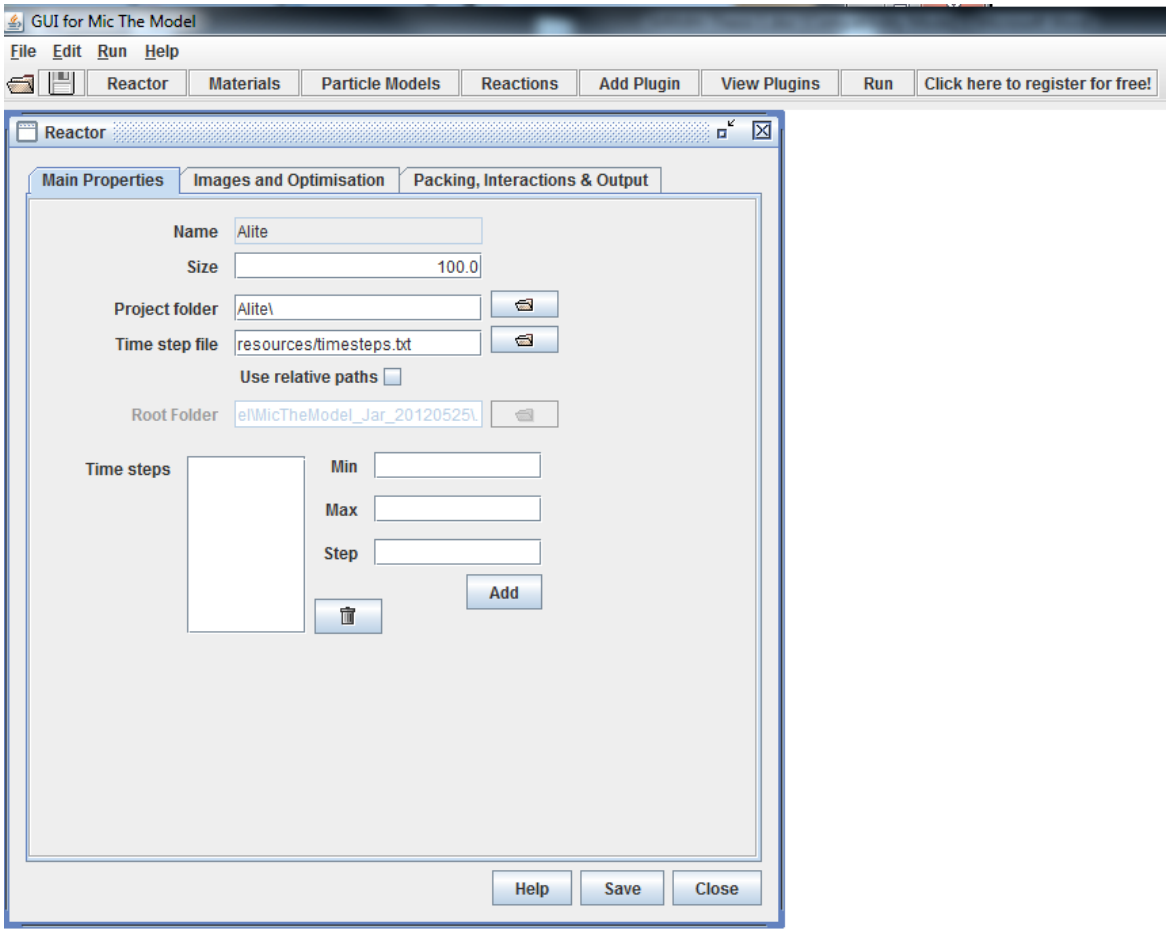

Figure 8.1 Reactor window in µic

Step 2 – Materials Defining

Clicking on the "Materials" tab, a new window is opened in which all constituents used for modeling are defined. The constituents and properties used for cement hydration modeling are summarized in Table 8.1. Initial fractions of some constituents are volume percentages of those constituents, and have been calculated through volumetric stoichiometry. Figure 8.2 also shows the Materials window in µic.

Table 8.1 Properties of all materials used for cement hydration modeling in µic

Name	Density	Initial fraction	Diffusivity	Color
Alite	3.21	0.2832	0.04	
Belite	3.28	0.0646	0.04	
Aluminate	3.03	0.0193	0.04	
C-S-H	2.00	0.0	0.04	
CH	2.20	0.0	0.04	
Ettringite	2.00	0.0	0.04	

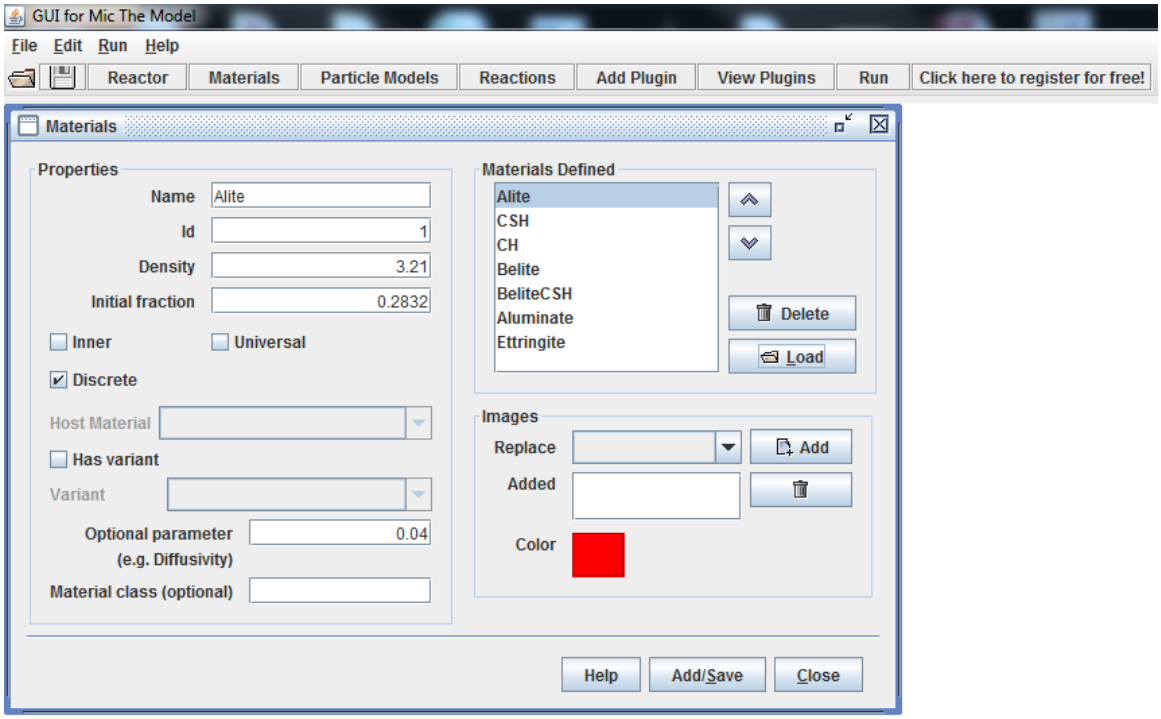

Figure 8.2 Materials window in µic

Step 3 – Particle Model

The "Particle Models" input section enables users to define reactant particles and their gradation, as well as layers of hydration products. Gradation results of different constituents are obtained by laser particle size distribution. For example, the layers of alite are alite (unreacted core C_3S) and C-S-H layer formed on the C_3S particles. Table 8.2 lists the reactants and corresponding products layers. Figure 8.3 shows a preview of Particle Models window.

Table 8.2 List of reactants and corresponding products used for modeling in μic

Reactant	Products Layer
Alite	Alite + C-S-H
Belite	Belite + C-S-H
Aluminate	Aluminate + Ettringite

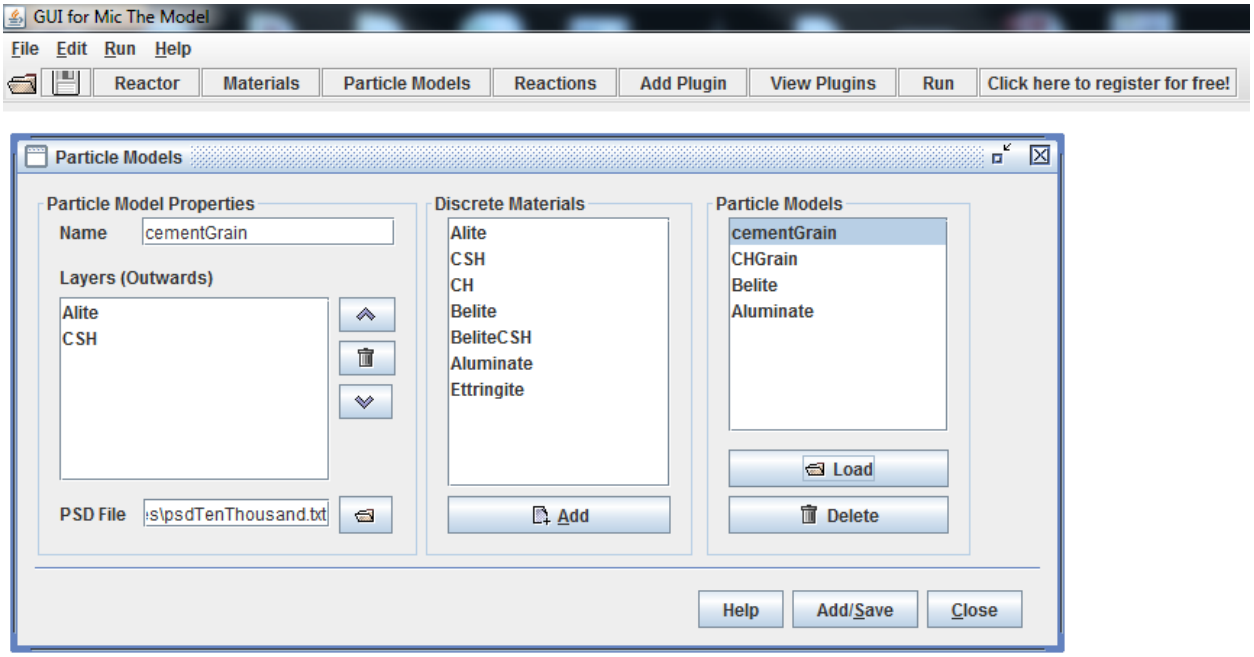

Figure 8.3 Particle Models window in μic

Step 4 – Reactions

A critical step in simulation in µic is to define reactions of different phases through mathematical equations. Hydrations of different phases of cement are typically expressed as mass equations, as previously shown in Eq. (1.1), Eq. (1.2), and Eq. (1.3). Since cement hydration is modeled in a paste cube and all fractions and calculations are volumetric-based, reactions equations should also be converted to volumetric equations. These conversions are done through stoichiometry and by assigning densities. Material densities used in this study are shown in Table 8.1. Equations (8.6), (8.7), and (8.8) show the volumetric equations for the reaction of different phases:

$$V_{C_3S} + 1.318V_H \rightarrow 1.569V_{C\text{-}S\text{-}H} + 0.593V_{CH} \qquad \text{Eq. (8.3)}$$

$$V_{C_2S} + 1.476V_H \rightarrow 2.166V_{C\text{-}S\text{-}H} + 0.189V_{CH} \qquad \text{Eq. (8.4)}$$

$$V_{C_3A} + 2.53V_{C\$H_2} + 5.27V_H \rightarrow 7.84V_{C_6A\$_3H_{32}} \qquad \text{Eq. (8.5)}$$

"Reactions" window allows users to define and customize different hydration equations. In this study, hydration equations (8.3), (8.4), and (8.5) are plugged into µic. As shown in Figure 8.4.

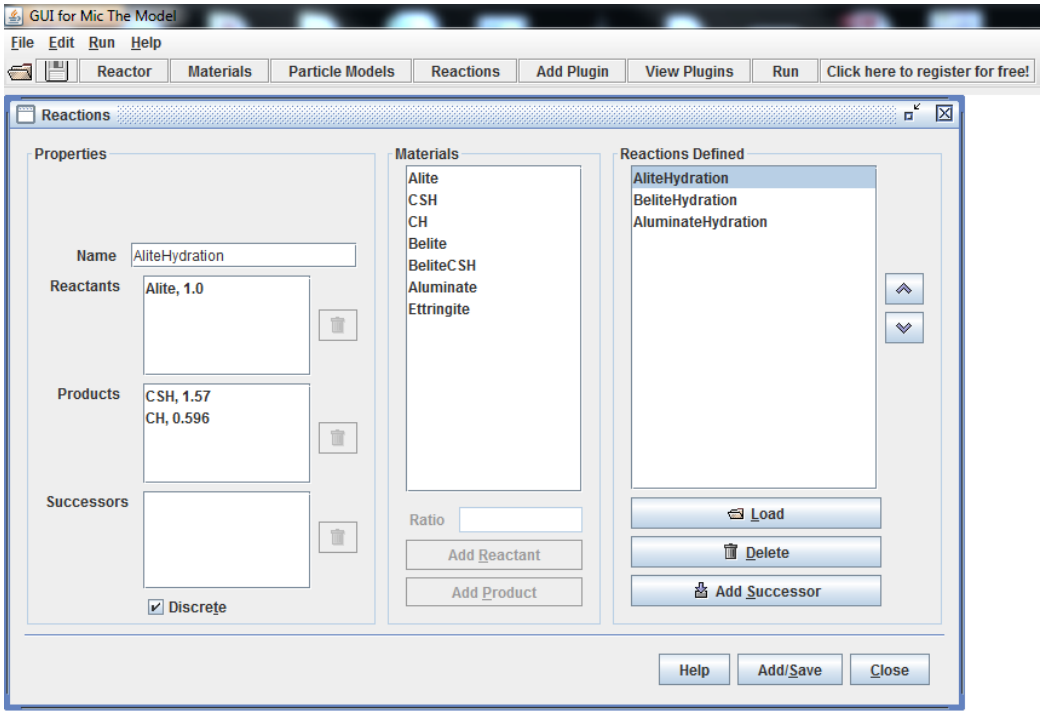

Figure 8.4 Particle Models window in µic

Step 5 – Plugins

"Plugins" is a list of several types of hydration model. Users are able to select desired model depending on objective of the modeling, or add new customized plugins in Java to the list. As mentioned earlier, this study uses Avrami model for cement hydration. Figure 8.5 shows how Avrami model is selected.

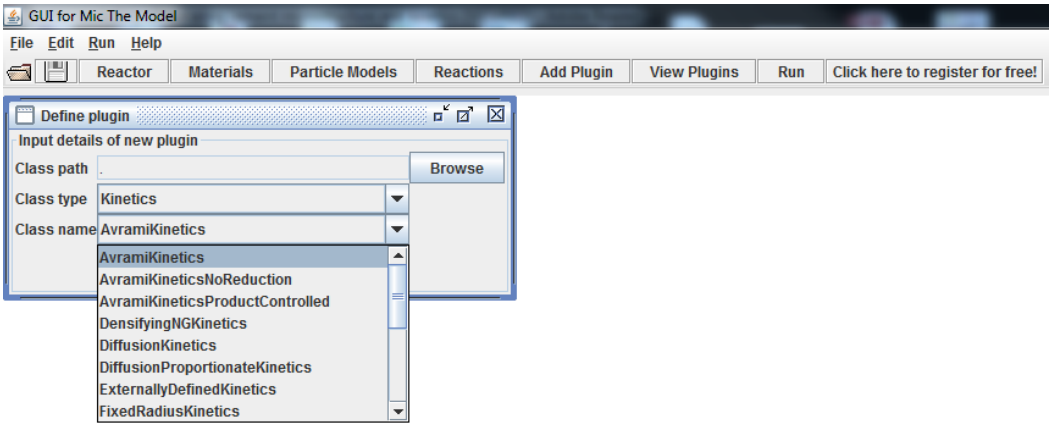

Figure 8.5 Selection of Avrami kinetics model

Then Avrami constants, starting time (set to zero), initial degree of hydration (set to zero), order of implementation of kinetics (set to one for all, as all reactions happen simultaneously), and types of reactions and reactants are determined. Figure 8.6 shows a set Avrami model for alite hydration.

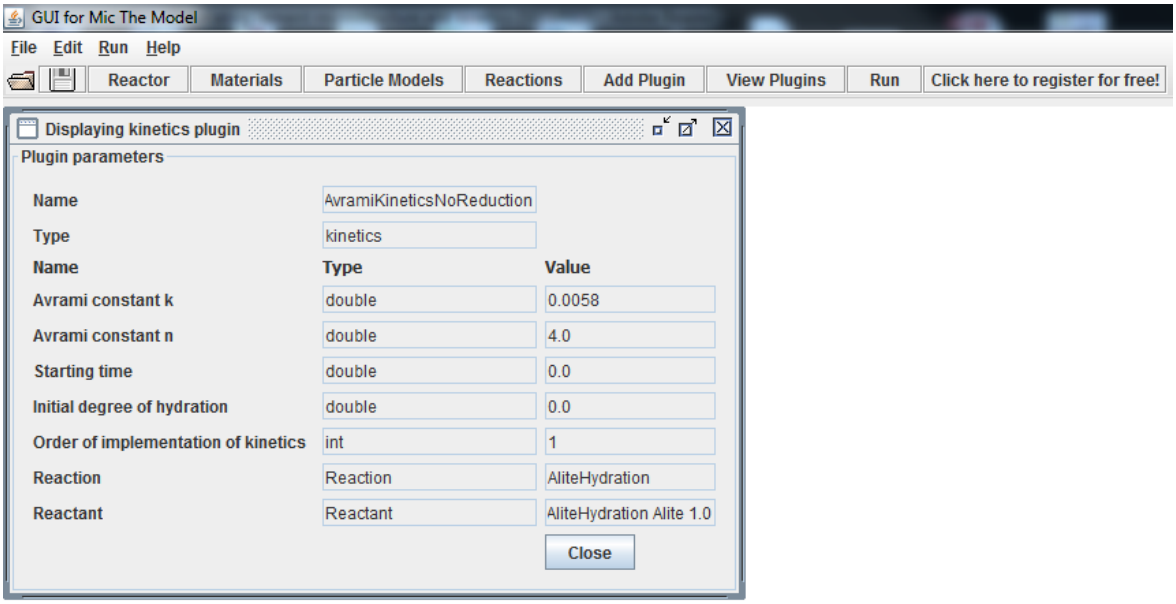

Figure 8.6 Avrami model set for alite hydration

Step 6 – View Plugins

This window allows users to control all determined plugins.

Step 7 - Run

After saving the project, users can run the model. Once the model runs, a folder in the name of project is automatically created which contains a cross section of simulated hydration at each time steps (Figure 8.7), as well as an excel file that gives the degree of hydration and changes in volume of all constituents at each time steps. The black pixels shown in Figure 8.7 are porosity.

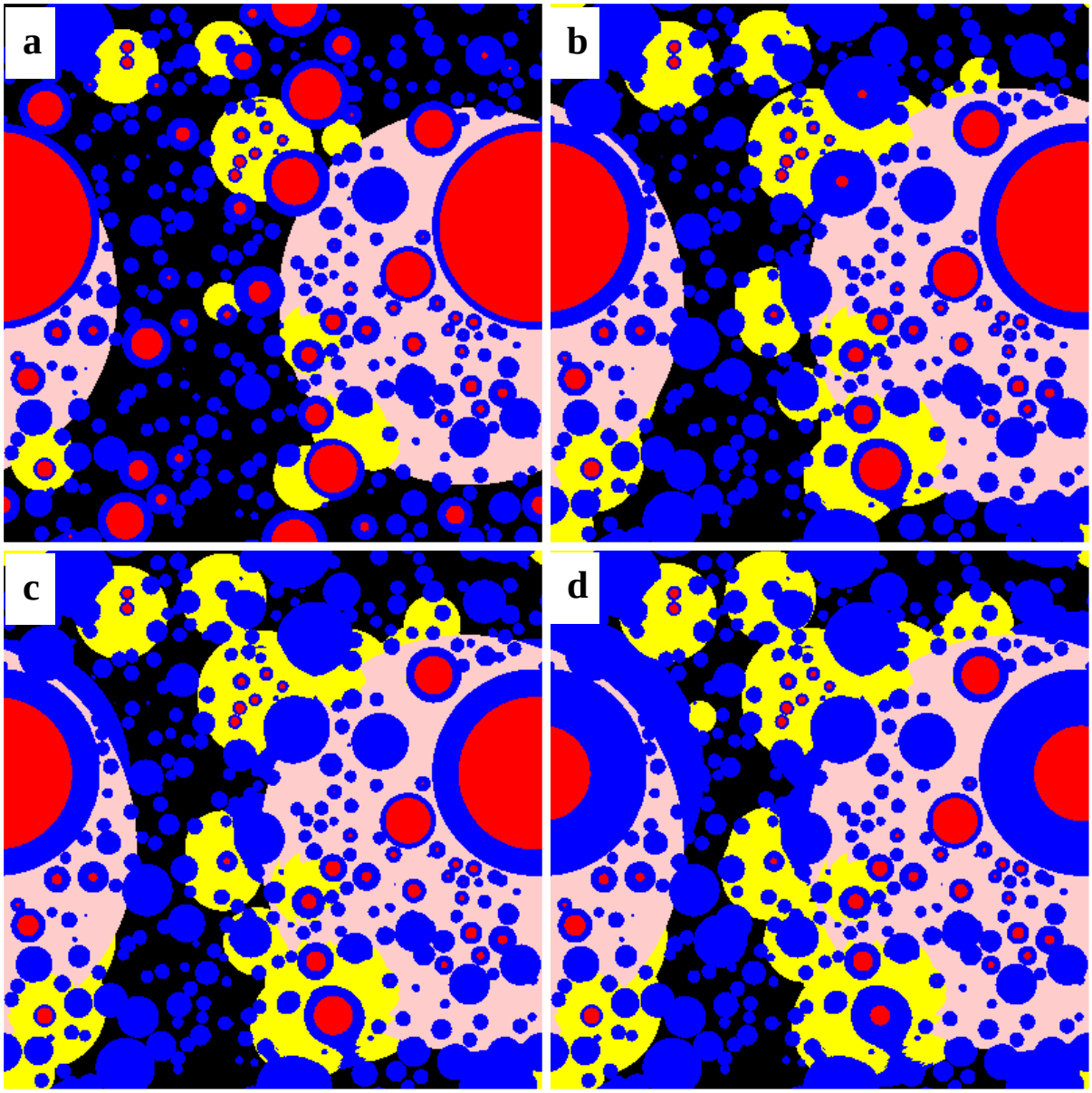

Figure 8.7 Cross sections of simulated cement hydration at 50°C: a. 1 day, b. 28 days, c. 91 days, and d. 365 days

Result of Modeling Cement Hydration

The Avrami constants found from fitting the model degree of hydration to the degree of hydration found from isothermal calorimetry for three compounds of cement are shown in Table 8.3 Figure 8.8 shows the fit obtained from the modeling to the measured data. These

values were used as fixed inputs for the next step of the modeling process: modeling glass cullet.

Table 8.3 Avrami constants of three phases obtained by μic

Name	Avrami Constants	
	k	*n*
Alite	5.8E–3	4.0
Belite	3.3E–3	4.0
Aluminate	7.0E–3	4.0

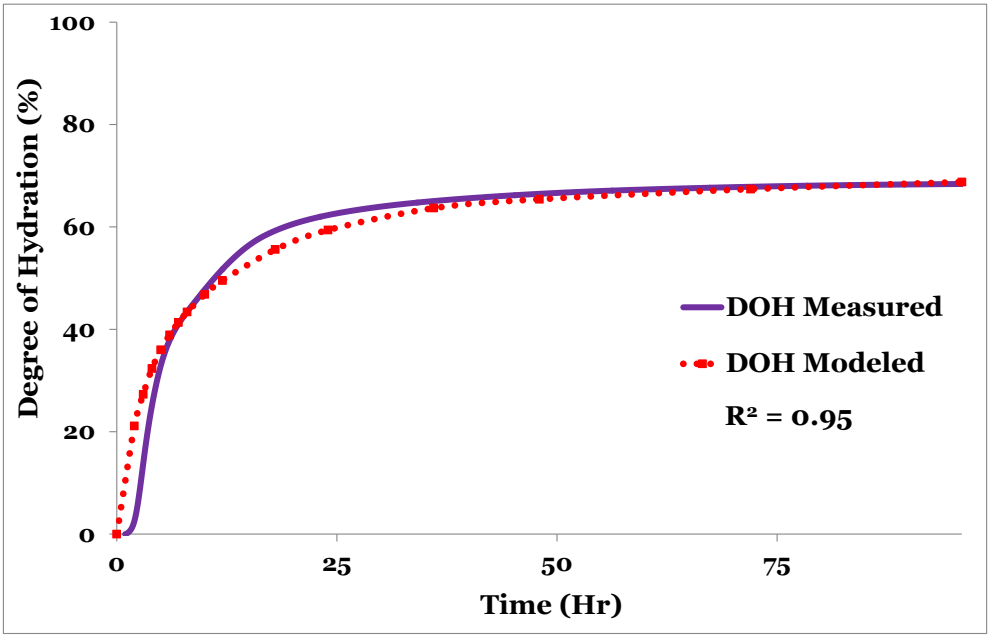

Figure 8.8 Fitting modeled to measured DOH results

Modeling of Glass Cullet Reactivity – Single type and particle size

Modeling of pozzolanic reaction of two glass types (i.e. clear and green) and one single particle size (<25 μm) of finely ground glass followed the same basic modeling steps as those explained for cement hydration modeling, with only a few alterations. Clear glass smaller than 25 μm, green glass smaller than 25 μm, and pozzolanic C-S-H were added to the previous constituents, but simulated through separate models to determine the reaction rate parameters

to use for each material by itself. Table 6.4 shows the properties of the individual types of glass in µic.

Table 8.4 Properties of glass particles used for pozzolanic reaction modeling in µic

Name	Density	Initial fraction	Diffusivity	Color
Clear < 25 µm	2.48	0.1455	0.0	
Green < 25 µm	2.50	0.1455	0.0	
Pozzolanic C-S-H	2.00	0.0	0.04	

In the "Particle Models" window, gradations of glass particles obtained from laser particle size distribution device were defined. Reactants and products layers on glass particles were also determined. Table 8.5 lists the glass reactants and corresponding hydration products.

Table 8.5 List of glass reactants and corresponding products used for modeling in µic

Reactant	Products Layer
Clear < 25 µm	G025 + C-S-HG025
Green < 25 µm	GG025 + C-S-HGG025

The pozzolanic reaction equation for glass cullet used in concrete was determined by Saeed et al. [63] and is shown determine in Eq. (8.9):

$$C_1S_{6.11}N_{1.1} + 6.15CH + 9.15H \rightarrow C_{7.15}S_{6.11}N_{1.1}H_{15.3} \qquad \text{Eq. (8.9)}$$

where N is shorthand for Na_2O. Using the material densities shown in Table 8.4 and the stoichiometric calculations from Eq. (8.9) give a volumetric-based equation shown in Eq. (8.10):

$$V_{C_1S_{6.11}N_{1.1}} + 1.027V_{CH} + 0.832V_{H} \rightarrow 2.806V_{C_{7.15}S_{6.11}N_{1.1}H_{15.3}} \qquad \text{Eq. (8.10)}$$

The last step for modelling the pozzolanic reactivity of glass cullet was to obtain the Avrami constants. These constants were attained through a trial-error process used in modeling to fit to the CH content calculated curve determined by TGA measurements.

Result of Simulation of Pozzolanic Reactivity of Glass Cullet

Clear smaller than 25 μm

Figure 8.9 shows the cross sections of simulated cementitious systems containing clear glass smaller than 25 μm. By fitting CH content modeled by μic to those measured by TGA as shown in Figure 6.10, the Avrami constants of pozzolanic reactivity of Clear glass smaller than 25 μm are k = 1.0899E–5 and n = 1.5.

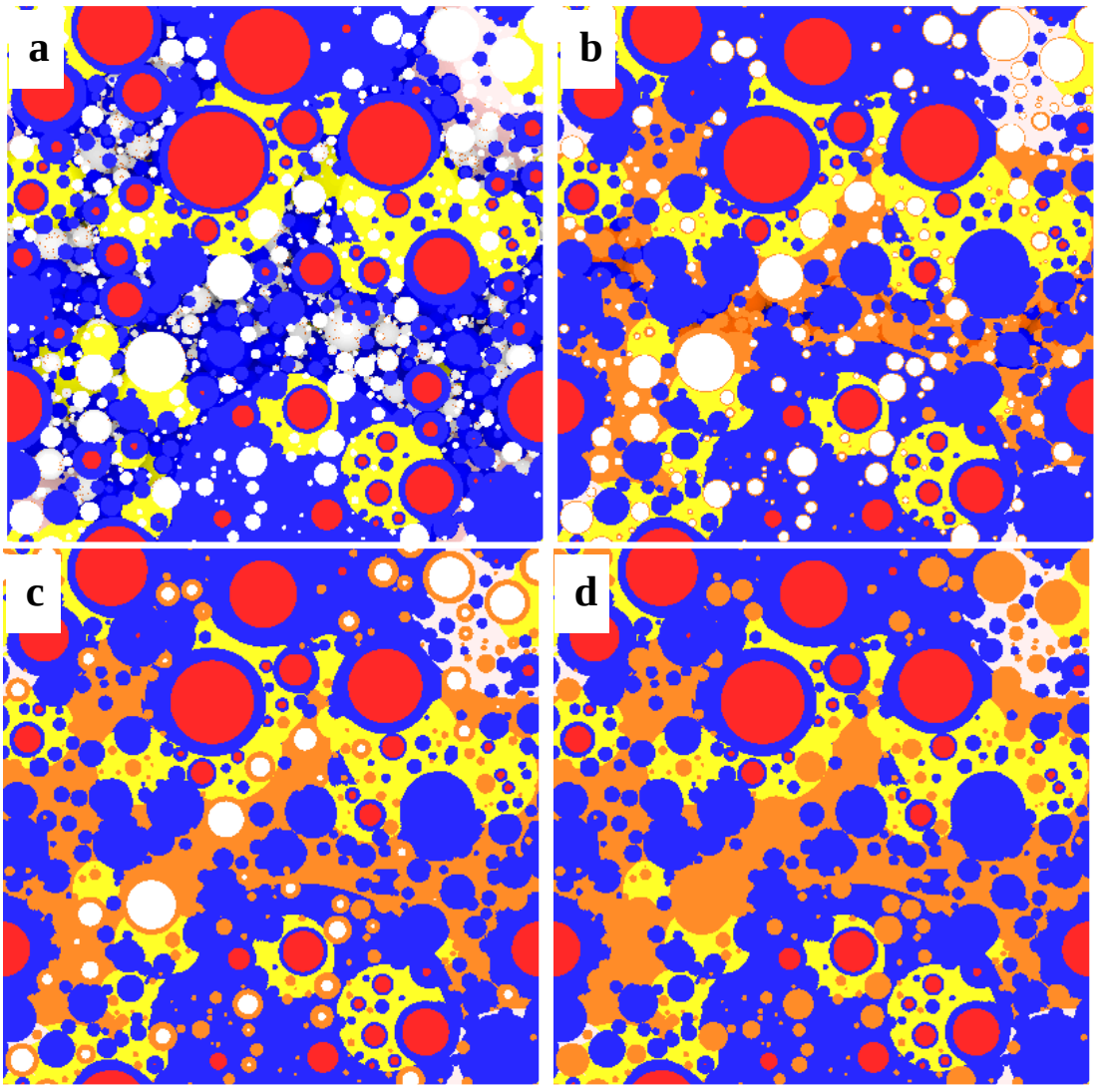

Figure 8.9 Cross sections of simulated pozzolanic reaction of Clear glass < 25 μm at 50°C: a. 1 day, b. 28 days, c. 91 days, and d. 365 days

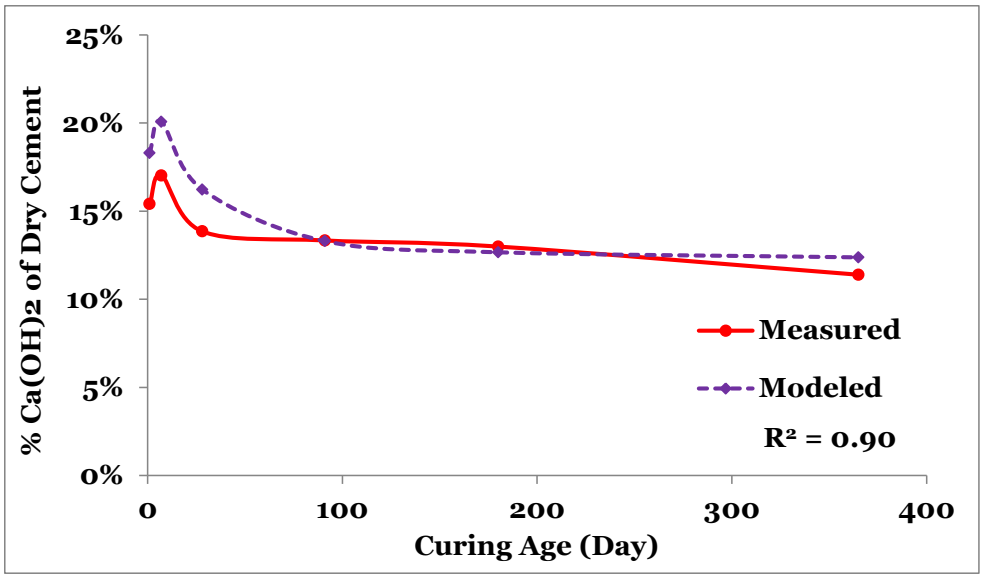

Figure 8.10 Fitting modeled to measured results of CH content for Clear glass < 25 µm at 50°C

Green smaller than 25 µm

Cross sections of simulated microstructures for cementitious systems containing green glass smaller than 25 µm are shown in Figure 8.11. Following the same method discussed for modeling clear glass, the Avrami parameters for the green glass smaller than 25 µm material were fit using the TGA measurements as shown in Figure 8.12. The Avrami parameters for the pozzolanic reactivity of Green glass smaller than 25 µm were found to be k = 1.0899E–5 and n = 1.5.

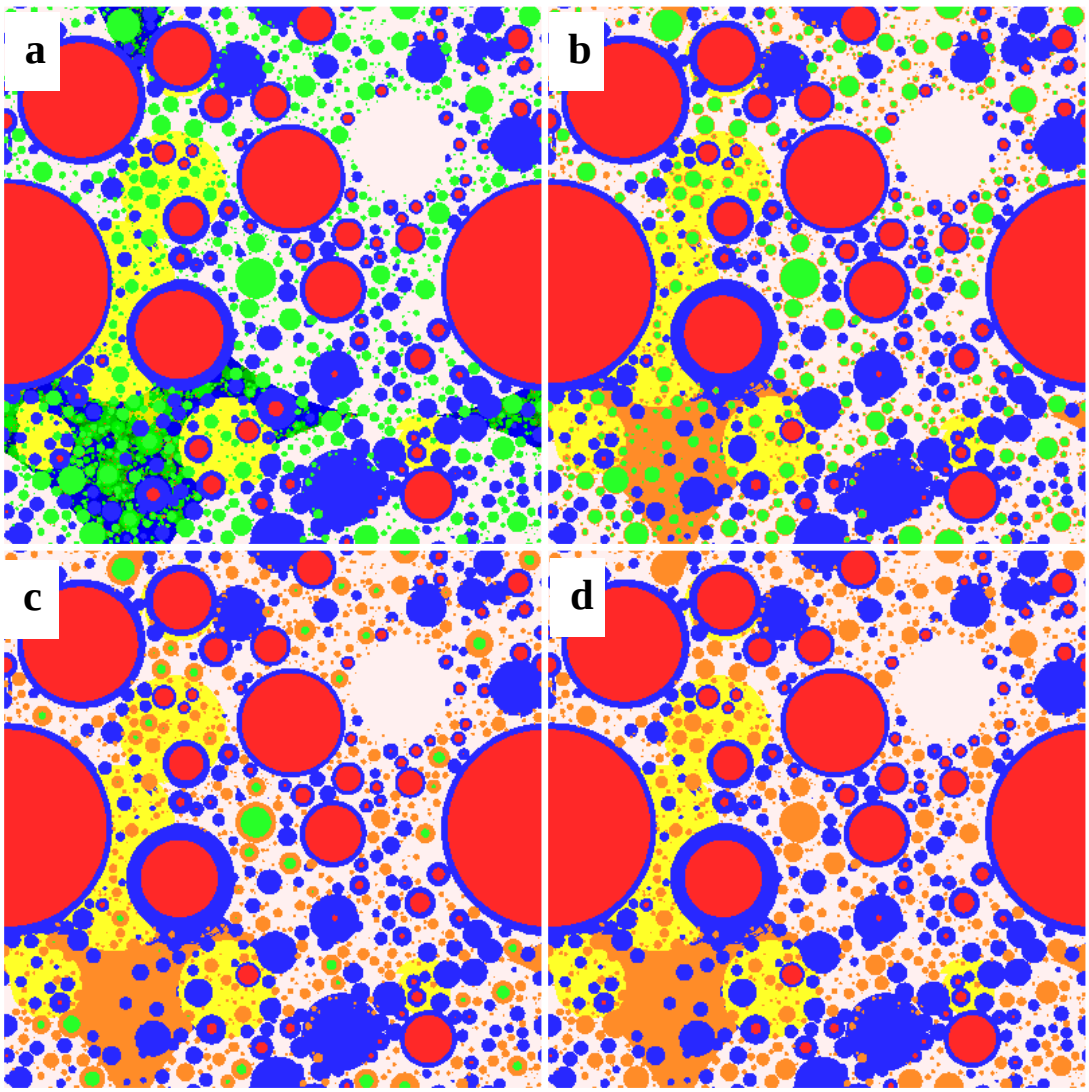

Figure 8.11 Cross sections of simulated pozzolanic reaction of Green glass < 25 µm at 50°C: a. 1 day, b. 28 days, c. 91 days, and d. 365 days

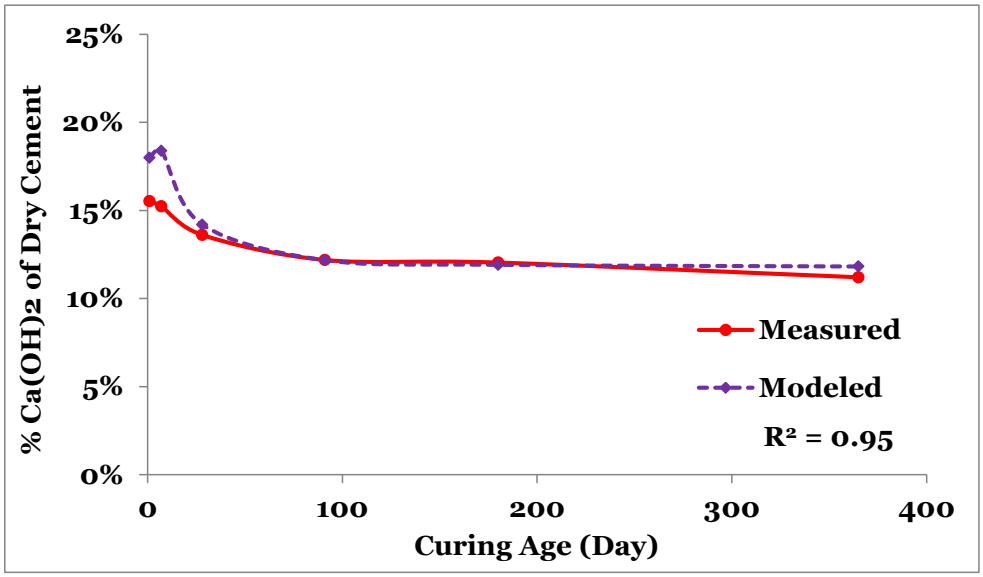

Figure 8.12 Fitting modeled to measured results of CH content for Green glass < 25 µm at 50°C

Combined glass types and particle sizes

The process of the modeling Mix 2 was the same as that previously outlined for cement and single glass particles. To model combined glass types and sizes (Mix 2), the fit Avrami constants for cement, Clear glass smaller than 25 µm, and Green glass smaller than 25 µm at 50°C obtained by modeling them in separate steps were used. The only difference between modeling Mix 2 and earlier materials is that the initial fractions of both Clear glass smaller than 25 µm and Green glass smaller than 25 µm are 0.07275 instead of 0.1455 (see Table 8.4). The first interesting point is that the modeling of Mix 2 pozzolanic reactivity was in well agreement with the calculated CH content obtained from the modeling of single particles (R^2=0.99) as shown in Figure 8.13. Results also showed that simulation for Mix 2 was not satisfactory and the differences between measured and modeled values are significant. In other words, the effect of particle sizes of on glass cullet pozzolanic reactivity could not be accounted for through linear addition as expected to be obtained by microstructural modeling. This

discrepancy might be caused by some errors in Avrami constants attained in modeling of cement and single glass particles. Another possible explanation for inaccurate modeling is the effect of elevated curing temperatures on reactivity and mechanical properties of cementitious systems containing Mix 2. As explained earlier, Mix 2 physical properties do not follow the linear-addition behavior. In other word, elevated curing temperatures is an important parameter not only in reactivity and mechanical properties of concrete containing mixed types and sizes of glass, but also in microstructural modeling.

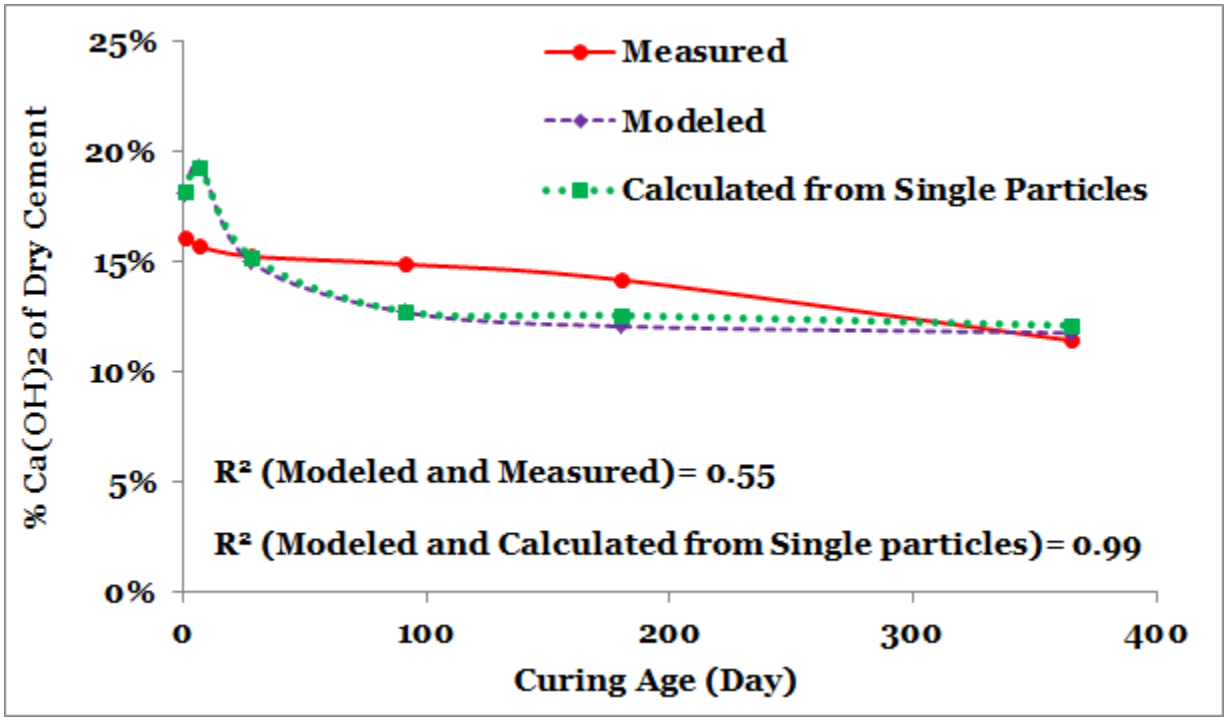

Figure 8.13 Fitting modeled to measured results of CH content for Mix 2 at 50°C

Chapter 9 - Conclusions and Recommendations

Conclusions

The objective of this study was to investigate how different glass particle size ranges and types, as well as various combinations of types and particle sizes of glass cullet as a SCM affect the reaction kinetics, microstructure, and performance of cementitious mixtures at varying temperatures. This study is the first research investigating the interactions between different particle sizes and types of glass cullet as SCM and their effects on performance and mechanical properties of cementitious mixtures. Based on experimental and modeling results, the findings from this study can be summarized as follows:

1- Curing temperature is one of the foremost factors affecting the pozzolanic behavior of glass cullet. The results of apparent activation energy calculation showed that glass, especially green glass, is temperature sensitive and has a higher tendency to participate in the pozzolanic reaction. This result is evidenced by a 9% increase in apparent activation energy, up to 70% reduction in portlandite content, and 22% increase in compressive strength at elevated temperature after 91 days of curing. In the case of cementitious systems containing mixed glass, the rate of reaction and pozzolanic reactivity are higher at elevated temperature.

2- Among three size ranges of glass cullet, smaller than 25 μm has considerable pozzolanic behavior even at one day, especially at 50°C, evidenced by the reduction in CH content of samples containing glass with an increased heat of hydration at 1 day. After seven days, calcium hydroxide content is noticeably reduced, reflecting higher pozzolanicity. This finding correlates well with the results of SEM imaging,

compressive strength, and water sorptivity tests. Portlandite content reduction can be explained by much higher surface area of smaller than 25 µm particles than other size ranges. Cementitious systems containing Mix 4 (Clear63-75µm+Green63-75µm) had the least reactivity, followed by Mix 3 (Clear63-75µm+Clear<25µm), Mix 1 (Green63-75µm+Green<25µm), and Mix 2 (Clear<25µm +Green<25µm) which was the most reactive combination. The simultaneous effect of mixing particle size, which is considered as surface area, on glass hydration kinetics could be accounted for through a linear addition.

3- Part of the reactivity of the cementitious system at low temperatures can be attributed to calcium carbonate; as AF_m phases containing calcium carbonate were shown to react faster at lower temperatures.

4- As evidenced by bottle leaching test results at various temperatures, dissolution tendency of aluminum and silica at pH ranges similar to concrete (i.e. 12.5 – 13.5) could be accounted for by the particle surface area. Thus, the alumina and silica ions of the finest glass particles (smaller than 25 µm which has the highest surface area) have a higher propensity to dissolve in pore solution which must occur before the glass can react, possibly accounting for another explanation for higher reactivity of smaller than 25 µm particles, specifically green glass and especially at 50°C.

5- The results of SEM image analysis indicated that hydration degrees of single glass cullet types and sizes, as well as combined glass cullet increase with an increase in curing temperature and reductions in particle size distribution result in more and denser C-S-H. The concurrent effect of types and particle sizes of glass cullet on

inner C-S-H density, accounted for as surface area, could be expressed as a linear addition.

6- Surface area is considered as an important factor on glass reactivity. Based on the findings, reaction kinetics, dissolution of silica and aluminum, and compressive strength could be directly correlated to the surface area through linear addition.

7- Rietveld refinement was used to quantify the portland cement degree of hydration and showed not only showed that increase in HOH and chemical shrinkage at later ages is the result of the glass pozzolanic reaction, but also verified that pozzolanic reaction is more pronounced for smaller particle sizes.

8- While mortar samples with glass cullet showed the cross-over effect on water absorption from 1 day to 91 days at 50°C, mortar samples containing glass powder for both the single particle size and type or combined types and size ranges, especially green smaller than 25 μm and Mix 2, had much lower water sorptivity at 91 days at 50°C, showing that using very finely ground glass cullet as SCM diminishes the cross-over effect.

9- Although the effect of particle sizes and types of glass cullet on reaction rate, pozzolanic reaction, and compressive strength at ambient temperatures could be accounted for by linear addition, their effect on compressive strength at elevated temperatures was markedly different, since compressive strength is mainly a function of pores size distribution and not just total amount of reaction. Due to more and larger pores creating weaker plane at elevated temperatures, compressive strength results of mixed glass were similar to those of weaker planes, and were not accounted for through linear correlation.

10- Some minor errors were seen in modeling cement and glass particles, especially at early ages. Despite acceptable fits of single type and size of glass cullet, microstructural modeling could not verify that the effect of particle size distribution on pozzolanicity of glass powder is linear. This inaccuracy can be attributed not only to some inherent limitations of microstructural modeling such as limited knowledge about mechanisms of hydration kinetics, but also to accumulation of minor errors in earlier steps of modeling, effects of some important factors such as curing temperatures and gradation, and accuracy of reaction equations.

Recommendations for Future Work

Although this study can address many aspects of performance and mechanical properties of cementitious mixtures containing finely ground glass cullet as SCM, it seems that a large body of works is still needed to comprehensively investigate the effect of using glass cullet in concrete. Recommendations for further research are:

1- The influence of pozzolanic reactivity of glass cullet on durability properties of concrete was beyond the scope of this research. It is strongly recommended that the long-term durability impacts of different types and size ranges of glass cullet and curing temperatures on concrete are investigated through lab research and field study to obtain better understanding of deterioration mechanisms for the concrete containing glass and to find best way to mitigate possible damages. Some mechanisms that deserve further research include salt scaling, sulfate attack, and ASR. ASR is a concern because a large amount of alkalis present in the glass.

2- To obtain a more accurate understanding of the effect of porosity on mechanical properties of concrete containing glass as SCM, it is recommended that a comprehensive research is done (e.g. Mercury Intrusion Porosimetry ASTM D4404-10) to study how different pore sizes, distribution, connectivity, and tortuosity can affect strength of cementitious materials containing glass cullet and how to account for these effects.

3- Ternary blends of glass cullet with other SCMs such as fly ash or slag could be considered as a mitigation method for ASR. It is recommended that the effect of combinations of glass cullet with other types of SCMs on durability be investigated.

4- With regard to microstructural modeling, it is recommended that a comprehensive stoichiometry study is performed on pozzolanic reaction of glass cullet to obtain a precise equation which can be used in microstructural modeling platforms like µic.

5- It is also recommended that a life-cycle analysis is performed to quantify economic and environmental benefits of glass as an SCM.

References

[1] Topçu, I. B., and Canbaz, M. (2004). Properties of concrete containing waste glass, Cement and Concrete Research, vol. 34, pp. 267-274.

[2] Shao, Y., Lefort, T., Moras, S., and Rodriguez, D. (2000). Studies on Concrete Containing Ground Waste Glass. Cement and Concrete Research, vol. 30(1), pp. 91-100.

[3] Byars, E. A., Morales-Hernandez, B., and Zhu, H. Y. (2004). Waste Glass as Concrete Aggregate and Pozzolan, Concrete, vol. 38(1), pp. 41-44.

[4] Shi, C., and Zheng, K. (2007). A Review on the Use of Waste Glasses in the Production of Cement and Concrete. Resources, Conservation and Recycling, vol. 52(2), pp. 234-247.

[5] Meyer, C. (2001). Recycled Glass - From Waste Material to Valuable Resource, Proceedings of the International Syposium: Recycling and reuse of Glass Cullet, Dundee, Scotland, pp. 1-10.

[6] Shao, Y., and Lehoux, P. (2001). Feasibility of Using Ground Waste Glass as a Cementitious Material, Proceedings of the International Syposium: Recycling and reuse of Glass Cullet, Dundee, Scotland, pp. 209-219.

[7] Dyer, T. D., and Dhir, R. K. (2001). Chemical Reactions of Glass Cullet Used as Cement Component. Journal of Material of Civil Engineering, vol. 13(6), pp. 412-417.

[8] Shayan, A., and Xu, A. (2004). Value-added Utilization of Waste Glass in Concrete. Cement and Concrete Research, vol. 34(1), pp. 81-89.

[9] Shayan, A., and Xu, A. (2006). Performance of Glass Powder as a Pozzolanic Material in Concrete: A Field Trial on Concrete Slabs. Cement and Concrete Research, vol. 36(3), pp. 457-468.

[10] Pereira-de-Oliveira, L. A., Castro-Gomes, J. P., and Santos, P. M. S. (2012). The Potential Pozzolanic Activity of Glass and Red-clay Ceramic Waste as Cement Mortars Components. Construction and Building Material, vol. 31, pp. 197-203

[11] Schwarz, N., and Neithalath, N. (2008). Influence of a fine glass powder on cement hydration: Comparison to fly ash and modeling the degree of hydration. Cement and Concrete Research, vol. 38, pp. 429-436

[12] United Nation Environmental Program (UNEP) (2010). Greening Cement Production has a Big Role to Play in Reducing Greenhouse Gas Emissions. http://na.unep.net/geas/getUNEPPageWithArticleIDScript.php?article_id=57 (downloaded on March 14, 2014)

[13] Van Oss, H. G. (2011). USGS Mineral Program Cement Report. United States Geological Survey (USGS) Report, pp. 38-39.

[14] Kosmatka, S. H., Kerkhoff, B., and Panarese, W. C. (2003). Design and Control of Concrete Mixtures, Portland Cement Association, 14th Edition, USA, pp. 360.

[15] Lin, F., and Meyer C. (2009). Hydration kinetics modeling of Portland cement considering the effects of curing temperature and applied pressure, Cement and Concrete Research, vol. 39, pp. 255–265.

[16] Kirby, D. M., and Biernacki, J. J. (2012). The effect of water-to-cement ratio on the hydration kinetics of tricalcium silicate cements: Testing the two-step hydration hypothesis, Cement and Concrete Research, vol. 42, pp. 1147–1156.

[17] Bishnoi, S. (2008). Vector Modelling of Hydrating Cement Microstructure and Kinetics, Doctoral Thesis, Swiss Federal Institute of Technology in Lausanne, Laboratory of Materials of Construction, pp. 166.

[18] Bullard, J. W., Jennings, H. M. , Livingston, R. A., Nonat, A., Scherer, G. W., Schweitzer J. S., Scrivener, K. L., and Thomas, J. J. (2011). Mechanisms of cement hydration, Cement and Concrete Research, vol. 41, pp. 1208–1223.

[19] Stein, H. N., and Stevels J. M. (1964). Influence of silica on the hydration of 3CaO, SiO_2, J. Appl. Chem., vol. 14, vol. 338–346.

[20] Juilland, P., Gallucci, E., Flatt, R., and Scrivener, K. (2010). Dissolution theory applied to the induction period in alite hydration, Cement and Concrete Research, vol. 40, pp. 831–844.

[21] Gartner, E. M., and Gaidis, J. M. (1989). Hydration mechanisms, I, in: J. Skalny (Ed.), Materials Science of Concrete, Vol. 1, American Ceramic Society, Westerville, OH, pp. 95–125.

[22] Garrault, S., and Nonat, A. (2001). Hydrated layer formation on tricalcium and dicalcium silicate surfaces: experimental study and numerical simulations, Langmuir, vol. 17, pp. 8131–8138.

[23] Garrault-Gauffinet, S., and Nonat, A. (1999). Experimental investigation of calcium silicate hydrate (C–S–H) nucleation, J. Cryst. Growth, vol. 200, pp. 565–574.

[24] Damidot, D., Nonat, A., and Barret P. (1990). Kinetics of tricalcium silicate hydration in diluted suspensions by microcalorimetric measurements, J. Am. Ceram. Soc., vol. 73(11), pp. 3319–3322.

[25] Arvidson, R. S., Fischer, C., and Luttge, A. (2009). Resolution of crystal dissolution and growth processes at multiple scales, Geochim. Cosmochim. Acta, vol. 72 (12), A34.

[26] Damidot, D., Bellmann, F., Möser, B., and Sovoidnich, T. (2007). Calculation of the dissolution rate of tricalcium silicate in several electrolyte compositions, Cement WapnoBeton, vol. 12/74 (2), pp. 57–67.

[27] Ménétrier, D., Jawed, I., Sun, T. S., and Skalny J. (1979). ESCA and SEM studies on early C_3S hydration, Cem. Concr. Res., vol. 9, pp. 473–482.

[28] Tadros, M. E., Skalny, J., Kalyoncu, R. S. (1976). Early hydration of tricalcium silicate, Journal of the American Ceramic Society, vol. 59 (7–8), pp. 344–347.

[29] Young, J. F., Tong, H. S., and Berger, R. L. (1977). Compositions of solutions in contact with hydrating tricalcium silicate pastes, Journal of the American Ceramic Society, vol. 60 (5–6), pp. 193–198.

[30] Damidot, D., and Nonat, A. (1994). C_3S hydration in diluted and stirred suspensions: (I) study of the two kinetic steps, Advances in Cement Research, vol. 6 (21), pp. 27–35.

[31] Barret, P., and Ménétrier, D. (1980). Filter dissolution of C_3S as a function of lime concentration in a limited amount of lime water, Cement and Concrete Research, vol. 10, pp. 521–534.

[32] Kondo, R., and Ueda, S. (1968). Kinetics of hydration of cements, Proceedings of the 5th international symposium on chemistry of cement, Tokyo, pp. 203-248.

[33] Pommersheim, J. M., and Clifton, J. R. (1979). Mathematical modeling of tricalcium silicate hydration, Cement and Concrete Research, Vol. 9, pp. 765-770.

[34] Gartner, E. M., and Gaidis, J. M. (1989). Hydration mechanisms, I, in: J.P. Skalny (Ed.), The Materials Science of Concrete, I, American Ceramic Society, pp. 95–125.

[35] Jennings, H. M., and Pratt, P. L. (1979). An experimental argument for the existence of a protective membrane surrounding Portland cement during the induction period, Cement and Concrete Research, vol. 9, pp. 501–506.

[36] Xie, T., and Biernacki, J. J. (2011). The origins and evolution of cement hydration models, Comp. Concr., vol. 8(6), pp. 647–675.

[37] Garrault, S., Behr, T., and Nonat, A. (2006). Formation of the C-S-H layer during early hydration of tricalcium silicate grains with different sizes, Journal of Physical Chemistry, Vol. 110, pp. 270-275.

[38] Bishnoi, S., and Scrivener, K. L. (2009). μic: a new platform for modeling the hydration of cements, Cem. Concr. Res., vol. 39(4), pp. 266–274.

[39] Bishnoi, S., and Scrivener, K. L. (2009). Studying nucleation and growth kinetics of alite hydration using μic, Cem. Concr. Res., vol. 39(10), pp. 849–860.

[40] Van Breugel, K. (1991). Simulation of hydration and formation of structure in hardening cement-based materials, PhD Thesis, Delft University of Technology, The Netherlands.

[41] Danielson, U. (1962). Heat of hydration of cement as affected bywater–cement ratio, Paper IV-S7, Proceedings of the 4th International Symposium on the Chemistry of Cement, Washington DC, USA, pp. 519–526.

[42] Taplin, J. H. (1969). A method for following hydration reaction in Portland cement paste, Australian Journal of Applied Sciences, vol. 10, pp. 329–345.

[43] Bresson, B., Meducin, F., and Zanni, H. (2002). Hydration of tricalcium silicates (C_3S) at high temperature and high pressure, Journal of Materials Science, vol. 37(24), pp. 5355–5365.

[44] Zhou, Q., and Beaudoin, J. J. (2003). Effect of applied hydrostatic stress on the hydration of Portland cement and C_3S, Advances in Cement Research, vol. 15(1), pp. 9–16.

[45] Knudsen, T. (1982). Modeling hydration of portland cement — the effect of particle size distribution, *in:* Young, J. F. (Ed.). Characterization and performance prediction of cement and concrete, United Engineering Trustees, Inc., New Hampshire, USA, pp. 125–150.

[46] Frigione, G., and Marra, S. (1976). Relationship between particle size distribution and compressive strength in Portland cement, Cement and Concrete Research, vol. 6(1), pp. 113–127.

[47] Bezjak, A. (1986). An extension of the dispersion model for the hydration of Portland cement, Cement and Concrete Research, vol. 16 (2), pp. 260–264.

[48] Lerch, W., and Ford, C. L. (1948). Long-term study of cement performance in concrete: chapter 3, Chemical and physical tests of the cements, ACI Journal, vol. 19(8), pp. 745–795.

[49] Escalante-Garcia, J. I. (2003). Nonevaporable water from neat OPC and replacement materials in composite cements hydrated at different temperatures, Cement and Concrete Research, vol. 33(11), pp. 1883–1888.

[50] Bentur, A., Berger, R. L., Kung, J. H., Milestone, N. B., and Young J. F. (1979), Structural properties of calcium silicate pastes: II, effect of the curing temperature, Journal of the American Ceramic Society, vol. 62(7–8), pp. 362–366.

[51] Chenevert, M. E., and Shrestha, B. K. (1991). Chemical shrinkage properties of oilfield cements, SPE Drilling Engineering, vol. 6(1), pp. 37–43.

[52] Hill, J., Whittle, B. R., Sharp, J. H., and Hayes, M. (2003). Effect of elevated curing temperature on early hydration and microstructure of composites, Proceedings of the Materials Research Society Symposium, vol. 757, pp. 699–703.

[53] Worrell, E., Price, L., Martin, N., Hendriks, C., and Meida, L. O. (2001). Carbon dioxide emissions from the global cement industry, Annual Review of Energy and the Environment, vol. 26, pp. 303-329.

[54] Lothenbach, B., Scrivener, K., Hooton, R. D. (2011). Supplementary cementitious materials, Cement and Concrete Research, vol. 41, pp. 1244–1256.

[55] National Ready Mixed Concrete Association (NRMCA) (2000). Concrete in Practice; What, why & how?, CIP 30 – Supplementary Cementitious Materials.

[56] ASTM (2012). Standard specification for coal fly ash and raw or calcined natural pozzolan for use in concrete. ASTM C618-12a, pp. 5.

[57] Folliard, K. J., Juenger, M., Schindler, A., Riding, K., Poole, J., Kallivokas, L. F., Slatnick, S., Whigham, J., and Meadows, J. L. (2008). Prediction model for concrete

behavior. Report No. FHWA/TX-08/0-4563-1, Texas Department of Transportation, pp. 78.

[58] Mak, S. L. (2000) Thermal reactivity of slag cement binders and the response of high strength concretes to in-situ curing conditions. Materials and Structures, vol. 33, pp. 29-37.

[59] Naik, T. R., and Kraus R. N. (2002). Temperature effects on high-performance concrete, 6th International Symposium on "Utilization of High Strength/High Performance Concrete", Report No. CBU-2002-07, Leipzig, Germany, pp. 1-18.

[60] United States Environmental Protection Agency (EPA) (2010). Municipal solid waste in the United States: 2009 Facts and Figures. Report No. EPA530-R-10-012.

[61] United States Environmental Protection Agency (EPA) website (2013). http://www.epa.gov/ wastes/conserve/materials/glass.htm. November 1st.

[62] Keep America Beautiful website (2013). http://www.kab.org/site/PageServer?pagename= Recycling_Facts_and_Stats, November 1st.

[63] Saeed, H. A., Ebead, U. A., Tagnit-Hamou, A., and Neale, K. W. (2011). Stoichiometric study of activated glass powder hydration. Advances in Cement Research, vol. 24(2), pp. 91-101.

[64] Johnson, C. D. (1974). Waste glass as coarse aggregate for concrete. J. Test. Eval., vol. 2(5), pp. 344–350.

[65] Figg, J. W., (1981). Reaction between cement and artificial glass in concrete. 5th Int. Conf. on Concrete Alkali Aggregate Reactions (ICAAR), pp. 252–257.

[66] Rajabipour, F., Maraghechi, H., and Fischer, G. (2010). Investigating the Alkali-Silica Reaction of Recycled Glass Aggregates in Concrete Materials, J. Mater. Civ. Eng., vol. 22, pp. 1201-1208.

[67] Tagnit-Hamou, A., and Bengougam, A. (2012). The Use of Glass Powder as Supplementary Cementitious Material. Concrete International, vol. 34(3), pp. 56.

[68] Shi, C., Wu, Y., Riefler, C., and Wang, H. (2005). Characteristics and Pozzolanic Reactivity of Glass Powders. Cement and Concrete Research, vol. 35(5), pp. 987-993.

[69] Nassar, R., and Soroushian, P. (2011). Field Investigation of Concrete Incorporating Milled waste Glass, Journal of Solid Waste Technology and Management, vol. 37(4), pp. 307-319.

[70] Bajad, M. N., Modhera, C. D., and Desai, A. K. (2011). Effect of Glass on Strength of Concrete Subjected to Sulphate Attack, International Journal of Civil Engineering Research and Development, vol. 1(2). pp. 1-13.

[71] Meena, A., and Singh, R. (2012). Comparative Study of Waste Glass Powder as Pozzolanic Material in Concrete, Bachelor Thesis, Department of Civil engineering, National Institute of Technology, Rourkela, India, pp. 46.

[72] Kou, S. C., and Xing, F. (2012). The Effect of Recycled Glass Powder and Reject Fly ash on the Mechanical Properties of fiber-reinforced Ultralight Performance Concrete, Advances in Material science and Engineering, pp. 8.

[73] Federico, L. (2013). Waste Glass – A Supplementary Cementitious Material, Ph.D. Dissertation, Department of Civil engineering, McMaster University, Hamilton, Ontario, Canada, pp. 99.

[74] Chini, A. R., Muszynski, L. C., Acquaye, L., and Tarkhan, S. (2003). Determination of Maximum Placement and Curing Temperatures in Mass Concrete to Avoid Durability Problems and DEF, Florida Department of Transportation, Final Report, pp. 167.

[75] Thomas, J. J., Biernacki, J. J., Bullard, J. W., Bishnoi, S., Dolado, J. S., Scherer, G. W., and Luttge, A. (2011). Modeling and simulation of cement hydration kinetics and microstructure development. Cement and Concrete Research, vol. 41, pp. 1257–1278.

[76] Pommersheim, J. M., and Clifton, J. R. (1979). Mathematical modeling of tricalcium silicate hydration, Cem. Concr. Res, vol. 9, pp. 765–770.

[77] Parrot in 2796: Parrot, L. J., and Killoh, D. C. (1984). Prediction of cement hydration, Br. Ceram. Proc., vol. 35, pp. 41–53.

[78] Tomosawa, F. (1997). Development of a Kinetic Model for Hydration of Cement, in: H. Justnes (Ed.), Proceedings of the Tenth International Congress on the Chemistry of Cement, Göteburg, Sweden.

[79] Tenoutasse, N., and De Donder, A. (1970). The kinetics and mechanism of hydration of tricalcium silicate, Silicates Ind., vol. 35, pp. 301–307.

[80] Brown, P. W., Pommersheim, J. M., and Frohnsdorff, G. (1985). A kinetic model for the hydration of tricalcium silicate, Cem. Concr. Res., vol. 15, pp. 35–41.

[81] Gartner in 2796: Gartner, E. M., and Gaidis, J. M. (1989). Hydration Mechanisms, I, in: J.P. Skalny (Ed.), Materials Science of Concrete, American Ceramic Society, Westerville, OH, pp. 95–125.

[82] Cahn, J. W. (1956). The kinetics of grain boundary nucleated reactions, Acta Metall. vol. 4, pp. 449–459.

[83] Thomas, J. J. (2007). A new approach to modeling the nucleation and growth kinetics of tricalcium silicate hydration, J. Am. Ceram. Soc., vol. 90, pp. 3282–3288.

[84] Frohnsdorff, G. J. C., Freyer, W. G., and Johnson P. D. (1968). The Mathematical Simulation of Chemical, Physical and Mechanical Changes Accompanying the Hydration of Cement, 5th Int. Congr. Chem. Cem., Tokyo, vol. 2, p. 321.

[85] Van Breugel, K. (1995). Numerical simulation of hydration and microstructural development in hardening cement paste (II): applications, Cem. Concr. Res., vol. 25, pp. 522–530.

[86] Bentz, D. P., and Garboczi E. J. (1991). A digitized simulation model for microstructural development, Ceram. Trans., vol. 16, pp. 211–226.

[87] Bullard, J. W. (2007). A three-dimensional microstructural model of reactions and transport in aqueous mineral systems, Modell. Simul. Mater. Sci. Eng., vol. 15, pp. 711–738.

[88] Navi, P., and Pignat, C. (1996). Simulation of cement hydration and the connectivity of the capillary pore space, Advanced Cement Based Materials, vol. 4, pp. 58-67.

[89] ASTM (2012). Standard Specification for Portland Cement. ASTM C150/150M, pp. 9.

[90] ASTM (2012). Standard Test Method for Compressive Strength of Hydraulic Cement Mortars (Using 2-in. or [50-mm] Cube Specimens), ASTM C109M, pp. 10.

[91] Riding, K., Silva, D. A., and Scrivener, K. (2010). Early age strength enhancement of blended cement systems by CaCl2 and diethanol-isopropanolamine. Cement and Concrete Research, vol. 40, pp. 935-946.

[92] Mehta, P. K. (2009). Global Concrete Industry Sustainability. Concrete International, vol. 31(2), pp. 45-48.

[93] Russ, J. C. (1986). Practical Stereology, Springer, pp. 196.

[94] Poole, J. L., Riding, K. A., Folliard, K. J., Juenger, M.,C., and Schindler, A. K. (2007) Methods for Calculating Activation Energy for Portland Cement, ACI Materials Journal, vol. 104(1), pp. 303-311.

[95] D'Aloia, L., and Chanvillard, G. (2002). Determining the "apparent" activation energy of concrete: E_a - Numerical simulations of the heat of hydration of cement. Cement and Concrete Research, vol. 32(8), pp. 1277-1289.

[96] ASTM (2012). Chemical Shrinkage of Hydraulic Cement Paste. ASTM C1608, pp. 5.

[97] Sarkar, S., Halder, A., and Bishnoi S. (2013). Shrinkage in concretes containing fly ash, UKIERI Concrete Congress, Jalandhar, India.

[98] Marsh B. K. (1984). Relationships between engineering properties and microstructure characteristics of hardened cement paste containing pulverized fuel ash as a partial cement replacement, PhD thesis, The Hatfield Polytechnic, UK.

[99] Zhang, X. (2007). Quantitative Microstructural Characterization of Concrete Cured Under Realistic Temperature Conditions, Doctoral Thesis, Swiss Federal Institute of Technology at Lausanne, pp. 282.

[100] ASTM (2013). Standard Test Method for Sampling and Testing Fly Ash or Natural Pozzolans for Use in Portland-Cement Concrete. ASTM C311/311M, pp. 10.

[101] Hall, C. (1989). Water Sorptivity of Mortars and Concretes: A Review, Magazine of Concrete Research, vol. 41(147), pp. 51-61.

[102] ASTM (2011). Measurement of Rate of Absorption of Water by Hydraulic Cement Concretes, ASTM C1585, pp. 6.

[103] White, W. B. (1992) Theory of Corrosion of Glass and Ceramics, In: D.E. Clarke and B.K. Zoitos editors, Corrosion of glass, ceramics and superconductors. Park Ridge, NJ, pp. 2–28.

[104] Holland, T. C. (2005). Silica Fume User's Manual, Federal Highway Administration Technical.

[105] Xu, W., and Chen, H. (2012). Microstructural modelling of cement-based materials via random packing of three-dimensional ellipsoidal particles. Procedia Engineering, vol. 27, pp. 332-340.

[106] Gallucci, E., Mathur, P., and Scrivener, K. (2010). Microstructural development of early age hydration shells around cement grains, Cement and Concrete Research, vol. 40, pp. 4–13.

[107] Thomas, J. J., Biernacki, J. J., Bullard, J. W., Bishnoi, S., Dolado, J. S., Scherer, G. W., and Luttge, A. (2011). Modeling and simulation of cement hydration kinetics and microstructure development. Cement and Concrete Research, vol. 41, pp. 1257–1278.

[108] Diamond, S. (2004). The microstructure of cement paste and concrete—a visual primer, Cement & Concrete Composites, vol. 26, pp. 919–933.

[109] Merzouki, T., Bouasker, M., Khalifa, N. E. H., and Mounanga, P. (2013). Contribution to the modeling of hydration and chemical shrinkage of slag-blended cement at early age, Construction and Building Materials, vol. 44, pp. 368–380.

[110] Bentz, D. P. (2008). Virtual Pervious Concrete: Microstructure, Percolation, and Permeability, ACI Materials Journal, vol. 105(3), pp. 297-301.

[111] Bentz, D. P. (2000). Influence of silica fume on diffusivity in cement-based materials II. Multi-scale modeling of concrete diffusivity, Cement and Concrete Research, vol. 30, pp. 1121–1129.

[112] Roy, D. M. (1993). Concrete microstructure, Strategic Highway Research Program (SHRP), National Research Council, Washington, DC 1993.

[113] Farjas, J., and Roura, P. (2006). Modification of the Kolmogorov-Johnson-Mehl-Avrami rate equation for non-isothermal experiments and its analytical solution, Acta Materialia, vol. 54(20), pp. 5573–5579.